SOLID STATE SPECTROSCOPY:

FAR INFRARED SPECTRA OF LANTHANIDE IONS IN CALCIUM, STRONTIUM AND BARIUM FLUORIDES

A thesis presented for the degree of
Doctor of Philosophy in Physics
in the University of Canterbury,
Christchurch, New Zealand.

by

E.J. Wood

1973

ACKNOWLEDGEMENTS

I would like to thank the following:

My supervisor, Dr J.A. Campbell, for his guidance and keen interest in all aspects of the project.

Mr R. Ritchie for growing the crystals.

Mr A. Edgar for the e.s.r. data.

The academic and technical staff of the Physics Department who, in diverse ways contributed to the success of this project.

My fellow research students for many enlightening discussions; in particular Phil Wilkinson, a cheerful room-mate.

The New Zealand University Grants Committee who provided a Postgraduate Scholarship.

Mrs M. Sewell for typing this thesis.

Finally sincere thanks to my wife Ruth for her many sacrifices and constant encouragement over the past four years.

CONTENTS

LIST OF FIGURES

LIST OF TABLES

ABSTRACT

The far infrared absorption spectra of trivalent lanthanide ion impurities in calcium, strontium and barium fluorides have been studied at $15^{o}K$ and $85^{o}K$. For calcium fluoride, lanthanide ions in the latter half of the series give rise to a pair of strong, broad absorption bands in the region 50-100 cm^{-1}. Simple lattice dynamical models involving mass changes and force constant reductions are used to interpret the results, and the bands are shown to arise from resonance modes of vibration of the lanthanide ion at a tetragonal site.

Lanthanide ions in strontium and barium fluorides activate phonons of the pure crystal at high-symmetry points in the Brillouin zone, so that the absorption spectra correspond approximately to the phonon density of states. With strontium fluoride the resemblance becomes less obvious for lanthanide ions towards the end of the series, where diminishing ionic radii are expected to cause reductions in the impurity-lattice coupling constants.

CHAPTER 1

INTRODUCTION

1-1 Aim of This Work

When a heavy impurity ion is introduced to a crystal lattice which is composed of lighter ions, the characteristic vibrations of the ions in the original lattice may be affected.

The object of this work was to establish far infrared spectroscopic facilities at the University of Canterbury and to use these facilities in a study of the effect on the lattice vibrations of adding heavy impurity ions, in particular the lanthanide ions, to single crystals of the alkaline earth fluorides (CaF_2, SrF_2 and BaF_2).

1-2 Far Infrared Spectroscopy

The far infrared region of the electromagnetic spectrum has been termed "the Cinderella of spectroscopy"[1] because until recently it has received relatively little experimental attention. The region falls between the microwave region and the near infrared, having no well defined limits but often taken as the wavelength range 20-1000 μm (10-500 cm^{-1}).

The region can be approached through either an extension of microwave techniques or optical techniques. Usually far infrared spectroscopy involves a combination of both techniques.

The extension of microwave techniques to shorter wavelengths involves a choice of two methods[2]: harmonic generation or provision of new sources whose fundamental frequencies are in the far infrared range. Although the only

successful method of very high resolution spectroscopy in the far infrared has been with a microwave source and harmonic generation, this has been limited to wavelengths close to 1 mm and such are the complications of the technique that it seems unlikely that it will be widely used[3].

Submillimetre wave sources have been produced but are extremely expensive, tunable over small ranges only, often fragile and always very difficult to operate[3].

Optical methods of investigating the far infrared have been affected by the lack of intense broad-band sources of radiation. In 1911 Rubens and Baeyer[4] found that a high-pressure mercury arc was an adequate source. Although it consumes several hundred watts of electric power, at most only 10^{-5}-10^{-4} watts (corresponding to the tail of the black-body curve) is radiated in the frequency range below 100 cm^{-1}. With no revolutionary broad-band source having been discovered, the mercury arc lamp is still the usual source used in far infrared spectroscopy.

High-powered far infrared lasers are now available[5,6] but the radiation is confined to a number of lines and at present these sources are tunable only over a limited frequency range. However tunable laser sources exist in the visible and near infrared[7]. Faries and coworkers[8] have generated far infrared radiation with a peak power of 1 mW in the frequency range 1.2 - 8.1 cm^{-1} using the difference frequency of two temperature-tuned ruby lasers. Utilizing a ruby laser as a source and stimulated polariton scattering in $LiNbO_3$, Johnson and coworkers[9] obtained a tuning range of 50-120 cm^{-1} with a peak power of 3 W at 50 cm^{-1}. The continued development of tunable far infrared lasers could revolutionize spectroscopy in this region.

As a consequence of no significant increase in source output, far infrared instrumentation has evolved by improvements in spectrometer efficiency and detector sensitivity[3,10,11]. Far infrared detectors may be conveniently divided into two categories, thermal and photoconductive, and with the important exception of the Golay pneumatic cell[12], almost all are solid state devices operating at liquid helium temperatures. Thermopiles, ferroelectric and pyroelectric detectors operate at room temperature while bolometers are used at room temperature for high power applications, e.g. laser power monitors.

With thermal detectors, incident radiation heats a receiving element and the resultant change in temperature gives a measure of the incident power. They include the Golay detector, the carbon[13] and the germanium[14] bolometers. Although thermal detectors respond over a wide range of the spectrum, they have slow response times (1 - 0.1 sec) compared with photoconductive detectors.

Photoconductive detectors, where absorbed radiation changes the conductivity of a semiconductor, are wavelength sensitive but with very fast response times (typically 10^{-6} sec.). They include the extrinsic germanium detectors[15] and the InSb or Putley detectors[16]. Cyclotron resonance absorption in a magnetic field gives the latter a tunable feature[17].

In spite of the obstacles, the wide range of phenomena with quantum transitions at far infrared frequencies, particularly in molecular and solid state physics[18-20] has recently spurred research in this region. Solid state research includes investigations of the lattice vibrational properties of perfect crystals, mixed crystals and crystals containing

impurities, resonance in ordered magnetic materials, superconductivity, electronic states of ions in crystals and cyclotron resonance in semiconductors.

A useful source of information is the recent bibliography of far infrared spectroscopy compiled by Bloor[21] while the books by Martin[2], Kimmitt[3], Moller and Rothschild[18] and Nudelman and Mitra[19] cover the applications and techniques of far infrared spectroscopy.

1-3 Lattice Vibrations and Infrared Absorption in Perfect Crystals[22,23,24]

A crystal lattice which contains more than one type of atom can be visualized either as being built up of repeated "unit cells" or as the intersection of two or more sublattices of identical atoms.

The atoms in a crystal are continuously oscillating about their equilibrium positions with an energy which is governed by the temperature. The atomic motions are characterised by (1) the frequency of oscillation, (2) the direction of motion relative to other atoms in the unit cell (polarization) and (3) phase with respect to corresponding atoms in neighbouring unit cells. Collectively, the atomic displacements have a wave-like phase variation through the crystal. This phase variation and hence the wavelength of these lattice vibrations in a perfect crystal is measured by the parameter $\underline{k}$ called the "wave vector", where $\underline{k} = \frac{2\pi}{\lambda}$. The direction of $\underline{k}$ is the direction of a wave of lattice vibrations. Modes of vibration where the atoms of a sublattice vibrate in phase have $k = 0$, i.e. infinite wavelength.

Dispersion curves relate the possible k values of the lattice vibrations to the permissible frequencies ω, by depicting the multivalued function $\omega_j(\underline{k})$. In a crystal with s atoms per unit cell the different polarizations of atomic motions give rise to 3s dispersion curves labelled by the index j. From the dispersion relation $\omega_j(\underline{k})$ can be obtained the phonon "density of states" $g(\omega)$ which is defined as the number of lattice vibrations (or phonons) per interval $\omega \rightarrow \omega+d\omega$. This function is normalized to unity over the range of lattice frequencies.

The polarizations of atomic motions and hence the lattice vibrations can be divided into two types. The three branches of $\omega_j(\underline{k})$ for which $\omega \rightarrow 0$ as $k \rightarrow 0$ are the dispersion curves of "acoustic" phonons where the atoms in a unit cell oscillate in phase with each other. The remaining 3s-3 branches are the dispersion curves of "optical" phonons where the atoms in a unit cell vibrate in antiphase. In crystals where the atoms are charged, the atomic motions of the optical modes impart a macroscopic, fluctuating dipole moment to the crystal, which may interact with an incident electromagnetic wave.

Typical lattice vibration frequencies lie in the range up to 10^{13} Hz in the far infrared and have a maximum wave vector $k_{max} \sim 3 \times 10^8$ cm^{-1} ($|\underline{k}| \leq \frac{\pi}{a}$, a is the lattice parameter). By comparison, the wave vector ($= \frac{2\pi\nu}{c}$) of a far infrared photon ($\sim$ 10-500 cm^{-1}) is very small.

The translational invariance of a perfect crystal leads to a selection rule which demands that in the processes of infrared absorption and simultaneous excitation or de-excitation of phonons, the total wave vector must be conserved.

As a consequence in "one-phonon" absorption, only modes with $k \approx 0$ can be excited by a photon.

Further selection rules are imposed by the point symmetry of the crystal and there is only strong interaction between an electromagnetic wave and the lattice vibrations if the crystal is ionic. The $k = 0$ optical modes of ionic crystals are strongly infrared active and are responsible for the characteristic "restrahlen" absorption. In homopolar crystals such as diamond, whose atoms are electrically neutral, infrared absorption by one-phonon processes is forbidden, but does occur weakly through multiphonon processes.

1-4 Impurity-Induced Infrared Lattice Absorption

When impurity atoms are introduced into a crystal lattice, it loses its translational symmetry and the $k = 0$ selection rule is relaxed so that electromagnetic waves can interact with all vibrational modes of the appropriate point symmetry. All modes which have a non-vanishing electric dipole moment, arising perhaps from a change in charge distribution from that of the perfect lattice or a change in atomic displacements near an impurity, will give rise to a more extensive one-phonon absorption than is allowed in the perfect crystal. The selection rules that determine which phonons of the perfect crystal can interact with infrared radiation when an impurity which affects only a single lattice point is present, have been worked out by Loudon[25]. He finds that all phonons can be impurity activated in the face-centred cubic and diamond lattices but that selection rules are operative in the rock-salt, zinc blende and calcium fluoride lattices.

The effects of impurities on the lattice vibrations and infrared absorption of crystals can be of at least two different kinds. The first type arises from the relaxation of the k = 0 selection rule which charged impurities are introduced into a homopolar crystal such as silicon or diamond. Then the absorption coefficient $\alpha(\omega)$ (see section 3-9) in the region of lattice frequencies is of the form [26]

$$\alpha(\omega) \propto A^2(\omega)\, g(\omega)$$

where $A(\omega)$ is the frequency dependent dipole moment and $g(\omega)$ is the density of states. The dipole moment function depends on the nature of the impurity. For a charged impurity atom which has similar mass and coupling constants to the rest of the lattice as the atom which it replaces, $A(\omega)$ is such that the absorption coefficient reflects the phonon density of states of the host crystal. However, for other impurities $A(\omega)$ can change rapidly near the maxima in the density of states, shifting the absorption peaks away from the frequencies of these maxima for the pure crystal.

The second type of impurity effect is the introduction of exceptional modes into the vibrational spectrum of the crystal. For example, it is possible for very heavy impurity atoms or atoms which are more weakly coupled to the surrounding lattice than the atoms which they replace, to give rise to so-called resonance modes (or quasilocalized or pseudolocalized modes) in the range of lattice frequencies (see fig. 1.1c). The oscillating impurity atom can lose energy by exciting phonons of the same frequency, but the damping effect is weak at low frequencies where the density of states is low, and narrow resonances result. If the impurity atom is charged then the

absorption coefficient $\alpha(\omega)$ will show a peak at the frequency of the resonance mode, corresponding to a minimum in the denominator of the frequency dependent dipole moment $A(\omega)$.

Another kind of exceptional mode which is introduced into the crystal is the "localized mode" which arises if the impurity atom is much lighter than the atom which it replaces, or if the impurity atom is coupled more strongly to the surrounding host crystal. Localized modes have frequencies above the maximum frequency of the host lattice and since they excite non-propagating modes of the crystal, nearly all the amplitude is at the impurity site (see fig. 1.1a).

If a crystal has a gap in its frequency spectrum, then it is possible for certain impurities to give rise to localized "gap modes" between the acoustic and optical branches, (see fig. 1.1b). Localized modes and gap modes will produce sharp absorption lines in the middle and far infrared if they are optically active.

A resonance mode is localized in frequency but not in space while a true localized mode is localized both in frequency and in space.

Theoretical understanding of impurity-induced infrared absorption is based mainly on the lattice dynamics of perturbed crystals. The study of defect lattice dynamics dates back to the work of Lord Rayleigh[29], but the modern theory was initiated by Lifshitz[30], who first predicted the existence of localized modes. Theoretical work was carried out in the almost complete absence of relevant experimental work until the discovery of the Mossbauer effect in 1958 stimulated a renewal of interest in lattice dynamical defect problems.

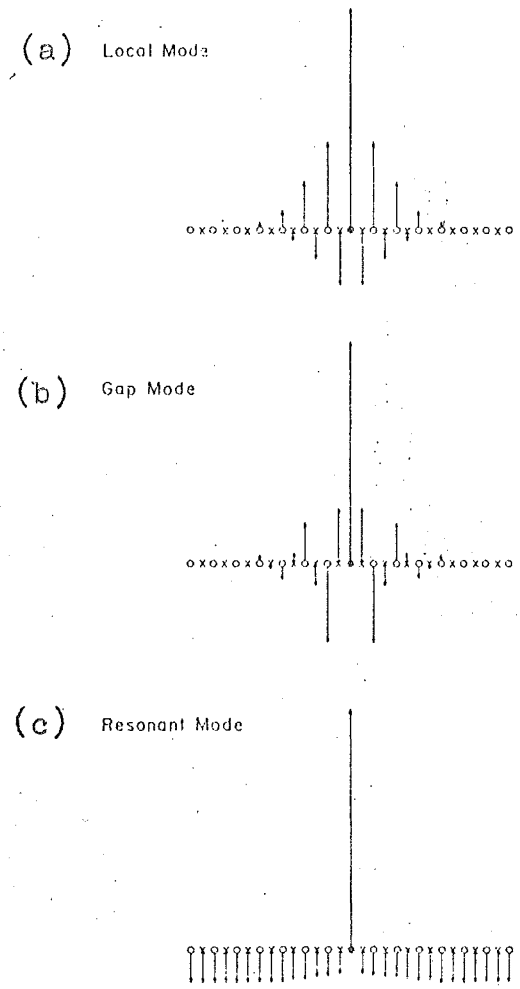

Fig (1.1) Atomic displacements for an infrared active impurity mode in a diatomic linear chain (18).
(a) Local mode (27)
(b) Gap mode (27)
(c) Resonant mode (28).

The accumulation of experimental data on impurity vibrations since then has been rapid, beginning with the first direct observation of localized modes in the infrared absorption spectra of U-centres in alkali halides by Schaefer[31]. The earliest experimental evidence for the existence of resonance modes came from thermal conductivity measurements on monovalent impurities in alkali halides[32] and in 1964 Sievers[33] observed an optically-active resonance mode identified with the substitional silver ion in KI.

In recent years many review articles on the theoretical and experimental aspects of defect lattice dynamics have been published, particularly with reference to impurity-induced infrared absorption[20,22,24,34-40]. Other techniques of studying the influence of impurities on the lattice dynamics of crystals include Raman scattering[41,42], vibronic spectra[43,44,45] and thermal conductivity[34].

Calcium fluoride with lanthanide impurity ions should in principle produce an example of a resonance mode. The bulk of this thesis is concerned with this system as it complements much of the work being done in this department on lanthanide ions in CaF_2, SrF_2 and BaF_2. This work has mainly involved optical and e.s.r. studies of calcium, strontium and barium fluorides containing lanthanide ions with H^- ions as charge compensators.

1-5 The Calcium Fluoride Lattice

The alkaline earth fluorides have been the subject of numerous spectroscopic investigations throughout the electromagnetic spectrum and consequently they occupy a special place as one of the model dielectrics in solid state spectroscopy.

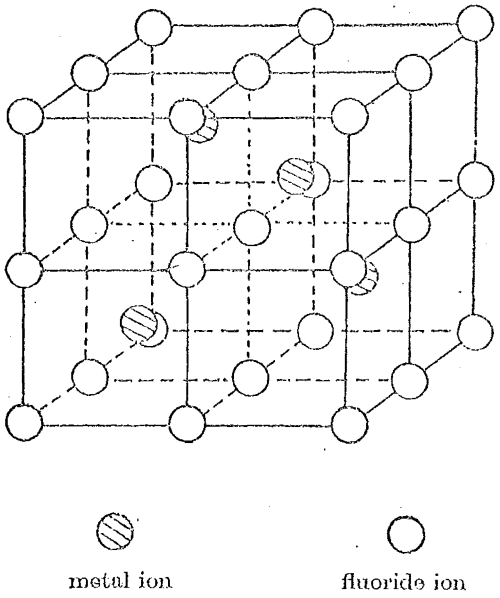

Fig (1.2) The calcium fluoride structure showing that each metal ion is surrounded by eight fluoride ions and each fluoride ion by four metal ions at the corners of a tetrahedron.

Their hardness and insolubility in water give good surfaces that are readily polished and do not deteriorate in a humid atmosphere. Consequently they have been widely used as optical materials for prisms, windows and as components in multilayer filters[3].

The calcium fluoride structure, which is also characteristic of strontium, barium, lead and cadmium fluorides, has the space group O_h^5 - Fm3m. The crystals consist of three interpenetrating face-centred cubic lattices and can be visualized as a cubic lattice of fluorine ions with divalent metal ions in every other body-centred position. The simple structure makes the alkaline earth fluorides an ideal subject for the detailed study of phonon dispersion curves and of the nature of the interaction of infrared radiation with ionic crystals.

The results from a wide range of physical measurements made on these fluorides are available, and certain of these results which are relevant to this work are given in table 1.1.

Elcombe and Pryor[53] have obtained the phonon dispersion curves of calcium fluoride by inelastic neutron scattering. Their observations were fitted by the "shell model" of lattice dynamics[54] and the results are shown in fig. (1.3). Their calculations of the density of states and Debye specific heat parameter θ_D, are also shown in fig. (1.4a) and fig. (1.4b) respectively.

The standard techniques of group theory can be used to show that the symmetry of the long wavelength ($k = 0$) modes of the calcium fluoride lattice is given by[49]

$$\Gamma(k = 0) = A_{2g} + 2A_{1u}$$

where A_{2g} and A_{1u} are irreducible representations of the space group. One of these A_{1u} representations corresponds to the (three) acoustic phonon branches, while the other six degrees of freedom correspond to the optical modes. The triply degenerate A_{2g} mode is Raman active and the infrared active A_{1u} mode is split into longitudinal and transverse branches, the latter being doubly degenerate. For the even A_{2g} mode, the calcium ions remain stationary while the two fluorine sublattices vibrate against each other. For the odd A_{1u} optic mode, the fluorines all have the same displacement and the calciums move in the opposite direction such that the centre of mass remains stationary.

Bosomworth[48] has investigated the far infrared absorption spectra of pure CaF_2, SrF_2 and BaF_2. As well as the strong one-phonon absorption arising from the infrared active transverse optical mode at zero wavevector ($k = 0$) he observes a temperature dependent two-phonon difference process as enhanced absorption at room and liquid nitrogen temperatures. Such a multiphonon process which is forbidden by the $k = 0$ selection rule in a perfect harmonic crystal, reflects the anharmonicity of the crystal lattice and the presence of non-linear terms in the crystal dipole moment[22].

The phonon dispersion curves and density of states have been obtained for strontium fluoride by Elcombe[50] and for barium fluoride by Hurrell and Minkiewicz[51]. Their results are shown in figs (1.5) and (1.6) respectively.

Table 1.1

	CaF_2	SrF_2	BaF_2	Reference
Lattice parameter $2r_0$ (A^o)	5.4630 (28°C)	5.7996 (26°C)	6.2001 (25°C)	(46)
Melting point (°C)	1360	1450 +	1280	(47)
$\omega_{TO}^{(a)}$ (cm^{-1}) (80°K)	267 ± 2	225 ± 2	189 ± 2	(48)
$\omega_{LO}^{(b)}$ (cm^{-1}) (80°K)	472	384	330	(48)
$n_0^{(c)}$ (80°K)	2.525	2.457	2.561	(48)
$\varepsilon_0^{(d)}$ (80°K)	6.38	6.04	6.56	(48)
$\varepsilon_\infty^{(e)}$ (80°K)	2.047	2.07	2.157	(48)
$\omega_R^{(f)}$ (cm^{-1})	326	280		(49,50)
			238	(51)
$\omega_D^{(g)}$ (cm^{-1}) 0°K	353	259	-	(52)
30°K	326	242	-	(50)
300°K	347	292	-	

(a) Frequency of transverse optic phonons at $\underline{k} = 0$ (A_{1u} mode).

(b) Frequency of longitudinal optic phonons at $\underline{k} = 0$ (A_{1u} mode).

(c) Refractive index at microwave frequencies.

(d) Electronic and ionic contribution to dielectric constant microwave frequencies.

(e) Electronic contribution to dielectric constant at infrared frequencies.

(f) Frequency of A_{2g} Raman mode.

(g) Debye frequency, calculated from Debye temperature θ_D.

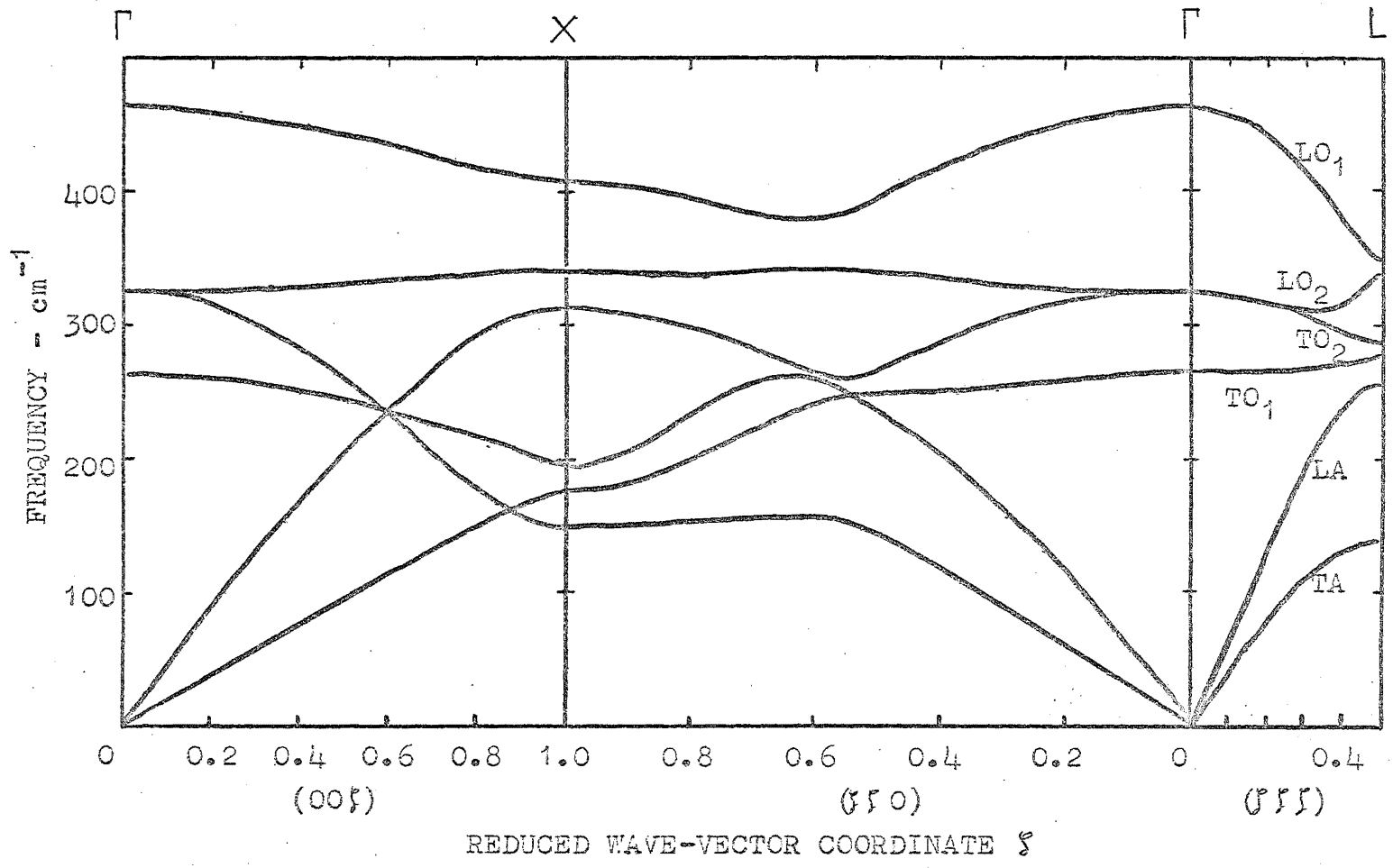

Fig (1.3) Phonon dispersion curves for calcium fluoride at 295°K in the (001), (110) and (111) directions. (Adapted from Elcombe and Pryor (53).)

(T - transverse, L - longtitudinal; A - acoustic, O - optic)

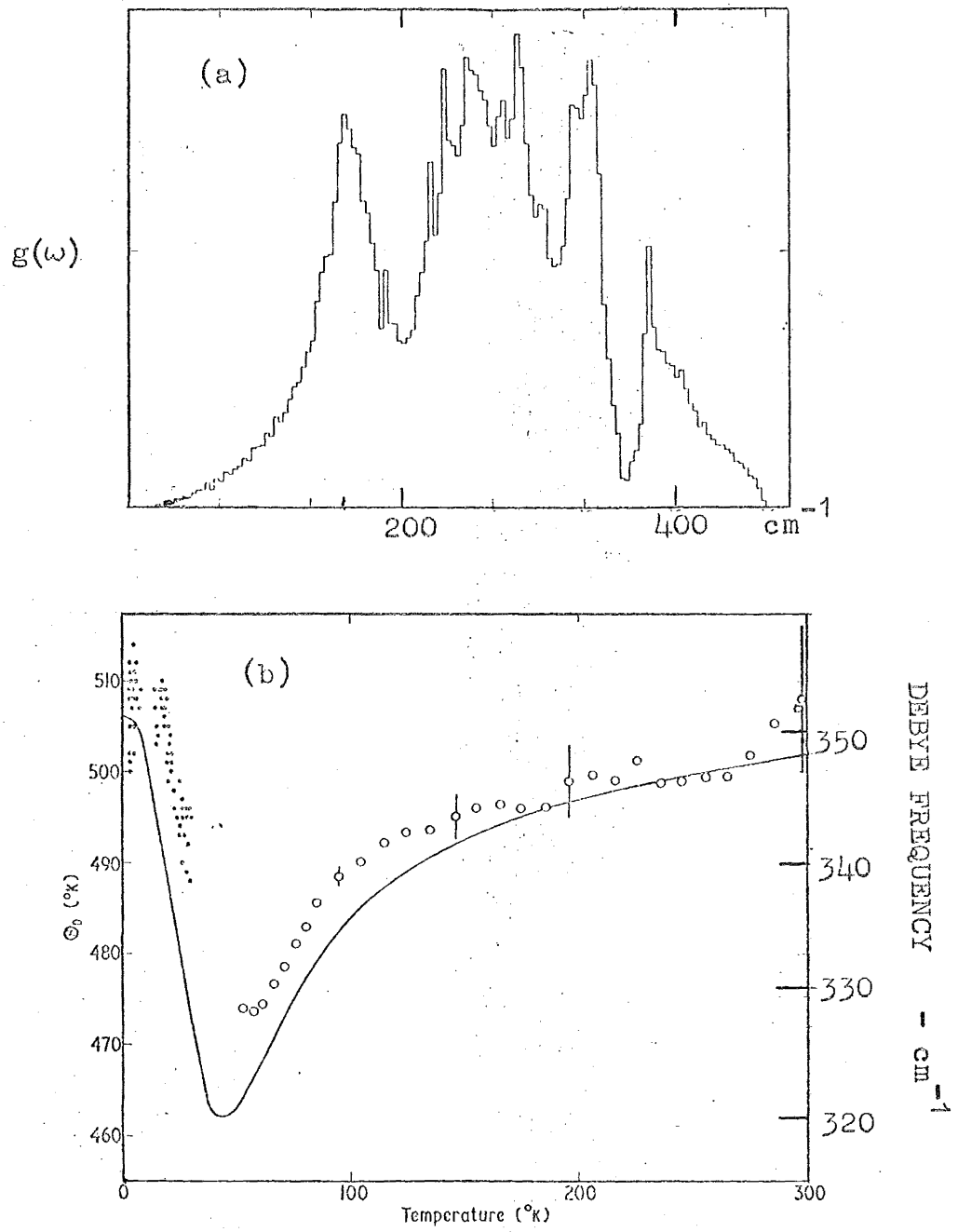

Fig (1.4) (a) Phonon density of states of CaF_2 calculated by Elcombe and Pryor (53).
(b) The Debye specific heat parameter Θ_0 and Debye frequency ω_0 from calculations of Elcombe and Pryor (solid curve) and two sets of experimental data (open and closed circles) (53).

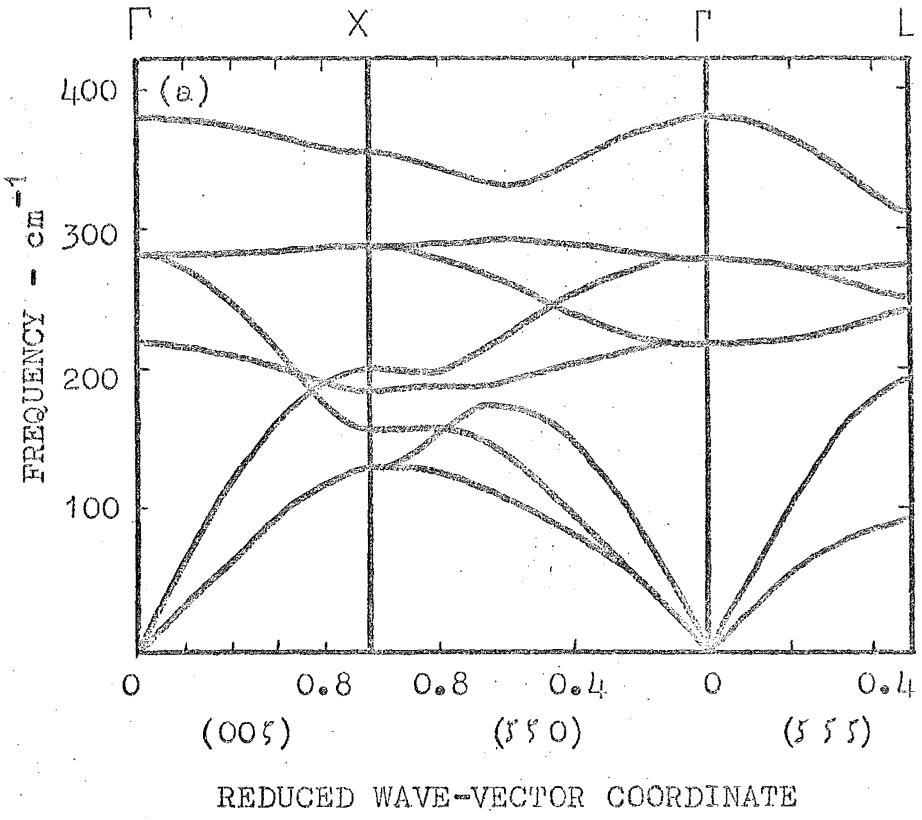

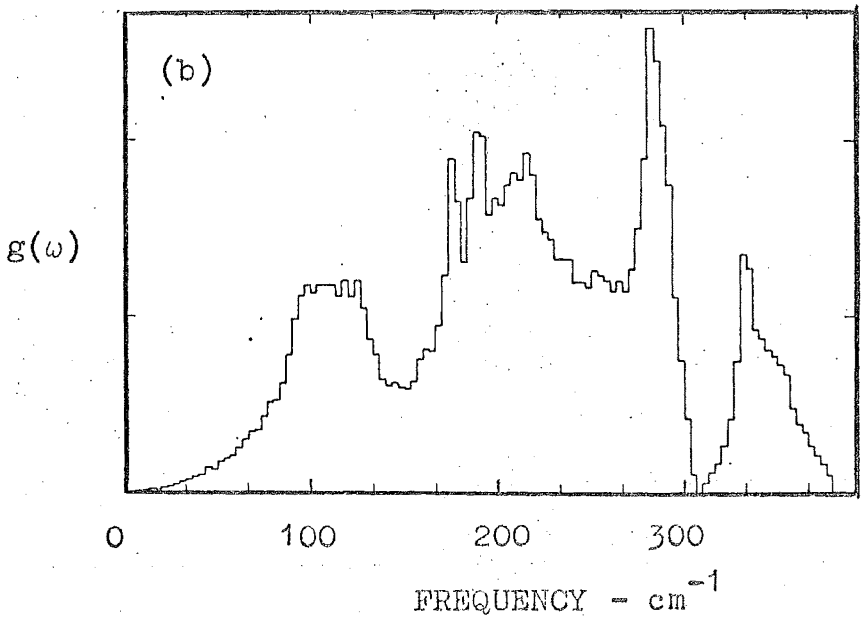

Fig (1.5) (a) Phonon dispersion curves for strontium fluoride at 295°K in the (001), (110) and (111) directions. (Adapted from Elcombe (50))

(b) Density of states of SrF_2 (50).

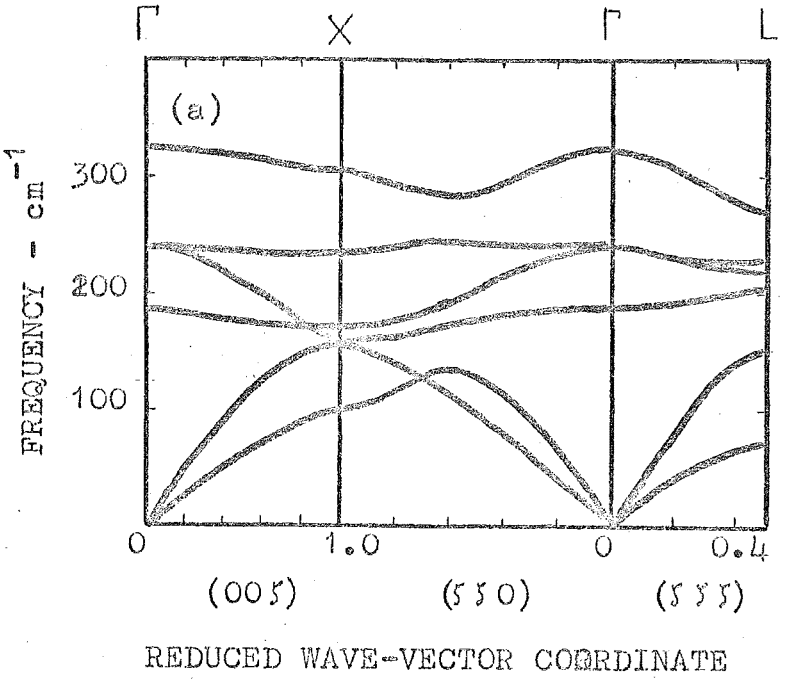

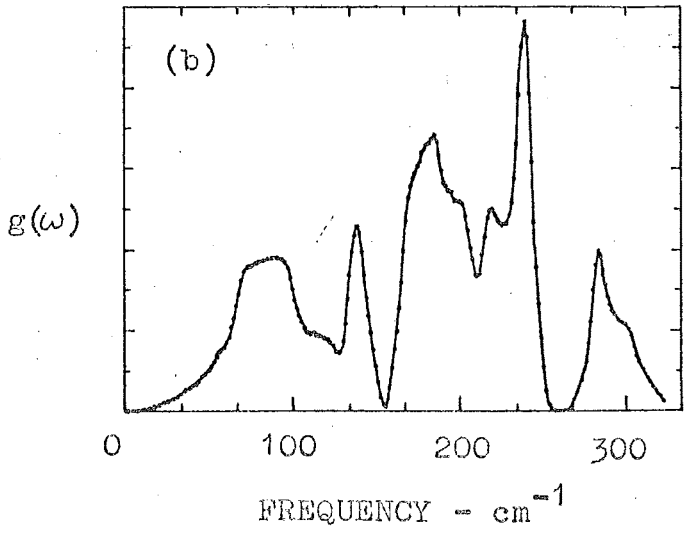

Fig (1.6) (a) Phonon dispersion curves for barium fluoride at 300°K in the (001), (110) and (111) directions. (Adapted from Hurrell and Minkiewicz (51).)

(b) Density of states of BaF_2 (50).

1-6 Lanthanide Ions in Calcium, Strontium and Barium Fluorides

Lanthanide ions can be introduced substitutionally at divalent cation sites when the crystals are grown from a melt containing both alkaline earth and lanthanide fluorines. The lanthanide ions have radii similar to the ions which they replace so that no serious disruption of the lattice results for impurity concentrations up to 5%.

Since lanthanide ions occur in the trivalent oxidation state and normally enter the crystal in this state, some form of charge compensation is required to balance the extra positive charge. Many charge compensation mechanisms are possible, the mechanism which predominates depending on the particular lanthanide ion, the lanthanide ion concentration, growing conditions, and history of the crystal. The various charge compensation mechanisms produce different lanthanide ion site symmetries and these have been identified by optical[55] and electron spin resonance[56] experiments.

If a crystal containing a low concentration ($\lesssim$ 0.3%) of lanthanide ions is grown under reducing conditions (by adding lead fluoride to the melt), then compensation is by means of excess fluorine ions. If the fluorine ion occupies an interstitial site some distance from the neighbourhood of the lanthanide ion then the lanthanide ion site symmetry is cubic (O_h). Paramagnetic resonance spectra exhibiting cubic symmetry have been observed[57,58]. If the compensating fluorine ion occupies the nearest interstitial site to the lanthanide ion (fig. (1.7)) then the symmetry is tetragonal ($C_{4v}(100)$). This charge compensation mechanism, which is the predominant one in many cases, has been well substantiated by paramagnetic resonance experiments of Bleaney et al.[59] and

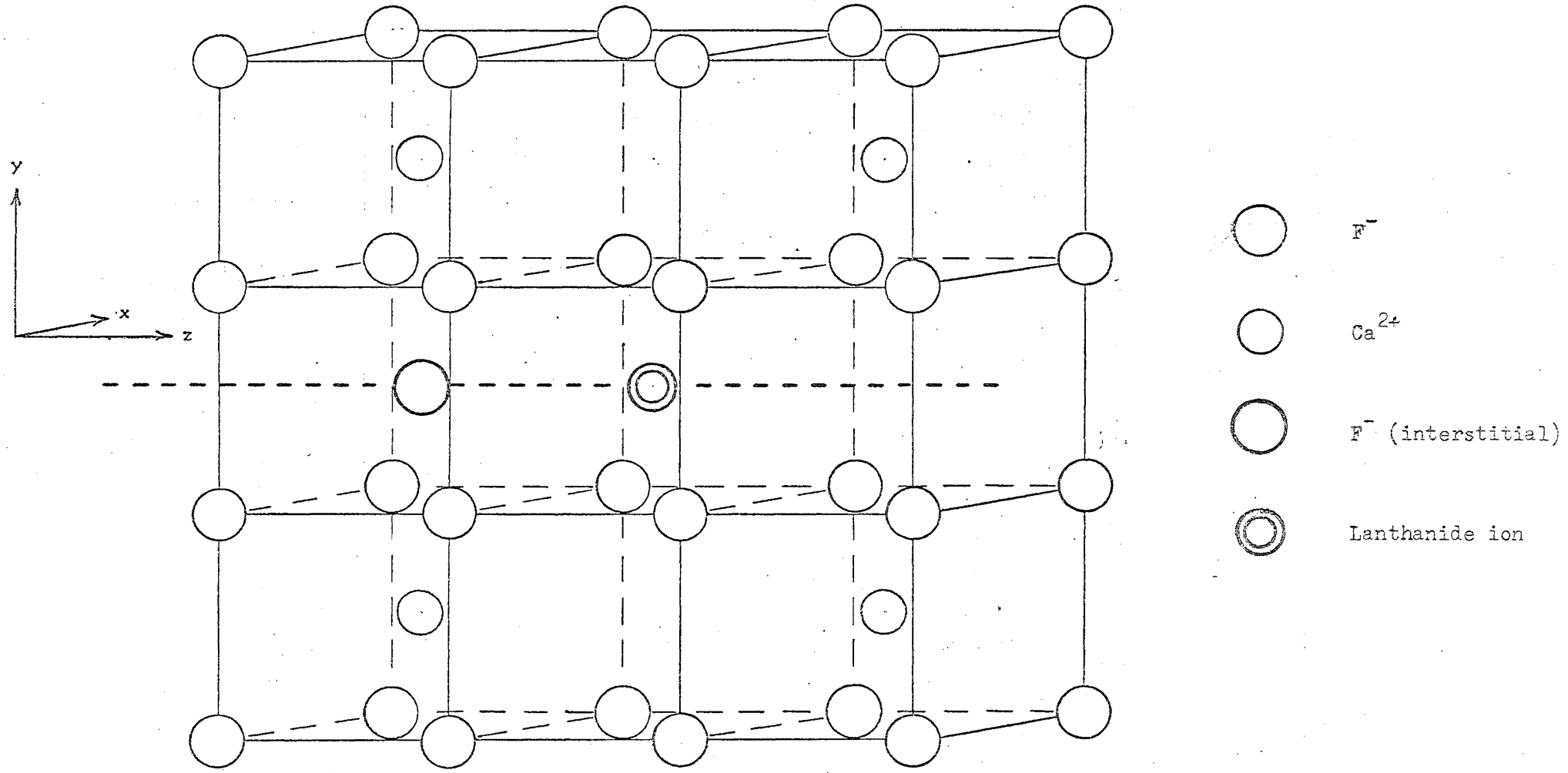

Fig (1.7) The tetragonal site

others[60,61]. Since the fluorine is not tightly bound to the lanthanide ion, it can diffuse through the crystal at high temperatures[62,63] to produce cubic sites. Lanthanide ions in the second half of the series have been found in sites of cubic symmetry in calcium fluoride more frequently than ions of the first half[55]. The stability of the former in cubic sites may be associated with their smaller ionic radii and different local distortions of the crystal lattice.

A less well-established centre in calcium fluoride[57] is the trigonal (C_{3v}(111)) site where it is possible that a fluorine ion is situated interstitially in the next nearest neighbour cube. This trigonal site is the dominant one in strontium and barium fluoride for lanthanide ions in the latter half of the series[64].

Heist and Fong[65] have theoretically predicted the occurrence of a third nearest neighbour monoclinic (C_s(210)) site whose presence has yet to be confirmed experimentally.

If crystals are grown under oxidizing conditions, the predominant site symmetry is trigonal which, up until recently, was believed to arise from replacement of one of the nearest-neighbour fluorine ions by an O^{2-} ion (Re^{3+}, F_7^- O^{2-})[66-68]. However, Reddy et al.[69] have shown that a better characterisation of this centre is Re^{3+} F^- O_4^{2-} where a calcium ion and eight fluorine ions are replaced by one fluorine ion, four oxygen ions and three anion vacancies.

Heating crystals in an atmosphere containing a small amount of water vapour causes the dissociation of H_2O molecules at the surface with OH^- replacing F^- to produce sites of trigonal symmetry[67,70]. An atomic model proposed by Reddy et al.[69] which agrees better with experiment is Re^{3+} H^- O_4^{2-},

similar to the oxygen centre above.

It is possible to obtain lanthanide ion sites of rhombic symmetry by adding sodium fluoride to the melt prior to growth[71,72]. Here the lanthanide ion is associated with a sodium ion which is on a nearest-neighbour divalent metal ion site.

At low concentrations ($\lesssim$ 0.3%) the lanthanide ion occurs as a single ion which requires some form of charge compensation. At higher concentrations ($\gtrsim$ 1%) it has been suggested that energetically favoured pairs of clusters of ions may occur. Thus it is possible for three divalent metal ions to be replaced by two trivalent lanthanide ions requiring no further charge compensation[61].

To date, most experimental work has involved investigations of individual lanthanide ions in alkaline earth fluorides at low concentration. Further work is needed on concentration dependence of site symmetries and trends along the series. This lack of knowledge coupled with the variety of possible growth conditions makes it impossible in general, to know in advance with any certainty, what proportions of different site symmetries will be present in a single crystal of an alkaline earth fluoride containing a given lanthanide ion.

1-7 Outline of Thesis

As an introduction to the technique of Fourier transform spectroscopy in the far infrared, Chapter 2 briefly outlines the principles involved and relates them to the main computer program which has been developed to perform the transform.

Experimental aspects are discussed in chapter 3, in particular the Grubb-Parsons spectrometer and modifications,

data processing and sample preparation.

Chapter 4 presents three simple theoretical models but of increasing sophistication, to show the necessary conditions for lanthanide ions to produce resonance mode peaks in the far infrared absorption spectra of calcium fluoride.

The experimental results for the pure and doped crystals which were investigated are presented in Chapter 5, leading on to discussion of the results in Chapter 6 and some conclusions in Chapter 7.

An appendix gives the listings of the various computer programs which have been developed for this work.

CHAPTER 2

PRINCIPLES OF FOURIER TRANSFORM SPECTROSCOPY

2-1 Introduction

If a monochromatic wave of wavenumber ω $(= \frac{1}{\lambda})$ and intensity S_0 is sent into a two-beam interferometer, the output is given by

$$I(x) = S_0(1 + \cos 2\pi\omega x) \tag{2.1}$$

where x is the optical path difference between the two beams.

For an arbitrary spectral input $S(\omega)d\omega$, the output is now

$$I(x) = \int_{-\infty}^{\infty} S(\omega)[1 + \cos 2\pi\omega x]d\omega$$

$$= \tfrac{1}{2} I(0) + \int_{-\infty}^{\infty} S(\omega) \cos 2\pi\omega x \, d\omega \tag{2.2}$$

where $$I(0) = \int_{-\infty}^{\infty} S(\omega) \, d\omega \tag{2.3}$$

The interferogram function

$$F(x) = I(x) - \tfrac{1}{2} I(0)$$

$$= \int_{-\infty}^{\infty} S(\omega) \cos 2\pi\omega x \, d\omega \tag{2.4}$$

is assumed to be symmetric about $x = 0$. Applying the Fourier integral theorem we obtain

$$S(\omega) = \int_{-\infty}^{\infty} F(x) \cos 2\pi\omega x \, dx$$

$$= 2 \int_{0}^{\infty} F(x) \cos 2\pi\omega x \, dx \tag{2.5}$$

which is the fundamental relation of Fourier transform spectroscopy (FTS).

Lowenstein[73] defines FTS as "the technique of determining a spectrum by the Fourier transformation of an interferogram, which is the record produced by a two-beam interferometer as the path difference is varied". Although this technique has been termed "a disagreeable indirect way to measure a spectrum"[74], in the far infrared FTS has several advantages over conventional grating monochromator techniques[75] which tend to outweigh the difficulties in computing the spectrum.

The "throughput advantage"[76] means that high resolution can be obtained without using narrow slits since the resolution depends primarily on the maximum path difference. With an interferometer, the whole spectrum reaches the detector for the entire experiment time so that, an improved signal-to-noise ratio results in the final spectrum or the experiment time is reduced in obtaining the same signal-to-noise ratio as a grating instrument. This "multiplex advantage"[77] is particularly significant in the far infrared where detector noise limits all measurements.

Although the general concept of FTS was realized by Fizeau, Rubens, Wood and Michelson[73], it was the emergence of electronics and computer science that made the technique feasible. The first modern worker in the field was Fellgett[77] who in 1951 recognized the multiplex advantage and converted the first interferogram to spectra, and shortly afterwards Jacquinot[76] pointed out the throughput advantage. These developments inspired the work of Connes[78], Mertz[74] and Strong, Vanasse and Gebbie[79,80] who initiated the use of this technique in the far infrared.

For further information on FTS, the reader may consult Bloor[21], Moller and Rothschild[18] and the review articles

by Richards[81] and Vanasse and Sakai[82].

2-2 The Michelson Interferometer

In principle, any two-beam interferometer will serve for FTS, but two types have proved to be the most useful in the far infrared. These are the lamellar grating interferometer developed by Strong and Vanasse[83] and the Michelson interferometer first used in the far infrared by Gebbie[84]. The former produces the two beams by wavefront division while the latter is an amplitude dividing device (fig. 2.1a) and is the type employed in this work.

In the Michelson interferometer the input radiation is divided by a beam-splitter into two beams of equal strengths (ideally). Two mirrors reflect the beams back to the beam-splitter where two recombined beams are formed, one travelling to the detector. If the distances from the beam-splitter to the mirrors are equal, the amplitude and phase of corresponding spectral elements in beams I and II will be the same and the resulting vector addition of the two energies will produce a "grand maximum" in the energy of beam III. Changing the distance of one mirror relative to the beam-splitter alters the phase relationships of the various spectral elements and the interference pattern generated will fluctuate in a manner determined by the spectral content of the energy.

For far infrared spectroscopy the beamsplitter is a thin film of mylar which acts as a Fabry-Perot interferometer in that it transmits a channel spectrum analogous to the various orders for an interference filter. The thickness of the film is chosen so that the beam-splitter transmits in the spectral region of interest (fig. 2.1(b)).

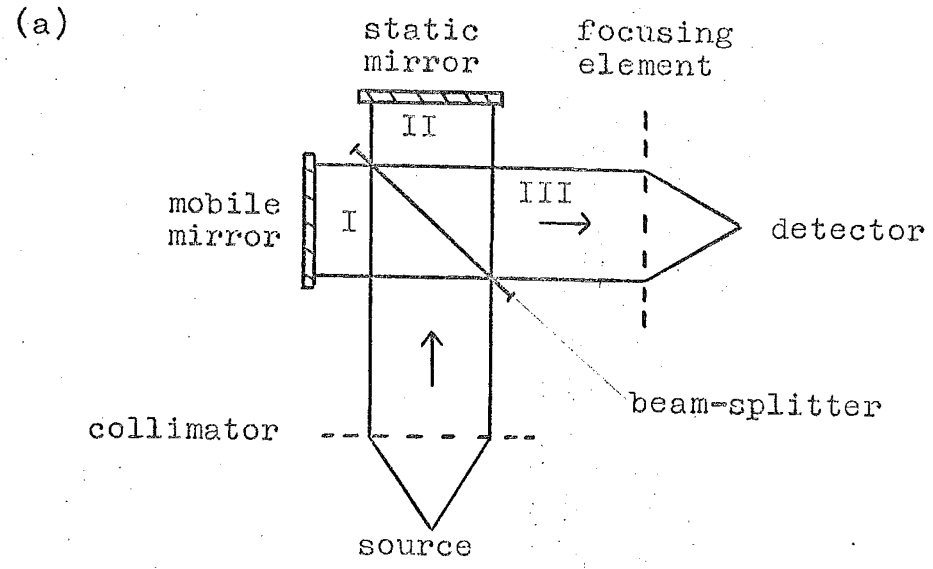

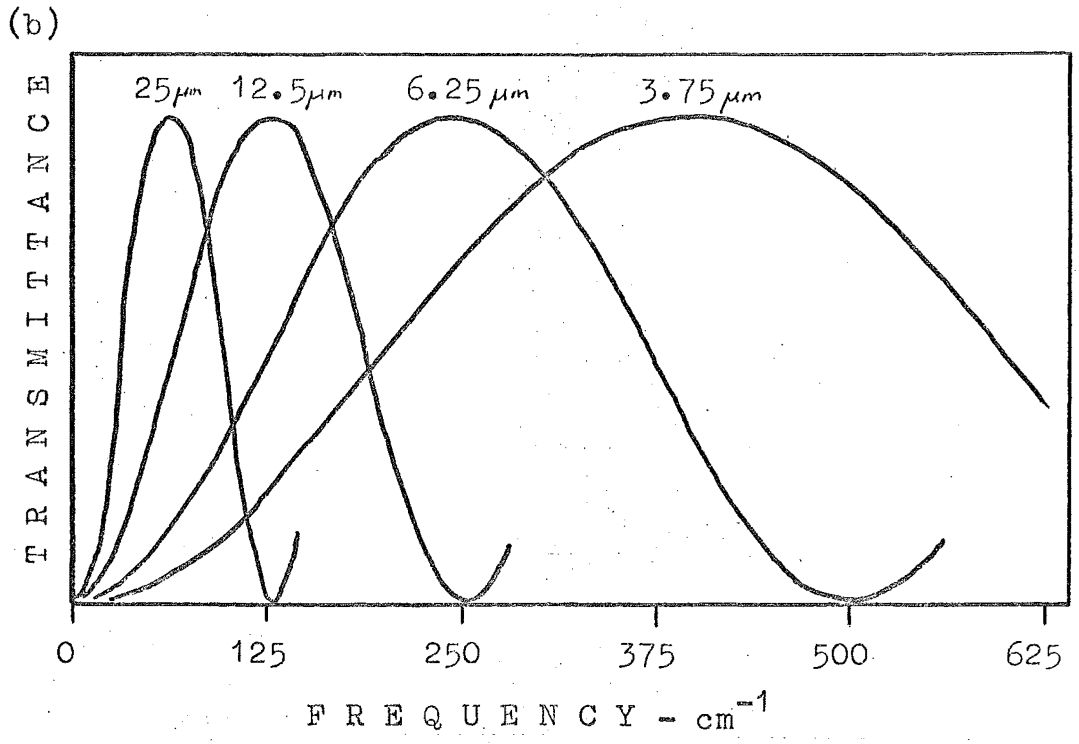

Fig2.1 (a) Basic Michelson system.
(b) Beam-splitter characteristics.

Two experimental approaches to FTS have been developed[81]; the periodic or rapid scan meathod of Genzel and coworkers[85], and the more widely used technique of aperiodic spectroscopy with digital Fourier transform. The latter involves sampling the interferogram at small uniform intervals of path difference as the mobile mirror scans either at constant velocity or in steps. In the far infrared the accuracy criterion is sufficiently relaxed that accurate sampling may be accomplished by driving a micrometer screw with a stepping motor.

In reality we do not realize the computation represented by equation (2.5), which is necessary for the faithful recovery of the spectrum because F(x) is not obtained as an analytical expression but is sampled at intervals of path difference. Consequently the set of points obtained may not be symmetric about x = 0. Also, because or physical limitations the maximum path difference is necessarily finite.

2-3 The Scanning Function

To express the finite movement of the mirror, a weighting function A(x), which is terminated at the maximum path difference x_{max}, is introduced in eqn (2.5) so that an approximate value of the integral is

$$S'(\omega) = \int_{-\infty}^{\infty} F(x)\ A(x)\ \cos\ 2\pi\omega x\ dx$$

$$= S(\omega) * \bar{A}(\omega) \qquad (2.6)$$

The computed spectrum is the convolution of the true spectrum $S(\omega)$ with a scanning function $\bar{A}(\omega)$. For a mere truncation of the interferogram at $\pm\ x_{max}$

$$A(x) = R(x) = \begin{cases} 1 & |x| \leq x_{max} \\ 0 & |x| > x_{max} \end{cases} \qquad (2.7)$$

This rectangular function has the Fourier transform (fig. 2.2)

$$\bar{R}(\omega) = 2\, x_{max} \frac{\sin 2\pi\omega x_{max}}{2\pi\omega x_{max}} \qquad (2.8)$$

Since $\bar{R}(\omega)$ has a finite width and sidelobes, the ability of the interferometer to resolve closely spaced spectral lines is limited. Convolution of $S(\omega)$ with $\bar{R}(\omega)$ produces a "smeared out" version $S'(\omega)$. The resolution is defined as the distance from the peak of the scanning function to its first zero, and for $\bar{R}(\omega)$ this is

$$\Delta\omega = \frac{1}{2x_{max}} \qquad (2.9)$$

Increasing x_{max} narrows the scanning function and thus improves the resolution.

The sidelobes of the scanning function $\bar{R}(\omega)$, which arise from the sharp cut-off at x_{max}, cause no problems if the spectrum is continuous but they introduce spurious lines into the computed spectrum in the regions of sharp discontinuities. The sidelobes can be reduced by introducing a smooth cut-off function into eqn (2.6):

$$S'(\omega) = \int_{-x_{max}}^{+x_{max}} F(x)\, A'(x) \cos 2\pi\omega x \, dx \qquad (2.10)$$

which is a process known as "apodization"[78,79,80]. The apodization function $A'(x)$ is chosen from functions whose Fourier transforms have small sidelobes (fig. 2.2). For example, the linear apodization function

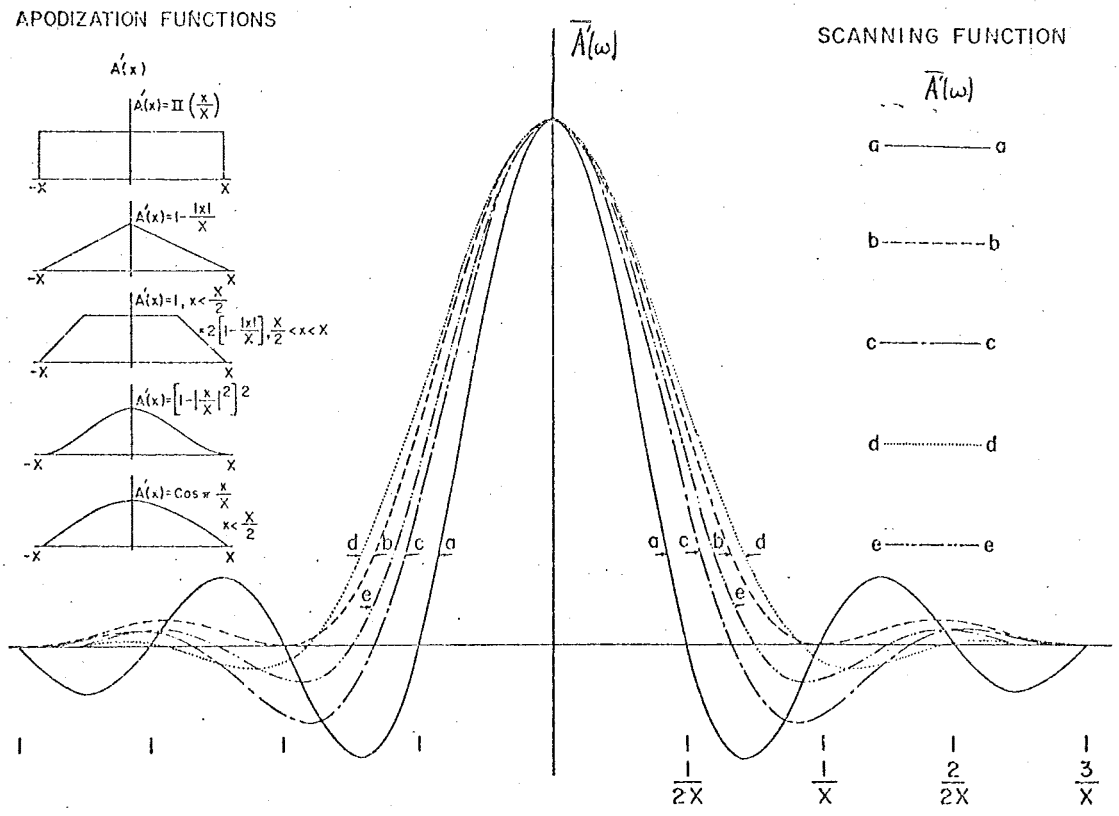

Fig (2.2) Selected apodization functions $A'(x)$ and their corresponding scanning functions $\bar{A}'(\omega)$. ($X \equiv x_{max}$)

$$A_1(x) = \begin{cases} 1 - \dfrac{x}{x_{max}} & |x| < x_{max} \\ 0 & |x| > x_{max} \end{cases} \qquad (2.11)$$

has the Fourier transform

$$\bar{A}_1(\omega) = x_{max} \left(\frac{\sin 2\pi\omega x_{max}}{2\pi\omega x_{max}} \right)^2 \qquad (2.12)$$

which has reduced sidelobes. However the width is twice that of $\bar{R}(\omega)$ and the resolution

$$\Delta\omega \approx \frac{1}{x_{max}} \qquad (2.13)$$

Apodization functions yield an improvement in the sidelobe level at the expense of resolution and signal-to-noise ratio. The process is useful for cleaning up noise spectra or for judging the significance of structure near strong narrow lines.

The main computer program which has been developed provides a choice of three apodization functions or no apodization for both single and double-sided interferograms. (See the appendix for the listings of SUBROUTINE APODS and SUBROUTINE APODD.)

2-4 Sampling[82]

The interferogram is sampled at uniform intervals of path difference Δx so that for computational purposes the Fourier integral (eqn 2.10) is replaced by a summation:

$$S'(\omega_n) = \frac{x_{max}}{M} \sum_{m=-M}^{M} A'(x_m)\, F(x_m) \cos 2\pi\omega_n x_m \qquad (2.14)$$

where

$$x_m = m\Delta x, \qquad \omega_n = \frac{n(\omega_2-\omega_1)}{N} \tag{2.15}$$

M is the number of interferogram points between x = 0 and x = x_{max} and N is the number of spectral points to be computed over the frequency range $(\omega_2-\omega_1)$. Eqn (2.14) can be written as

$$S'(\omega_n) = \Delta x \int_{-\infty}^{\infty} D(x)\ A'(x)\ F(x)\ \cos 2\pi\omega_n x\ dx \tag{2.16}$$

Each delta function of the Dirac comb function (fig. 2.3a)

$$D(x) = \sum_{m=-\infty}^{\infty} \delta(x-m\Delta x) \tag{2.17}$$

extracts a discrete sample from the interferogram. Its Fourier transform (fig. 2.3b) is

$$\bar{D}(\omega) = \frac{1}{\Delta x} \sum_{n=-\infty}^{\infty} \delta\left(\omega - \frac{n}{\Delta x}\right) \tag{2.18}$$

so that in the spectral domain, eqn (2.16) becomes

$$S'(\omega) = \bar{D}(\omega) * \bar{A}'(\omega) * S(\omega). \tag{2.19}$$

The spectral distribution $\bar{A}'(\omega) * S(\omega)$ (fig. 2.3c) appears as sidebands on each delta function of the comb $\bar{D}(\omega)$ (fig. 2.3d) Ambiguities due to overlap of these sidebands must be avoided by choosing the delta function separation sufficiently large (Δx small). For a band limited spectrum extending from $0 - \omega_{max}$ the condition for no overlap is

$$\Delta x \leq \frac{1}{2\omega_{max}} \tag{2.20}$$

which is the same result as is obtained from sampling theory[87]. In general the whole electromagnetic spectrum is folded on the

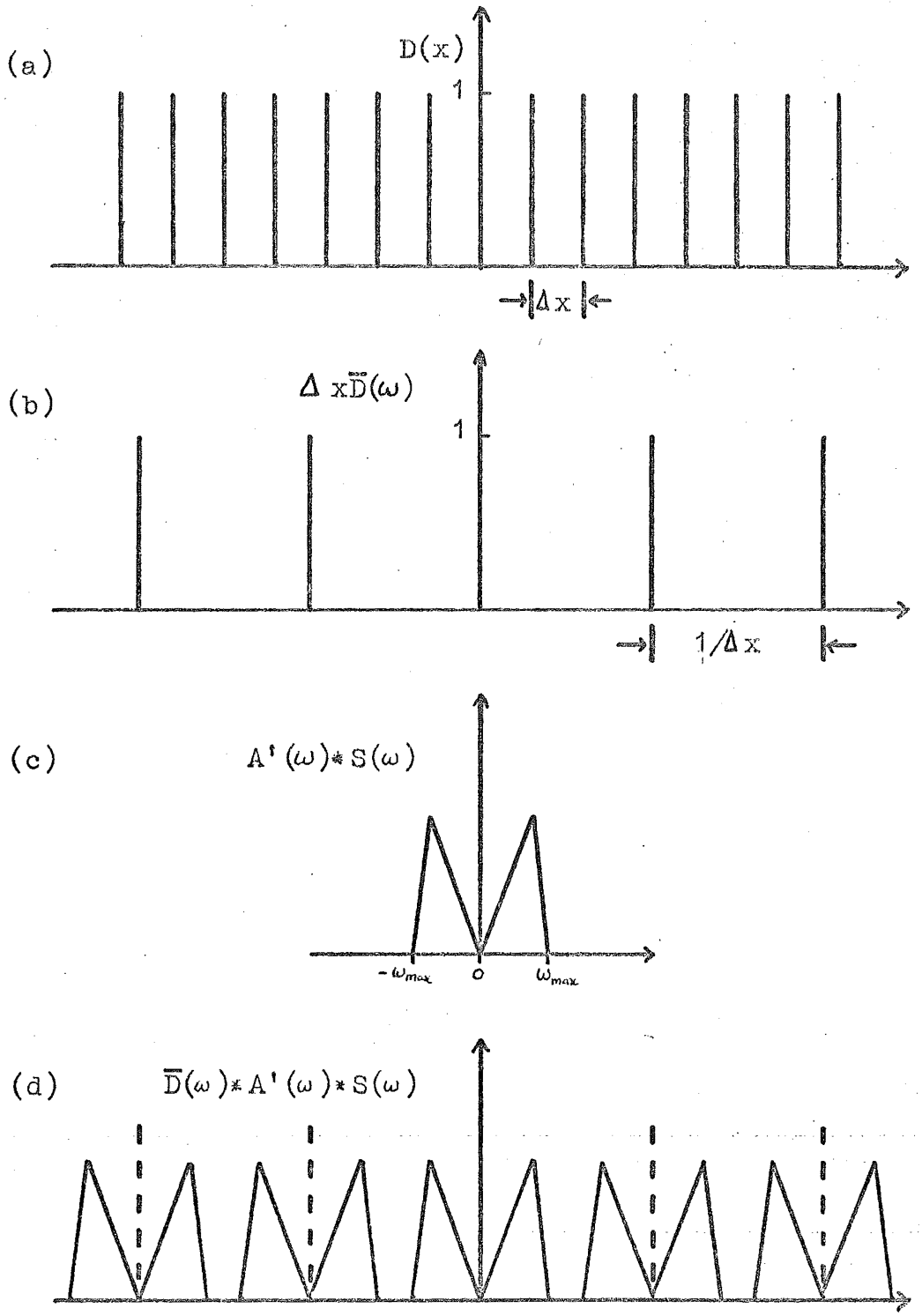

Fig (2.3) Repetition of numerically calculated spectra where $\Delta x < 1/2\omega_{max}$.

region $0 < \omega < \omega_{max}$ and to obtain an unambiguous spectrum, it is necessary to use filters to isolate one of these folds. However, in FTS the filtering problem is less severe than in a grating monochromator system.

With $\Delta x = 10$ microns the upper limit is 500 cm^{-1}
On occasions when examining highly absorbing samples, a long time constant ~30 seconds is desirable. To reduce the experiment time the mirror is scanned manually and the interferogram is sampled at intervals of 40 microns, which sets an upper limit of 125 cm^{-1}.

2-5 Asymmetric Interferograms

The interferogram function F(x) is necessarily real and ideally is an even function:

$$F(x) = \int_{-\infty}^{\infty} S(\omega) \cos 2\pi\omega x \, d\omega$$

$$= \int_{-\infty}^{\infty} S(\omega) \, e^{-2\pi i\omega x} \, d\omega \qquad (2.21)$$

However, compensation errors or phase errors which destroy the basic symmetry may arise. The first type, which are errors resulting from lack of symmetry in the optical path, are in general nonlinear functions of frequency but the magnitude is only of a few degrees. The second, more important types, arise because of displacment between the digitizing command and the interferogram, and the phase error $\phi(\omega)$ is a linear function of frequency. To eliminate the asymmetry eqn (2.21) can be modified:

$$F'(x) = \int_{-\infty}^{\infty} S(\omega) \, e^{-i\phi(\omega)} \, e^{-2\pi i\omega x} \, d\omega \qquad (2.22)$$

Hence

$$S(\omega)\ e^{-i\phi(\omega)} = \int_{-\infty}^{\infty} F'(x)\ e^{2\pi i\omega x}\ dx \qquad (2.23)$$

$$= P(\omega) + i\ Q(\omega)$$

so that

$$S(\omega) = \sqrt{P^2(\omega) + Q^2(\omega)} \qquad (2.24)$$

$$\phi(\omega) = -\arctan \frac{Q(\omega)}{P(\omega)} \qquad (2.25)$$

This "amplitude" method of computing the spectrum of an asymmetric interferogram suggested by Connes[78] has several disadvantages:

1. A double-sided interferogram is required, which when compared with the single-sided interferogram suitable for the cosine transform means double the data acquisition time and four times the computation time.

2. The signal-to-noise ratio is decreased, particularly at low frequencies[88].

It is possible to avoid these difficulties by use of the fact that in practice the phase error $\phi(\omega)$ and hence $\cos\phi(\omega)$ and $\sin\phi(\omega)$ are smooth functions of ω. Then a short double-sided interferogram can be used to calculate $\phi(\omega)$ so that only a short extension of the interferogram past zero path difference is required[88]. Having obtained $\phi(\omega)$, the Fourier transform of $e^{i\phi(\omega)}$ is calculated:

$$M(x) = \int_{-\infty}^{\infty} e^{i\phi(\omega)}\ e^{-2\pi i\omega x}\ d\omega \qquad (2.26)$$

and the phase-corrected interferogram function is obtained by the convolution

$$F(x) = F'(x) * M(x). \qquad (2.27)$$

Finally, use of the symmetric Fourier transform produces the spectrum $S(\omega)$.

Consider an interferogram $F(x)$ which is sampled at intervals Δx that are off-centre by an amount ε, then the phase error is linear:

$$\phi(\omega) = 2\pi\omega\varepsilon \qquad (2.28)$$

The transform of $e^{2\pi i\omega x}$ over the range $\omega \leqslant 1/2\Delta x$ gives the correction function

$$M(x) = \frac{1}{\Delta x} \frac{\sin \pi[(x-\varepsilon)/\Delta x]}{\pi[(x-\varepsilon)/\Delta x]}$$

$$= \frac{1}{\Delta x} \operatorname{sinc} \frac{x-\varepsilon}{\Delta x} . \qquad (2.29)$$

Since $F'(x)$ is sampled at discrete points $\varepsilon+n\Delta x$, the convolution is

$$F(m\Delta x) = \frac{1}{\Delta x} \sum_{n=m-p}^{m+p} F'(\varepsilon+n\Delta x) \operatorname{sinc}[(m-n)\frac{x}{\Delta x} - \frac{\varepsilon}{\Delta x}] \qquad (2.30)$$

where p is chosen to suit the accuracy required; for 1%, $p > 20$. Connes[78] has shown that negligible asymmetry results from a phase error where $\varepsilon/\lambda \leqslant 0.01$ and λ is the shortest wavelength present. For $\lambda = 20$ μm ($\omega = 500$ cm^{-1}), $\varepsilon \leqslant 0.2$ μm can be ignored.

The main computer program which has been developed (see listing in appendix) has facilities for handling both double and single-sided interferograms using the procedures outlined above. The second method[88] forms the basis for SUBROUTINE ERROR, but the distance off-centre ε is obtained by fitting a

polynomial to the three points either side of the maximum point and employing numerical differentiation.

2-6 Computation of Spectra

From eqn 2.14 the spectrum of a symmetric interferogram F(x) with apodization function A'(x) is obtained by performing the summation

$$S'(\omega_n) = \Delta x[F(0) + 2 \sum_{m=1}^{M} A'(x_m)\, F(x_m) \cos 2\pi\omega_n x_m] \qquad (2.31)$$

An "amplitude" Fourier transform of a double-sided interferogram is obtained from

$$P(\omega_n) = F(0) + \sum_{m=1}^{M} [A'(x_m)F(x_m) + A'(-x_m)F(-x_m)]\cos 2\pi\omega_n x_m \qquad (2.32a)$$

$$Q(\omega_n) = \sum_{m=1}^{M} [A'(x_m)F(x_m) - A'(-x_m)F(-x_m)]\sin 2\pi\omega_n x_n \qquad (2.32b)$$

$$S'(\omega_n) = \Delta x\sqrt{P^2(\omega_n) + Q^2(\omega_n)} \qquad (2.32c)$$

The simplest (and slowest) way of evaluating these equations is the direct sum method, involving M multiplications and finding M cosines in eqn (2.31) for each spectral point. To speed up the calculation of the cosines and sines Connes[78] proposed the use of the Chebyshev recursion formulae:

$$\cos(p+1)x = 2\cos x \cos px - \cos(p-1)x \qquad (2.33a)$$

$$\sin(p+1)x = 2\cos x \sin px - \sin(p-1)x \qquad (2.33b)$$

A further reduction in computer time is obtained by using Watt's method[89,90] employing the recursion relation

$$t_n = 0$$

$$t_{n-1} = y_{n-1} \tag{2.34}$$

$$t_r = 2t_{r+1}\cos\theta - t_{r+2} + y_r$$

so that

$$t_0 - t_1\cos\theta = \sum_{r=0}^{n-1} y_r \cos r\theta \tag{2.35a}$$

$$t_1\sin\theta = \sum_{r=0}^{n-1} y_r \sin r\theta \tag{2.35b}$$

For these methods, the computation time is proportional to NM.

A recent development has been the fast Fourier transform [91,92] based on the Cooley-Tukey algorithm. This method has a computation time proportional to N log M so that a vast improvement is obtained over the times of the conventional methods, especially for large values of M and N. However, it has certain disadvantages arising from the requirement $M = N = 2^p$, (p an integer). In Fourier spectroscopy this means that the resolution and frequency interval will not be simple numbers and the spectrum is calculated over a wider frequency range than is normally required so that editing may be necessary. Also significantly greater computer memory is required.

The computer program uses Watt's method to evaluate eqns (2.31), (2.32a) and (2.32b). (See appendix for the listings of SUBROUTINE COSINE and SUBROUTINE COMP). With spectra of moderate to low resolution there is little advantage in using the fast Fourier transform because the computer time for execution of the program is determined more by the time involved in reading the interferogram off paper tape, plotting the spectrum and producing punched card output of the spectrum.

Fig (3.1) External view of the Grubb-Parsons IS3 Spectrometer and the cryostat.

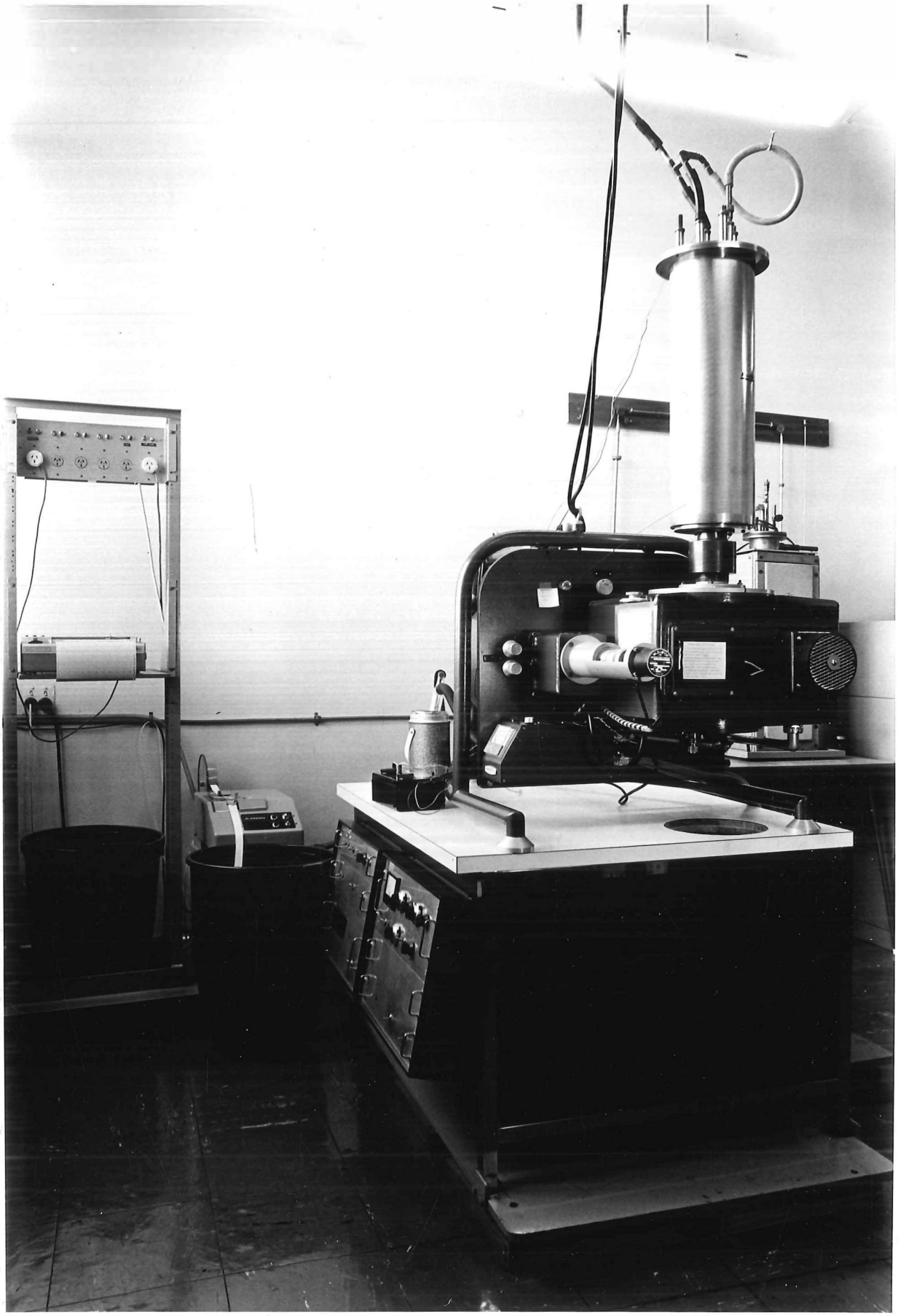

CHAPTER 3

EXPERIMENTAL DETAILS

A. THE FOURIER TRANSFORM SPECTROMETER

The spectrometer which was used in this work was a Grubb-Parsons IS3 interferometer which relies on a Michelson system for its operation (fig. 3.1). Several modifications have been made to the basic instrument to improve its usefulness for solid state spectroscopy in the far infrared.

3-1 Optical Unit (fig. 3.2)

(i) The bulkhead, which is rigidly attached to a tubular frame forms the constructional basis of the instrument and separates the sampling region from the analyzing and detecting region.

(ii) The sample chamber contains a high pressure mercury lamp (1) cooled by conduction, a chopper and reference generator system (2), a pair of scatter plates (3) and (4), and primary (5) and secondary (6) focussing mirrors. The chopper motor rotates a vane which interrupts the energy at $16\frac{2}{3}$ Hz, and is also coupled to a generator which produces a reference signal for the lock-in amplifier. At the centre of this chamber (7) where the radiation is brought to a focus, the sample is mounted either in a sample holder or at the tip of a cryostat (see section 3-5). The radiation passes through to the main chamber via a radiation port (8) which normally contains a high density polythene window of 5.5 mm thickness.

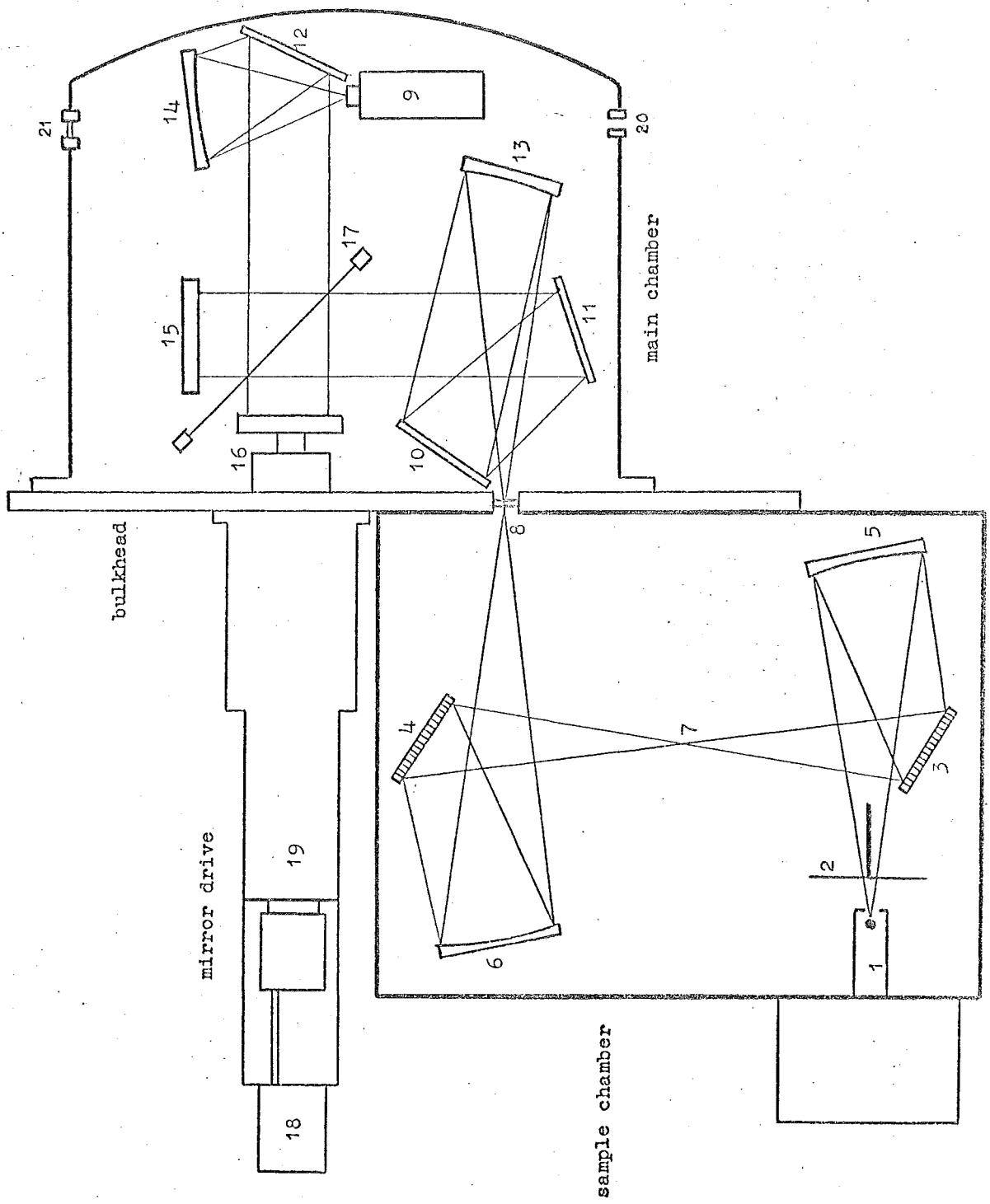

Fig (3.2) Grubb-Parsons IS3 Spectrometer - Optical unit.

(iii) The main chamber houses the Michelson system and Golay detector (9) together with the associated optics consisting of plane beam-deflecting mirrors (10,11,12), a primary collimator mirror (13) and a focussing mirror (14). The Michelson system comprises a static mirror (15), a mobile mirror (16) and a mylar beam-splitter (17). Beam-splitters of five different thicknesses are supplied (3.75 μm, 6.25 μm, 12.5 μm, 25 μm, 50 μm). (See fig. 2.1b for their characteristics.) Two extra ports have been made in the wall of the main chamber. One (20) is to provide access for a lightpipe coupled to a bolometer system. The other (21) contains a viewing window to enable the radiation beam to be aligned while the main chamber is closed.

(iv) In the mirror drive assembly a stepping motor (18) with 200 steps per revolution drives the mobile mirror a distance of 2.5 μm per pulse via an accurate micrometer thread (19). The normal resolution setting enables double or single-sided interferograms of up to 0.2 cm^{-1} resolution to be obtained, and by relocating the mirror sufficient mirror travel for 0.1 cm^{-1} single-sided interferograms is available.

3-2 Electronics System (fig. 3.3)

The signal from the Golay detector is amplified by a $16\frac{2}{3}$ Hz lock-in amplifier and is fed via a digital voltmeter to an encoder unit whose output is coupled to an Addo paper tape punch. The amplifier comprises a phase sensitive detection system with an associated phase shifter. Time constants of ½, 1, 2 and 4 seconds are available, and additional values of 8 secs and 30 secs have been added for use when obtaining noisy interferograms from highly absorbing samples. The latter value

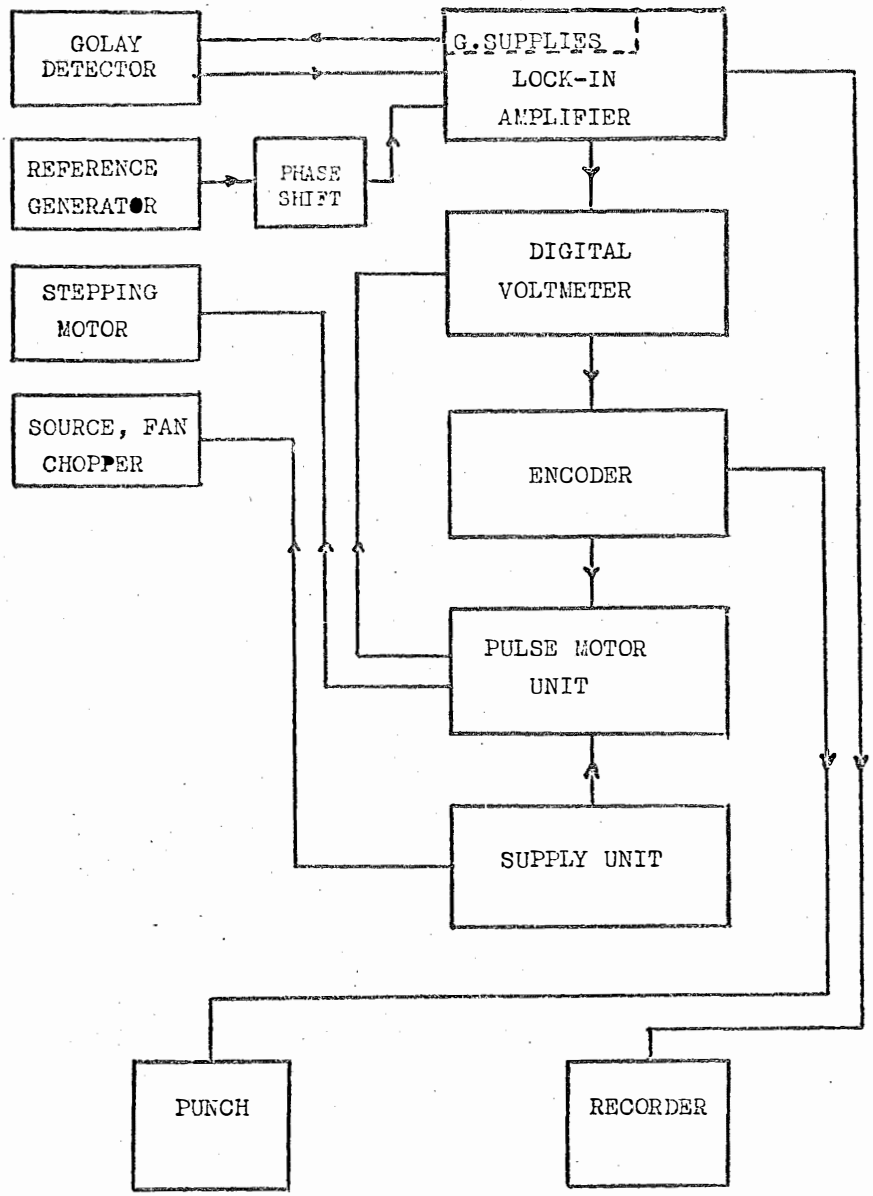

Fig (3.3) Grubb-Parsons IS3 Spectrometer - Electronics system.

necessitates using the manual sampling technique which is mentioned in section 2-4.

Pulse intervals of ½, 1, 2, 4 and 8 seconds are available. Each pulse causes the stepping motor to advance the mirror 2.5 μm, producing a path difference change $\Delta x = 5$ μm. This sets a limit ω_{max} on the range of frequencies over which the spectrum can be calculated:

$$\omega_{max} = \frac{1}{2\Delta x} = 1000 \text{ cm}^{-1}.$$

This value is much higher than required.

A modification to the pulse motor unit made it possible to feed a pair of pulses to the motor for every single pulse which is sent to the digital voltmeter. This produces a sampling interval of 10 μm ($\omega_{max} = 500$ cm^{-1}). Further improvements will make it possible to feed up to 10 closely-spaced pulses to the motor, enabling sampling intervals up to 50 μm ($\omega_{max} = 100$ cm^{-1}) to be obtained.

The pulse shift control for the reference signal was shifted from a rather inaccessible position within the electronics console to position on the instrument control panel to allow for ease of realignment when a different chopper system is substituted for the present one.

3-3 Filtration

In section 2-4 it was pointed out that in order to avoid ambiguities arising from spectral overlap, adequate filtration of the radiation is necessary. To this end, the Grubb-Parsons interferometer has several forms of filtration in its optical system.

Direct ultraviolet radiation from the mercury source damages polythene and may damage certain samples. For this reason scatter plates producing appreciable scattering above 500 cm^{-1} are mounted in the sample chamber.

The polythene window transmits nonselectively from 10-500 cm^{-1} (apart from a narrow band close to 70 cm^{-1}) with a cut-off at about 680 cm^{-1}. It transmits again in the near infrared.

The Golay cells which were supplied have both diamond and crystalline quartz windows. Quartz cuts off sharply at 250 cm^{-1} so for work in the 250-500 cm^{-1} region the diamond window Golay cell must be used. A further precaution is to cover the Golay window with black polythene film which acts as a blocking filter for near infrared and visible.

In operating the interferometer manually with a sampling interval of say 40 μm (ω_{max} = 125 cm^{-1}) the filtering out of frequencies above 125 cm^{-1} is usually done by the sample itself particularly if thick samples of calcium fluoride doped with lanthanide ions are being investigated.

3-4 Vacuum System

Atmospheric water vapour is highly absorbing in the far infrared. For this reason the sample chamber and main chamber are evacuated while the interferometer is in operation.

A Genevac rotary pump with a displacement of 224 litres per minute was supplied with the interferometer, but extremely strong vibrations produced by this pump necessitated its replacement by a quieter Speedivac model ES200.

Low temperature work made it essential for a diffusion pump to be incorporated in the vacuum system. Although a 1 inch oil diffusion pump was found to be adequate, a 4 inch Edwards pump with a liquid air cold trap in the pumping line was used for most of the work.

3-5 Cryostat

In order to begin low temperature studies with the minimum amount of modification to the system, a liquid nitrogen/liquid helium cryostat requiring no windows was designed and constructed in the Physics Department's workshop. The construction of the tail section of the cryostat is shown in fig. 3.4 while an external view of the upper section which contains the liquid nitrogen and liquid helium cans is shown in fig. 3.1.

A hollow copper tube (1) extends from the inner can down to a copper block (2) which is surrounded by a radiation shield (3) during operation. The sample (4) is attached using "Frigilene" to a copper holder (5) which is clamped to its "twin" (6) in the copper block by a phosphor-bronze clip (7). A narrow tube (8) passes through the copper block enabling a continuous flow of liquid to cool the sample effectively.

The whole cryostat can be raised or lowered by means of an elevation mechanism (9) or rotated about its central axis. A plate (10) covers the large port in the top of the interferometer sample chamber, where an O ring ensures a good vacuum seal. The vacuum jacket of the cryostat, and the sample space is open to the chamber, so to avoid condensation on the sample, an efficient vacuum system is necessary, (see section 3-4).

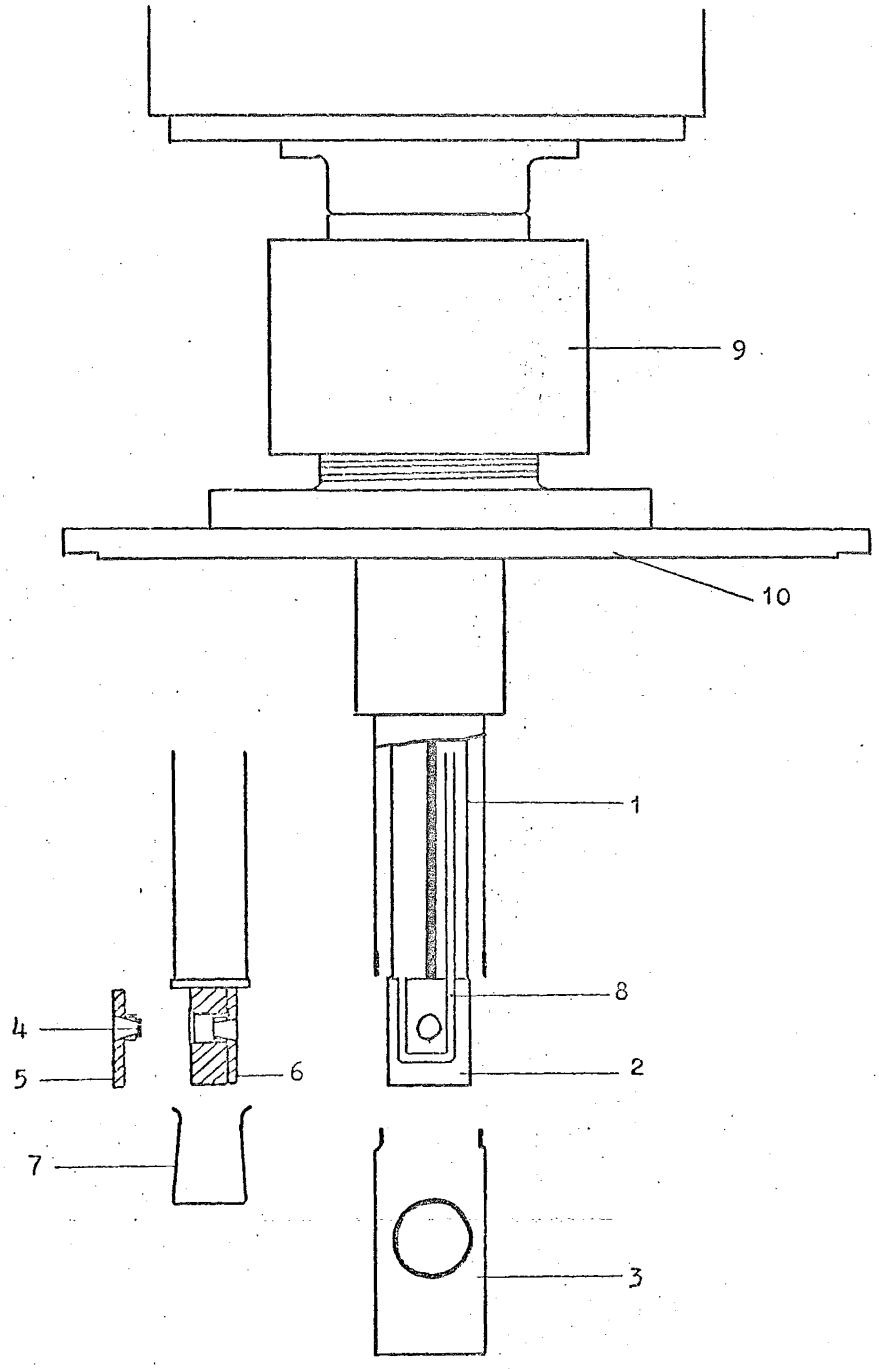

Fig. 3.4 Tail section of cryostat.

Temperatures were measured using a copper-constantan thermocouple with the reference junction at the bath temperature. The other junction was soldered into a hole in the sample holder using Wood's metal. Temperatures measured were 85°K with liquid nitrogen and 15°K with liquid helium. (These figures have an uncertainty of about ±3°K.) It is expected that radiation would raise the sample temperature by a few degrees above these values, but since the phenomena being studied were not strongly temperature dependent, more accurate determination of the sample temperature was not considered necessary.

The system proved to be quite efficient as regards usage of liquid helium. Only 5 litres of liquid helium was necessary to cool down the inner can and give 4-5 hours running time. However, in spite of its efficiency and simplicity of operation several drawbacks limit the usefulness of this cryostat arrangement.

(i) Its low temperature capability is limited. The sample, holder and block are near the mercury lamp as well as being exposed to the space of the sample chamber so that the likelihood of obtaining sample temperatures below 15°K is very improbable.

(ii) The small aperture of the sample holder (5 mm dia.) causes about 70% of the available radiation to be lost, and this is a shame in the far infrared. Nevertheless, it does enable extremely thin samples to be studied as single crystals.

(iii) Only one sample can be studied during one run. To change samples involves warming the cryostat up to room temperature before releasing the vacuum. Consequently, if liquid helium is being used it is possible to run only one

sample per day.

(iv) Flexing in the cryostat, arising from temperature changes, causes displacement of the copper block relative to the radiation beam, results in drifts and step functions in the interferogram. Slow drifts in interferograms introduce increased noise in spectra at very low frequencies and alter line shapes to a small extent at higher frequencies, while step functions contribute to the noise at all frequencies. (Noise spikes and steps are more of a problem than drift in FTS, in direct contrast to grating spectroscopy.) These problems make the recording of low temperature spectra at a resolution better than 0.5 cm^{-1} rather futile unless the samples are highly transmitting.

3-6 The Germanium Bolometer

In order to obtain measurements at lower temperatures and to study several samples during one run, a liquid helium-cooled germanium bolometer system was constructed and coupled to the spectrometer by means of a light-pipe leading from the main chamber of the optical unit. Unfortunately the germanium elements did not have the optimum concentration of gallium impurities, resulting in a poor sensitivity. Another problem was in directing sufficient radiation down the light-pipe. For these reasons, the germanium bolometer was not used to obtain any of the results for this work.

B. DATA PROCESSING

3-7 Obtaining the Spectrum

The output from the Grubb-Parsons interferometer is an interferogram on paper tape, each data point being represented by four binary-coded decimal digits. A FORTRAN program has been developed which is compatible with the University of Canterbury IBM 360/44 computer (see appendix for listing). This program has procedures for reading the tape, performing apodization and symmetrization of the interferogram and converting it to a transmittance spectrum in the wave number domain (fig. 3.5a) (see Chapter 2). The output spectrum is plotted by the lineprinter as a series of points on an arbitrary transmittance scale, as well as being produced on punched cards. Two features of the program are worth mentioning at this stage.

(1) Either single or double sided interferograms are accepted, each type receiving somewhat different treatments. Double-sided interferograms require no symmetrization so that in checking that the interferogram contains sufficient data points both sides of the central maximum, only the resolution required must be taken into account. The symmetrization of a single-sided interferogram requires three points before the central maximum to enable the zero error to be calculated (see section 2-5). The next step, a convolution procedure requires that there be a "margin" at both ends of the interferogram. The result is that single-sided interferograms must have a margin of 50 points before the central maximum, and 20 points after the central maximum in addition to the number of points determined by the required resolution.

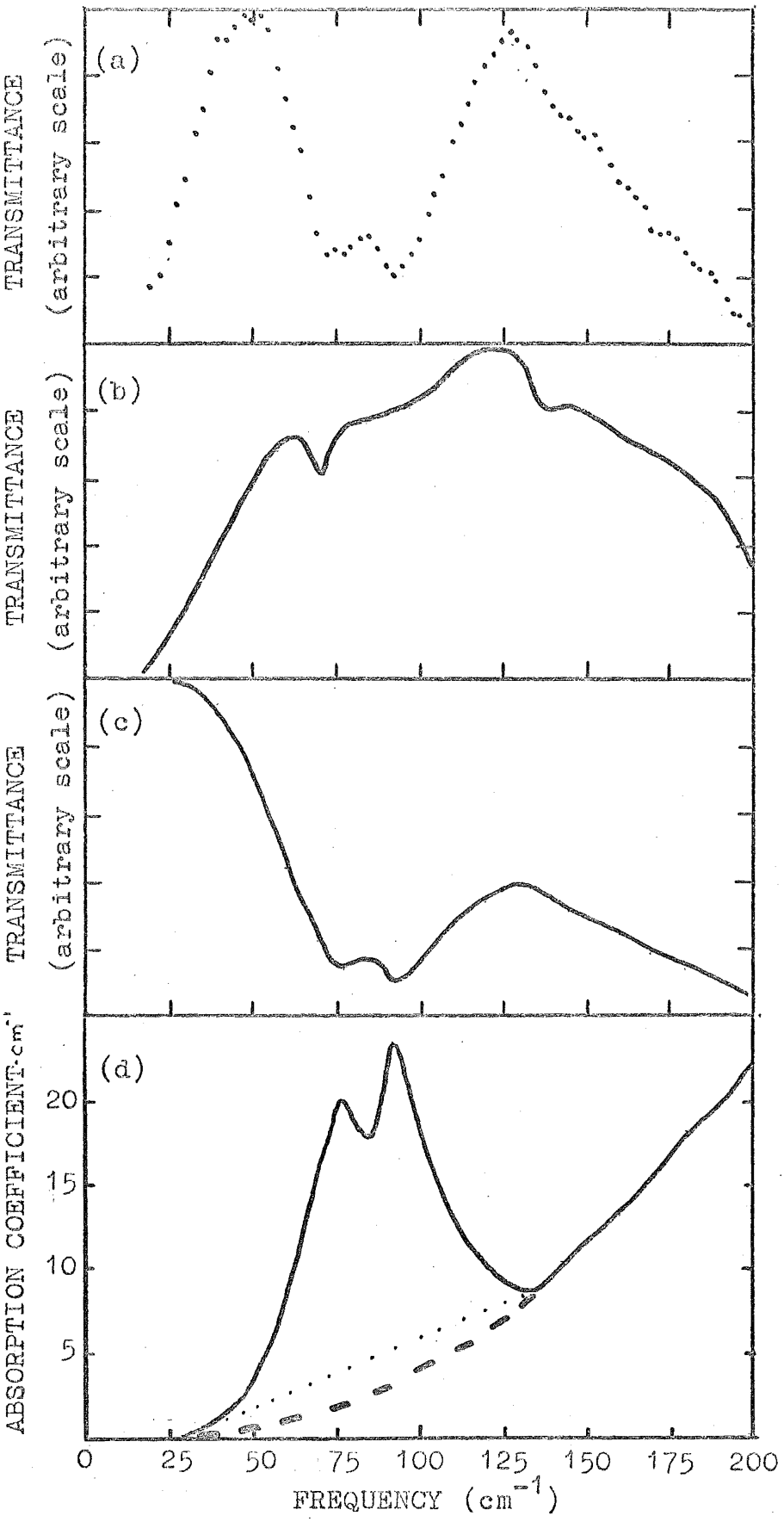

Fig (3.5) Steps in processing the spectra.
(a) "Raw" spectrum of CaF_2 - 0.3% Lu (0.95mm) at 15°K.
(b) Spectrum of CaF_2 (0.95mm) at 15°K (averaged).
(c) Ratioed spectrum in transmittance.
(d) Absorption spectrum.

(2) Three apodization functions are available as well as the choice of no apodization:

(i) Linear - $A_1(x) = 1 - \frac{x}{x_{max}}$

(ii) Quadratic - $A_2(x) = (1 - \frac{x^2}{x_{max}^2})^2$

(iii) Cosine - $A_3(x) = 1 + \cos(\pi \frac{x}{x_{max}})$.

As mentioned in section (2-3), apodization reduces the side-lobe level at the expense of resolution and signal noise. Since different functions do this to varying extents, the choice of apodization function depends on which feature one wishes to optimise.

This work has mainly involved the study of reasonably broad spectral features at moderate resolution (1-5 cm^{-1}). In this situation the choice of apodization function is not critical and in all the work we have settled for single-sided interferograms and linear apodization.

3-8 Production of Ratioed Spectra

In a conventional spectrometer, a double-beam system is usually employed which permits a direct ratio of the instrument background spectrum and the sample spectrum to be obtained, thus eliminating the influence of the spectrometer on the sample spectrum. In an interferometer this is not possible because the ratio of two functions does not go over under a Fourier transformation to the ratio of the transformed functions.

If a spectrum is required which is not influenced by the transmittance of the interferometer, the "raw" spectrum produced by the Fourier transform program must be ratioed point-for-point with the background spectrum of the instrument.

In the investigation of the influence of impurities on the far infrared spectra of crystals, the background spectrum is usually that of the pure host crystal of the same thickness and temperature as the perturbed crystal under examination (fig. 3.5b). The resulting spectra shows the enhancement of absorption brought about by the presence of the impurity.

A second computer program RUTB has been developed to accept as input the punched card output from the Fourier transform program (see appendix for listing). Up to five background spectra and five sample spectra are averaged to improve the signal-to-noise ratio and the results are ratioed (fig. 3.5c). If ratioing is attempted at points where the background spectrum is tending to zero (i.e. near beamsplitter cutoff or host crystal cutoff) spurious results are obtained which distort the resulting spectrum. Most of the spectra in this work have been computed between 20 and 240 cm^{-1} which are close to the 12.5 μm beamsplitter cutoff frequencies. It has been found convenient to delete several points at the extremities of the ratioed spectrum where the transmittance values are likely to be spurious. Another feature of the RUTB program is that any number of data points may be inserted between existing data points using a subroutine based on Newton's forward difference formula[93].

3-9 Conversion to Absorption Coefficient Scale

For purposes of comparison it is advantageous to convert a spectrum from a transmittance scale to an absorption coefficient scale. An extension to the RUTB program performs this conversion, the particular method depending on whether the spectrum is of a pure or doped crystal.

With pure crystals the conversion must take account of energy losses through reflection, and each data point in the transmittance spectrum is operated on by the following computational sequence[48,94]:

1. An approximate value of the reflectivity R is calculated by means of the formula

$$R = \frac{(n_0-1)^2}{(n_0+1)^2} \tag{3.1}$$

where n_0 is given in table 1.1.

2. A preliminary value of the absorption coefficient α is found from

$$S = \frac{(1-R)^2 e^{-\alpha d}}{1-R^2 e^{-2\alpha d}} \tag{3.2}$$

where d is the crystal thickness in centimetres

S is the transmittance value of a data point after ratioing.

3. The imaginary part of the refractive index is calculated using

$$k = \frac{\alpha\lambda}{4\pi} \tag{3.3}$$

in order to recompute R:

$$R = \frac{(n_0-1)^2 + k^2}{(n_0+1)^2 + k^2} \tag{3.4}$$

4. An improved value of α can then be calculated using eqn (3.2).

5. The real part of the refractive index n at a particular frequency ω is found from

$$n(\omega) = \sqrt{\frac{\varepsilon_0 \omega_{TO}^2 - \varepsilon_\infty \omega^2}{\omega_{TO}^2 - \omega^2}} \qquad (3.5)$$

the values of ε_0, ε_∞, and ω_{TO} being given in table 1.1.

6. Finally R is calculated using

$$R = \frac{(n-1)^2 + k^2}{(n+1)^2 + k^2} \qquad (3.6)$$

so that the final value of α for the data point can be found by using eqn (3.2) again.

The procedure for doped crystals is considerably simpler since we are only in the enhancement of absorption produced by the impurity. No account is taken of the enhancement of reflectivity since this is determined mainly by the real part of the refractive index. If radiation of intensity I_0 is incident on a crystal of thickness d and radiation of intensity I is transmitted through the crystal, then, where reflection losses are neglected, the absorption coefficient α is defined by

$$\frac{I}{I_0} = e^{-\alpha d} \qquad (3.7)$$

The corresponding expression relating the result of ratioing the spectrum of a doped crystal against the spectrum of the pure host crystal ($S'(\omega)/S(\omega)$) and the enhancement of absorption by the impurity is

$$\frac{S'(\omega)}{S(\omega)} = e^{-\alpha(\omega)d} \qquad (3.8)$$

It is necessary to set the maximum value of S'/S in the frequency range under consideration to unity so that the minimum value of α is zero. If the true maximum value of S'/S

lies outside the frequency range (e.g. < 20 cm^{-1}), the values of α may be a little too low, particularly if α is changing rapidly with frequency. In general for the spectra studied, α tends to zero at zero frequency. The "starting point", which is usually at about 25 cm^{-1}, is close enough to zero frequency to ensure that the error introduced into the absorption coefficient is small.

The absorption spectrum (fig. 3.5d) is punched onto cards for use as input to a third program FUN (see appendix for listing).

3-10 Integrated Absorption Coefficient

Frequently, the enhancement of the absorption coefficient produced by an impurity in a crystal consists of an absorption line or band superimposed on a sloping baseline. In order to measure the strength of the absorption band, the program FUN constructs a straight baseline across the limits of the band (dotted line in fig. 3.5d) and calculates the integrated absorption coefficient which is represented by the area between the curve and the straight baseline. This area is calculated using the trapezoidal rule.[93] Apart from the obvious uncertainties in the integrated absorption strength introduced by the use of this rule, other uncertainties arise from the method of constructing the baseline if the absorption band is rather broad. The straight line is a necessary approximation because the true shape of the baseline cannot be determined with any accuracy. To take account of the curvature of the baseline, the approximate shape is estimated (dashed line in fig. 3.4d) and the area between the straight and curved baseline is calculated. This result is added to that

obtained from FUN, so that all estimates of the integrated absorption coefficient which are given in Chapter 5 take account of possible background curvature.

C. SAMPLE PREPARATION

Several boules of calcium fluoride with lanthanide ion concentrations of 1.0 atoms per cent were purchased from the Hebrew University of Jerusalem[95], to provide samples for preliminary investigations. The samples for further work were obtained from crystals of calcium, strontium and barium fluoride doped with lanthanide ions, which were grown in the Physics Department using the ADL Model MP crystal growing furnace. The temperature gradient (Bridgman-Stockbarger) technique was used where the crystals are grown from a melt containing both metal and lanthanide fluorides. The metal fluorides were all Optovac stock[96].

In most cases lead fluoride was added to the melt as a scavenger to produce F^- charge compensation (see section 1-6). Where O^{2-} compensation was desired, crystals were grown from the lanthanide oxide. Attempts were also made to produce Na^+ compensation by adding up to 5 atoms per cent to the melt. Lanthanide ion concentrations varied from 0.03 to 3.0 atoms per cent although 0.3 atoms per cent samples with a thickness of about 1 mm proved to be the most convenient.

Other impurities were added to the alkaline earth fluorides. These included the fluorides of yttrium, lithium, sodium, nickel, calcium, barium and strontium, with concentrations of 0.3 atoms per cent. Calcium fluoride crystals containing chlorine and oxygen were grown by adding

calcium chloride (1%) and calcium oxide (0.1%) respectively to the melt.

Calcium fluoride samples were cut from the boule using a diamond saw, and were then ground to the desired size and thickness by various grades of silicon carbide. (Polishing samples with tin oxide produced no change in spectra from just grinding with 800 grade silicon carbide.) Rather than cut strontium and barium fluoride crystals, it was easier to cleave them along (111) planes. In grinding, all samples were slightly wedged to eliminate multiple reflections which give rise to periodicities in far infrared spectra. This created some uncertainty in the measured value of sample thickness, typical variations being ±0.03 mm.

CHAPTER 4

RESONANCE MODES OF LANTHANIDE IONS IN CALCIUM FLUORIDE

4-1 Dynamics of a Crystal Lattice with Impurities[35,38]

Consider a crystal composed of N unit cells, each cell being a parallelpiped bounded by three co-planar vectors $\underline{a}_1$, $\underline{a}_2$, $\underline{a}_3$. The position of the ℓ^{th} unit cell is $\underline{r}(\ell)$ where $\underline{r}(\ell) = \ell_1\underline{a}_1 + \ell_2\underline{a}_2 + \ell_3\underline{a}_3$ (ℓ an integer), and if $\underline{r}(\kappa)$ is the position of the κ^{th} atom in a unit cell ($\kappa = 1,2,\ldots,s$) then the position vector of the κ^{th} atom in the ℓ^{th} unit cell is $\underline{r}(\ell\kappa) = \underline{r}(\ell) + \underline{r}(\kappa)$. Defining the displacement of atom $(\ell\kappa)$ from its equilibrium position as $\underline{u}(\ell\kappa) = \underline{r}\,(\ell\kappa) - r_0(\ell\kappa)$ then in the harmonic approximation the equations of motion of the perfect crystal can be written as

$$M_\kappa \ddot{u}_\alpha(\ell\kappa,t) = - \sum_{\ell'\kappa'\beta} \Phi^o_{\alpha\beta}(\ell\kappa,\ell'\kappa')u_\beta(\ell'\kappa',t) \qquad (4.1)$$

The cartesian axes are labelled by α,β; M_κ is the mass of the κ^{th} atom and the harmonic coefficient $\Phi^o_{\alpha\beta}(\ell\kappa,\ell'\kappa')$ is the force exerted in the α direction on the atom at $\underline{r}(\ell\kappa)$ when the atom at $\underline{r}(\ell'\kappa')$ is displaced a unit distance in the β direction. Assuming the time dependence $\underline{u}(\ell\kappa,t) = \underline{u}(\ell\kappa)\exp(i\omega t)$ we obtain

$$\sum_{\ell'\kappa'\beta} \{M_\kappa\omega^2\delta_{\ell\ell'}\delta_{\kappa\kappa'}\delta_{\alpha\beta} - \Phi^o_{\alpha\beta}(\ell\kappa,\ell'\kappa')\}u_\beta(\ell'\kappa') = 0$$

or $$\underline{\underline{L}}\,\underline{u} = 0 \qquad (4.2)$$

with the condition for nontrivial solutions $|\underline{\underline{L}}| = 0$.

The introduction of an impurity into a crystal destroys the translational symmetry, the crystal symmetry being reduced from a structure with N operations of the translation group to a structure that retains only the point symmetry around the defect with ~10 operations. The loss of periodic symmetry means that the crystal's normal modes of vibration are modified from the usual plane wave form and may be no longer specified by wave vector $\underline{k}$.

Instead the normal modes may be specified according to the irreducible representations of the appropriate point group, which are small in number compared with the N values of $\underline{k}$. A simplifying feature is that the defect is localized in a small region of the crystal.

Point defects such as impurities change the masses of some of the atoms as well as the force constants for their interactions with their surroundings so that the equations of motion become

$$\sum_{\ell'\kappa'\beta} \{M_{\ell\kappa}\omega^2\delta_{\ell\ell'}\delta_{\kappa\kappa'}\delta_{\alpha\beta} - \Phi_{\alpha\beta}(\ell\kappa,\ell'\kappa')\}u_\beta(\ell'\kappa') = 0$$

$$\text{or} \quad (\underline{\underline{L}} - \delta\underline{\underline{L}})\underline{u} = 0 \tag{4.3}$$

$$\text{where } \delta L_{\alpha\beta}(\ell\kappa,\ell'\kappa') = -\omega^2(M_{\ell\kappa}-M_\kappa)\delta_{\ell\ell'}\delta_{\kappa\kappa'}\delta_{\alpha\beta}$$

$$+ \{\Phi_{\alpha\beta}(\ell\kappa,\ell'\kappa') - \Phi^o_{\alpha\beta}(\ell\kappa,\ell'\kappa')\} \tag{4.4}$$

has 3n x 3n nonzero elements (n is the total number of lattice sites influenced by the impurity atom).

For the perfect harmonic crystal the classical Green's function is defined as the inverse of the dynamical matrix $\underline{\underline{L}}$[97]:

$$G_{\alpha\beta}(\ell\kappa,\ell'\kappa';\omega^2) = L^{-1}_{\alpha\beta}(\ell\kappa,\ell'\kappa')$$

$$= \frac{1}{N\sqrt{M_\kappa M_{\kappa'}}} \sum_{j\underline{k}} \frac{W_\alpha(\kappa,j\underline{k})W_\beta(\kappa,j\underline{k})}{\omega^2-\omega_j^2(\underline{k})} \exp[i\underline{k}.(\underline{r}(\ell\kappa) - \underline{r}(\ell'\kappa'))] \tag{4.5}$$

where $\omega_j(\underline{k})$ is the frequency of the normal vibrational mode of the crystal described by wave vector $\underline{k}$ and branch index j, while $\underline{W}(\kappa,j\underline{k})$ is the associated unit polarization vector. We can rewrite eqn (4.3) as

$$\underline{u} = \underline{\underline{G}}\ \delta\underline{\underline{L}}\ \underline{u} \tag{4.6}$$

Assuming that the impurity atom affects only a few of its neighbours, matrix partitioning techniques can be used to simplify the problem:

$$\delta\underline{\underline{L}} = \begin{pmatrix} \delta\underline{\underline{\ell}} & 0 \\ 0 & 0 \end{pmatrix} \tag{4.7a}$$

$$\underline{\underline{G}} = \begin{pmatrix} \underline{\underline{g}} & \underline{\underline{G}}_{12} \\ \underline{\underline{G}}_{21} & \underline{\underline{G}}_{22} \end{pmatrix} \tag{4.7b}$$

$$\underline{u} = \begin{pmatrix} \underline{u}_1 \\ \underline{u}_2 \end{pmatrix} \tag{4.7c}$$

and obtain the set of 3n equations

$$\underline{u}_1 = \underline{\underline{g}}\ \delta\underline{\underline{\ell}}\ \underline{u}, \tag{4.8}$$

The condition for nontrivial solutions is

$$|I - \underline{\underline{g}}\ \delta\underline{\underline{\ell}}| = 0. \tag{4.9}$$

The roots of eqn (4.9) are the normal mode frequencies which are perturbed by the presence of an impurity atom. The size of the matrix $\underline{\underline{g}}\delta\underline{\underline{\ell}}$ depends on the type of impurity and the host

crystal. For an impurity, whose mass and coupling constants differ from those of the atom which it replaces, in a body-centred cubic lattice n = 9 so that $\underline{\underline{g}}\ \delta\underline{\underline{\ell}}$ is a 27 x 27 matrix. However, the methods of group theory can be used to simplify the problem by diagonalizing the matrix into blocks corresponding to different irreducible representations of the appropriate point symmetry group[38]. Only the modes corresponding to an irreducible representation transforming according to a polar vector, can couple with electromagnetic radiation. For a substitutional impurity having O_h symmetry, only the normal modes which transform according to the irreducible representation A_{2u} are infrared active.

4-2 The Brout-Visscher Model

For an isotopic impurity in a cubic Brovais lattice, the secular equation which determines the lattice frequencies is[98]

$$D(\omega) = 1 + \frac{\Delta m}{mN} \sum_{\underline{k}} \frac{\omega^2}{\omega^2 - \omega^2(\underline{k})} = 0 \qquad (4.10)$$

where m+Δm is the impurity mass and the sum is over the N phonons of the perfect lattice. For $\frac{\Delta m}{m} >> 1$ a solution to eqn (4.10) is found which produces a resonance within the range of lattice frequencies[99]. This resonance mode occurs at a frequency ω_r:

$$\omega_r = \omega_D \left(\frac{m}{3\Delta m} \right)^{\frac{1}{2}} \qquad (4.11)$$

with a full width at half maximum Γ:

$$\Gamma = \frac{1}{6} \pi \left(\frac{m}{\Delta m}\right) \omega_D \qquad (4.12)$$

where ω_D is the Debye frequency of the crystal lattice (ω_D = 345 cm^{-1} is used here). Table (4.1) gives the frequencies and widths of resonance modes arising from lanthanide ion impurities in a cubic Bravais lattice of calcium ions.

Table 4.1

The Brout-Visscher Model

	ε	$\omega_r (cm^{-1})$	Γ (cm^{-1})	ω_r/Γ
Lanthanum	-2.47	123	66	1.86
Dysprosium	-3.06	111	58	1.91
Lutetium	-3.36	106	52	2.04
Uranium	-4.94	87	36	2.42

The mass difference parameter ε is given by

$$\varepsilon = 1 - \frac{M'}{M} \tag{4.13}$$

where M is the mass of the host crystal atoms and M' is the impurity mass.

This simple model predicts a shift of the resonance frequency to lower frequencies for heavy atoms, together with a reduction in the width of the mode. However, the changes in going from dysprosium to lutetium are small.

4-3 The Isotopic Impurity in Calcium Fluoride

In forming a realistic theoretical description of the influence of substitutional lanthanide ions on the lattice dynamics and far infrared absorption spectra of calcium fluoride it is necessary to consider a "defect subspace"

containing nine ions: the lanthanide impurity and its eight nearest-neighbour fluorine ions. The simplest case to consider is the isotopic impurity which occupies a calcium site of O_h symmetry. The impurity is assumed to have the same charge and coupling constants as the calcium ion which it replaces, so that the mass is the only parameter altered.

We will consider the impurity to be in the unit cell labelled $\ell = 0$ at a site on the calcium sublattice denoted by the index $\kappa = 1$. The defect matrix $\delta\underline{\underline{L}}$ has elements

$$\delta L_{\alpha\beta}(\ell\kappa,\ell'\kappa') = \varepsilon M_1\omega^2\delta_{\alpha\beta}\delta_{\ell 0}\delta_{\ell' 0}\delta_{\kappa 1}\delta_{\kappa' 1} \tag{4.14}$$

where

$$\varepsilon = 1 - \frac{M_1'}{M_1} \tag{4.15}$$

M_1 is the mass of the calcium ion and M_1' is that of the lanthanide impurity ion.

In the defect subspace, the elements of the matrix $\underline{\underline{g}}\ \delta\underline{\underline{\ell}}$ are

$$(\underline{\underline{g}}\ \delta\underline{\underline{\ell}})_{\ell\kappa\alpha,\ell'\kappa'\beta} = \delta_{\ell 0}\delta_{\ell' 0}\delta_{\kappa 1}\delta_{\kappa' 1}\varepsilon M_1\omega^2 G_{\alpha\beta}(01,01;\omega^2) \tag{4.16}$$

where the Green's function $G_{\alpha\beta}(01,01;\omega^2)$ is given by

$$G_{\alpha\beta}(01,01;\omega^2) = \frac{1}{NM_1}\sum_{j\underline{k}}\frac{W_\alpha(1,j\underline{k})W_\beta(1,j\underline{k})}{\omega^2 - \omega_j^2(\underline{k})} \tag{4.17}$$

Having O_h symmetry about the lattice point (01) means that $G_{\alpha\beta}(01,01;\omega^2)$ vanishes unless $\alpha = \beta$ and $G_{xx}(01,01;\omega^2) = G_{yy}(01,01,\omega^2) = G_{zz}(01,01;\omega^2)$ [38]. In the defect subspace, the matrices $\underline{\underline{g}}$ and $\underline{\underline{g}}\ \delta\underline{\underline{\ell}}$ simplify to

$$\underline{\underline{g}} = g\ \underline{\underline{I}} \tag{4.18a}$$

$$\underline{\underline{g}}\ \delta\underline{\underline{\ell}} = g\ \delta\ell\ \underline{\underline{I}} \tag{4.18b}$$

where $g = G_{xx}(0l,0l;\omega^2)$ (4.19a)

and $\delta\ell = \varepsilon M_l \omega^2$ (4.19b)

The Green's function for the perturbed crystal in the impurity subspace is given by[38]

$$\underline{\underline{\bar{g}}} = \underline{\underline{g}}\,(I - \underline{\underline{g}}\;\underline{\underline{\delta\ell}})^{-1} \tag{4.20}$$

Using the simplifications of eqn (4.18), eqn (4.20) becomes

$$\bar{g} = g(1 - g\;\delta\ell)^{-1} \tag{4.21a}$$

where $\underline{\underline{\bar{g}}} = \bar{g}\,I$ (4.21b)

Related to this matrix is the t-matrix defined by[34]

$$\underline{\underline{t}} = \underline{\underline{\delta\ell}}\,(I - \underline{\underline{g}}\;\underline{\underline{\delta\ell}})^{-1} \tag{4.22a}$$

which in this case simplifies to

$$t = \delta\ell\,(1 - g\;\delta\ell). \tag{4.22b}$$

The infrared absorption induced by impurities in a crystal lattice is given by[34]

$$\alpha(\omega) = \frac{(n_\infty^2+2)^2}{9n(\omega)}\,\frac{4\pi N e^{*2}}{c\,\mu\,V}\,\frac{\omega}{(\omega_{T0}^2 - \omega^2)^2}\,\mathrm{Im}\langle 0,T0_l|\underline{\underline{t}}(\omega^2-i0)|0,T0_l\rangle \tag{4.23}$$

where n_∞ = refractive index at high frequencies

$n(\omega)$ = refractive index at frequency ω

N = number of impurities in a unit volume

V = unit cell volume

μ = reduced mass of a unit cell

c = velocity of light

$|0,T0_l\rangle$ = eigenvector of the transverse optic phonon at zero wavevector, polarized in the l direction.

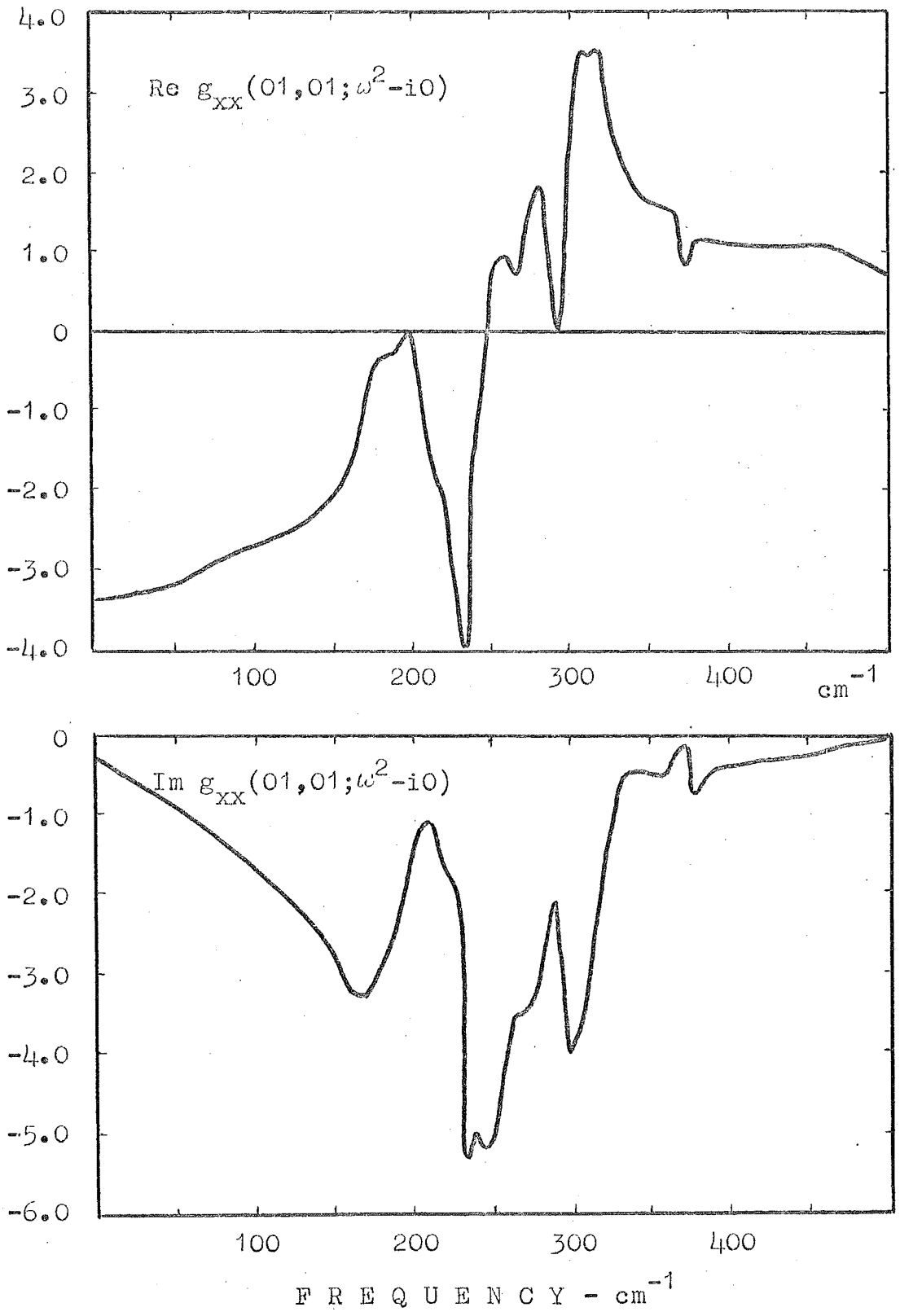

Fig (4.1) The real and imaginary parts of the Green's function $g_{xx}(01,01;\omega^2-i0)$ (49).

(The units are $1/m_F\omega^2_{max}$, where m_F is the fluorine mass and $\omega^2_{max} = 472$ cm^{-1}.)

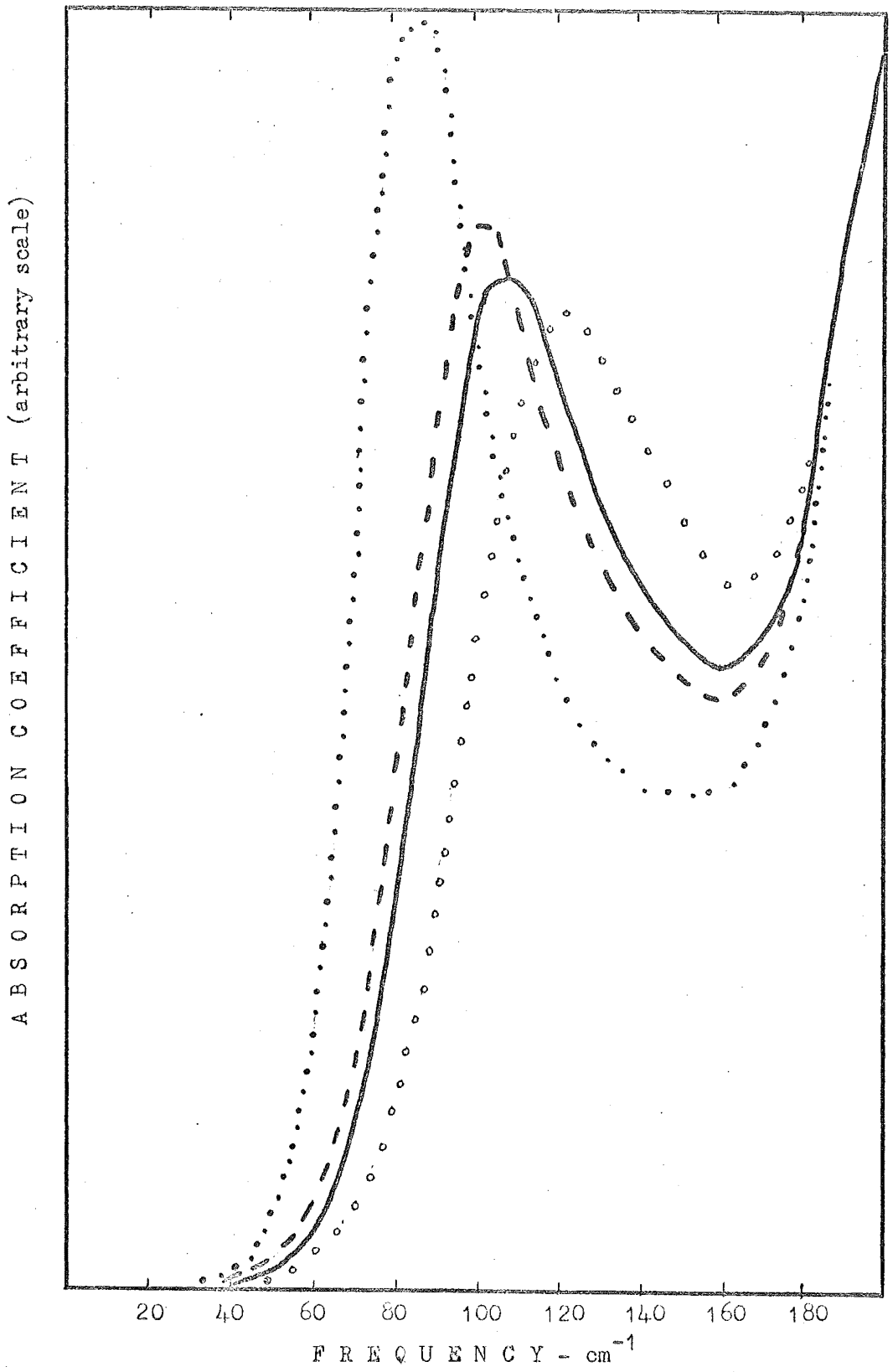

Fig (4.2) Absorption spectra arising from isotopic impurities in calcium fluoride.

Impurity mass:
- o o o o Lanthanum
- ——— Dysprosium
- – – – – Lutetium
- • • • • Uranium

For an isotopic impurity in calcium fluoride, the matrix element in eqn (4.23) simplifies thus:

$$\mathrm{Im}\langle T0_1,0|\underline{\underline{t}}(\omega^2-i0)|0,T0_1\rangle = \mathrm{Im}\ t(\omega^2-i0) = \frac{g_2(\omega^2)}{(1-g_1(\omega^2)\delta\ell)^2 + (g_2(\omega^2)\delta\ell)^2} \tag{4.24}$$

where $$g(\omega^2-i0) = g_1(\omega^2) + ig_2(\omega^2) \tag{4.25}$$

Lacina and Pershan[49] have calculated the Green's functions $g_{\alpha\beta}(\ell\kappa,\ell'\kappa';\omega^2-i0)$ for calcium fluoride using a rigid model of a harmonic fluorite lattice[100]. Their results for $g_{xx}(01,01;\omega^2-i0)$ are shown in fig. (4.1). These have been used to calculate the absorption spectrum arising from isotopic impurities in calcium fluoride, for several lanthanide masses (fig. 4.2). Since it is anticipated that the effective charge e* will deviate from the expected value, only the frequency-dependent factors of eqn (4.23) were computed so that the absorption coefficient scale is arbitrary. As expected, the results from the Brout-Visscher model compare more favourably at lower frequencies with these results. For lutetium and dysprosium an absorption band at about 100 cm^{-1} produced by a resonance mode of the impurity is predicted.

4-4 Force Constant Changes

The isotopic impurity model is rather unphysical for trivalent lanthanide ions in calcium fluoride because

(i) The lanthanide ion has a different charge and coupling constants from the calcium ion;

(ii) The lanthanide site symmetry may not be cubic;

(iii) Motion of the nearest-neighbour fluorine ions may

alter the lanthanide coupling constants.

A refinement of the isotopic impurity model attempts to take account of these factors. Because of the large mass difference between the calcium and lanthanide ions, the approximation is made that the vibration amplitude of the lanthanide ion at the resonance mode frequency is much greater than the vibration amplitude of the lighter F^- ions which surround it[101]. This enables us to use "effective force constants" in the x, y, z directions (see fig. 1.7) rather than the central and non-central force constants. A further simplification is that the motion of the lanthanide ion in a particular direction is affected only by the effective force constant in that direction.

The defect subspace is formed by the altered masses and force constants of the lattice. Therefore the matrix $\delta\underline{\ell}$ is of the form[101]

$$\delta\underline{\ell} = \begin{pmatrix} \Delta\Phi_{xx} + \varepsilon M_1\omega^2 & 0 & 0 \\ 0 & \Delta\Phi_{yy} + \varepsilon M_1\omega^2 & 0 \\ 0 & 0 & \Delta\Phi_{zz} + \varepsilon M_1\omega^2 \end{pmatrix} \qquad (4.26)$$

where $\Delta\Phi_{xx}$, $\Delta\Phi_{yy}$, $\Delta\Phi_{zz}$ are the effective force constant changes in the x, y and z directions respectively. For lanthanide sites of cubic symmetry $\Delta\Phi_{xx} = \Delta\Phi_{yy} = \Delta\Phi_{zz}$ while for sites of tetragonal symmetry (fig. 1.7) $\Delta\Phi_{xx} = \Delta\Phi_{yy} \neq \Delta\Phi_{zz}$. Since the motions in the three directions are uncoupled, the defect matrix $\delta\underline{\ell}$ simplifies to

$$\delta\ell = \Delta\Phi + \varepsilon M_1\omega^2 \qquad (4.27)$$

where $\Delta\Phi = \Delta\Phi_{xx}, \Delta\Phi_{yy}, \Delta\Phi_{zz}$.

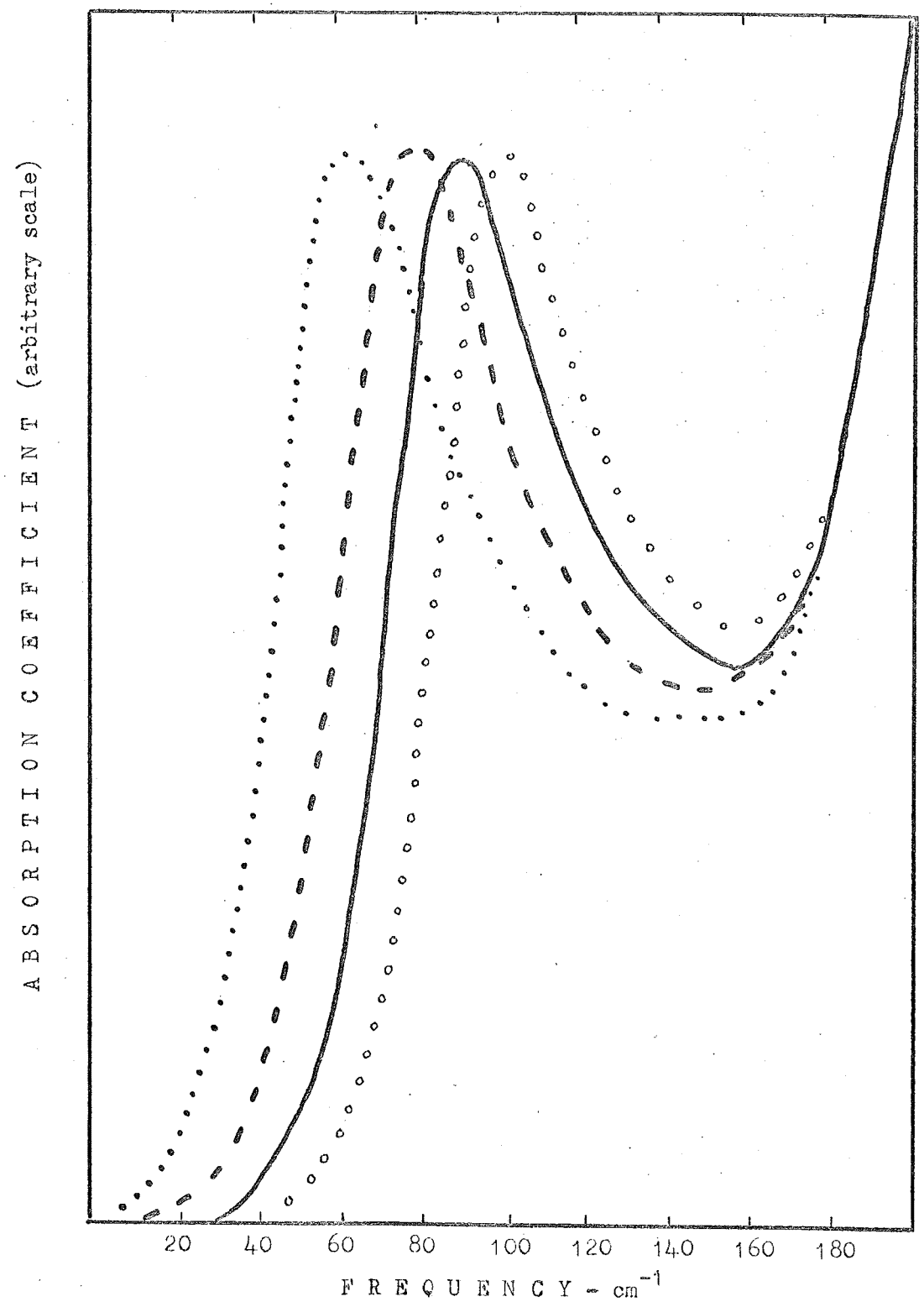

Fig (4.3) Absorption spectrum (calculated) arising from lutetium impurities in calcium fluoride, with reduced effective force constants.

Force constant: o o o o $\phi = \phi^{\circ}$ (isotopic impurity)

——— $\phi = 0.83\,\phi^{\circ}$

– – – – $\phi = 0.65\,\phi^{\circ}$

. . . . . $\phi = 0.48\,\phi^{\circ}$

Using the expression in eqn (4.22b), the method of section 4-3 has been used to calculate the absorption spectrum of calcium fluoride with lutetium impurities having reduced effective force constants (fig. (4.3)). It is estimated that for a resonance to occur in the region of 90 cm^{-1}, the force constants must soften by about 20% while for a resonance at 60 cm^{-1} a 50% reduction is necessary.

For a lanthanide ion at a cubic site, the force constant changes are identical in the x, y, z directions so that a triply-degenerate resonance mode will result. For a lanthanide ion at a tetragonal site, a different effective force constant in the x and y directions from that in the z direction will give rise to two resonance modes having single and double degeneracies. The absorption spectrum in this case will display two peaks, reflecting the superposition of the two modes.

While recognizing the limitations of this model, we feel that useful information is obtained about the weakening of coupling constants which must occur for a resonance mode of an impurity to occur at a frequency lower than the resonance mode frequency of an isotopic impurity.

CHAPTER 5

EXPERIMENTAL RESULTS

5-1 Far Infrared Spectra of Undoped Calcium, Strontium and Barium Fluorides

The absorption spectra of pure calcium fluoride were obtained at 15°K and 85°K for samples from three different sources (fig. (5.1))

(a) Optovac stock;

(b) Optovac stock regrown at Canterbury under same conditions as for doped crystals;

(c) boule obtained from Hebrew University of Jerusalem. In each case there is an enhancement of the absorption at the higher temperature for all frequencies, attributed to a two-phonon difference process by Bosomworth[48] (see section 1-5). There are significant differences in the spectra of the three samples particularly at 15°K. While sample (a) is virtually transparent to all frequencies up to 200 cm^{-1}, sample (b) is more highly absorbing over this range, particularly above 120 cm^{-1}. Presumably the differences must be attributed to strains and lattice defects produced by the growing process.

The absorption spectrum of sample (c) at 15°K shows two absorption bands centred at 100 cm^{-1} and 145 cm^{-1} with full widths at half-height of about 20 cm^{-1}. The stronger 145 cm^{-1} band is displayed by all the Hebrew University (Israeli) doped calcium fluoride crystals to about the same extent. Since this band occurs close to the peak in the phonon density of states (fig. 1.4) its rather narrow width precludes the possibility that a resonance mode of an impurity is involved.

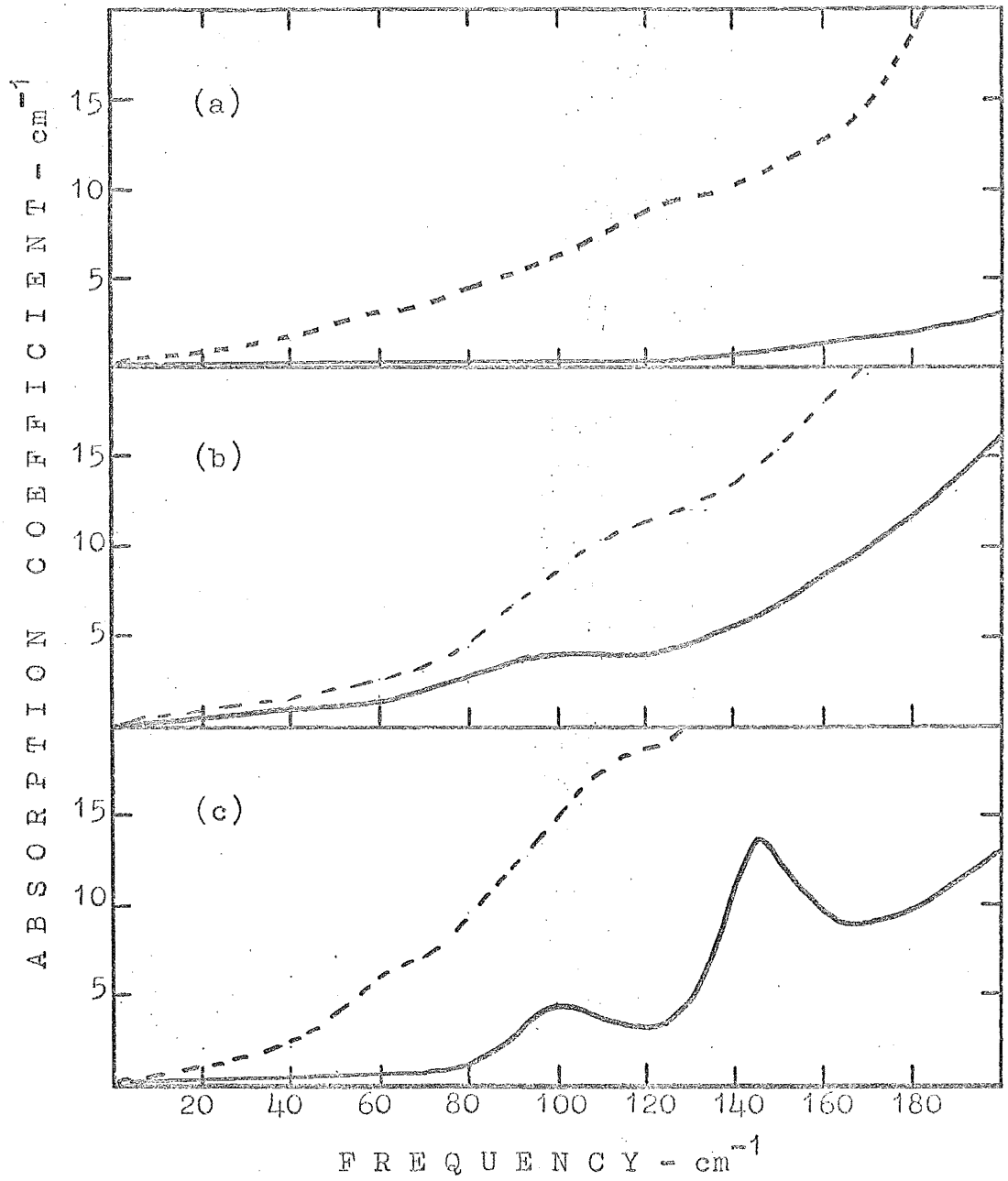

Fig (5.1a-c). The far infrared absorption spectra of calcium fluoride at 15°K (———) and 85°K (- - -).
(a) Optovac stock.
(b) Regrown Optovac stock.
(c) Israeli stock.

However, as mentioned in section 1-4 certain impurities in crystals can produce modifications to the absorption spectrum which reflects the density of states.

Since this structure is not observed for Optovac material nor in the results of Bosomworth[48] who used very pure calcium fluoride, extraneous impurities must either occur naturally in the Israeli material or be introduced by the crucible during growth. An analysis of B.D.H. extra pure grade CaF_2, the starting material for all Israeli crystals, has been supplied together with other major contaminants in similar grade CaF_2 (Merck, Suprapur) (see table 5.1). This table also presents the results of spectrographic analysis on Israeli nominally pure CaF_2 carried out by Chemistry Division, D.S.I.R. In this analysis impurities looked for, but not detected, included the lanthanides, alkali metals and many transition metals.

Table 5.1

Contaminants of calcium fluoride

BDH analysis[104]	ppm*	Other contaminants	ppm	Chem.Division analysis	ppm
Silicate	500	Barium	500	Strontium	1500
Sulphate	100	Strontium	100	Nickel	1500
Chlorine	50	Sodium	10	Magnesium	300
Iron	50	Lithium	5	Barium	150
Lead	50	Potassium	5	Aluminium	100

* ppm ≡ parts per million.

On the strength of these analyses, certain metal ions were added to calcium fluoride in the following nominal concentrations: 0.3% Ni^{2+}, 1% Ba^{2+}, 0.3% Y^{3+}, 2.0% Sr. (Yttrium was included because it has been reported to be a common contaminant of lanthanide-ion doped calcium fluoride[102].) Without exception, the spectra of these crystals at 85°K revealed no features corresponding to the 145 cm^{-1} band in nominally pure Israeli calcium fluoride. However, it was found that the introduction of certain negative ions into calcium fluoride produces some features of interest. The following calcium compounds were added to CaF_2 and grown: 0.1% CaO, 0.3% $CaCl_2$, 0.3% Ca_2SiO_3. All produced a rather narrow absorption band in the region 150-160 cm^{-1} (see fig. 5.2). The crystal which was supposed to contain silicate ions showed no evidence of this in its middle infrared spectra. Instead a sharp line at 956 cm^{-1} which seems to be due to the local mode of the hydride ion in calcium fluoride[103] was observed. In these systems it is not certain what ion is exciting the absorption band so close to the peak in the density of states, and this phenomenon warrants further investigation. The source of the extraneous absorption band which is present in Israeli calcium fluoride, but not in crystals grown at Canterbury from Optovac stock, has yet to be fully explained.

The absorption spectra of strontium and barium fluorides are shown in fig. (5.3). In comparing spectra (a) and (b) it is apparent that the growth process perturbs the crystal, producing an enhancement of absorption. The absorption spectra of barium fluoride at 85°K displays structure around 55 cm^{-1} corresponding to a peak in the two-phonon density of states[48].

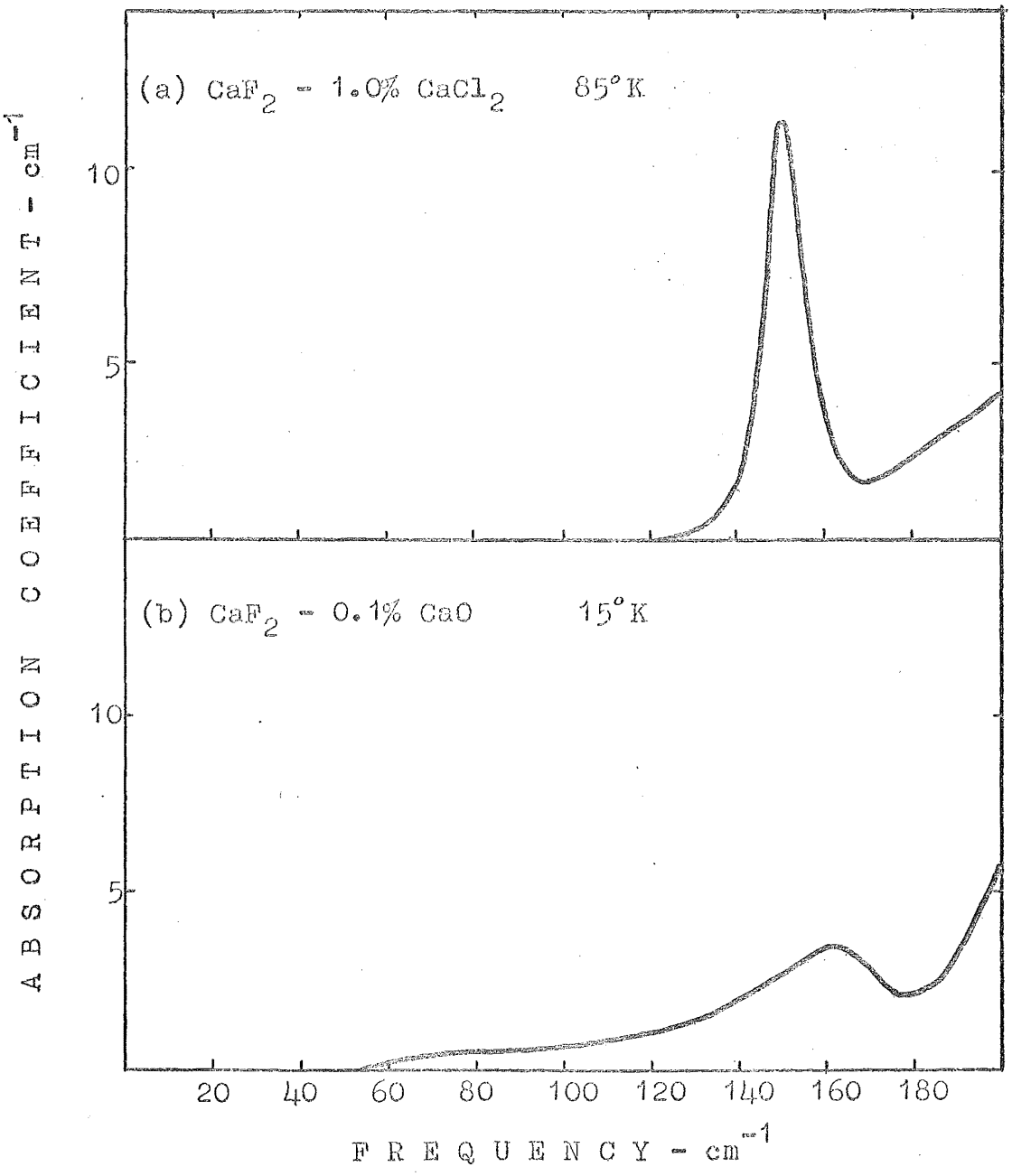

Fig (5.2). Far infrared absorption spectra of Cl^- and O^{2-} in calcium fluoride.

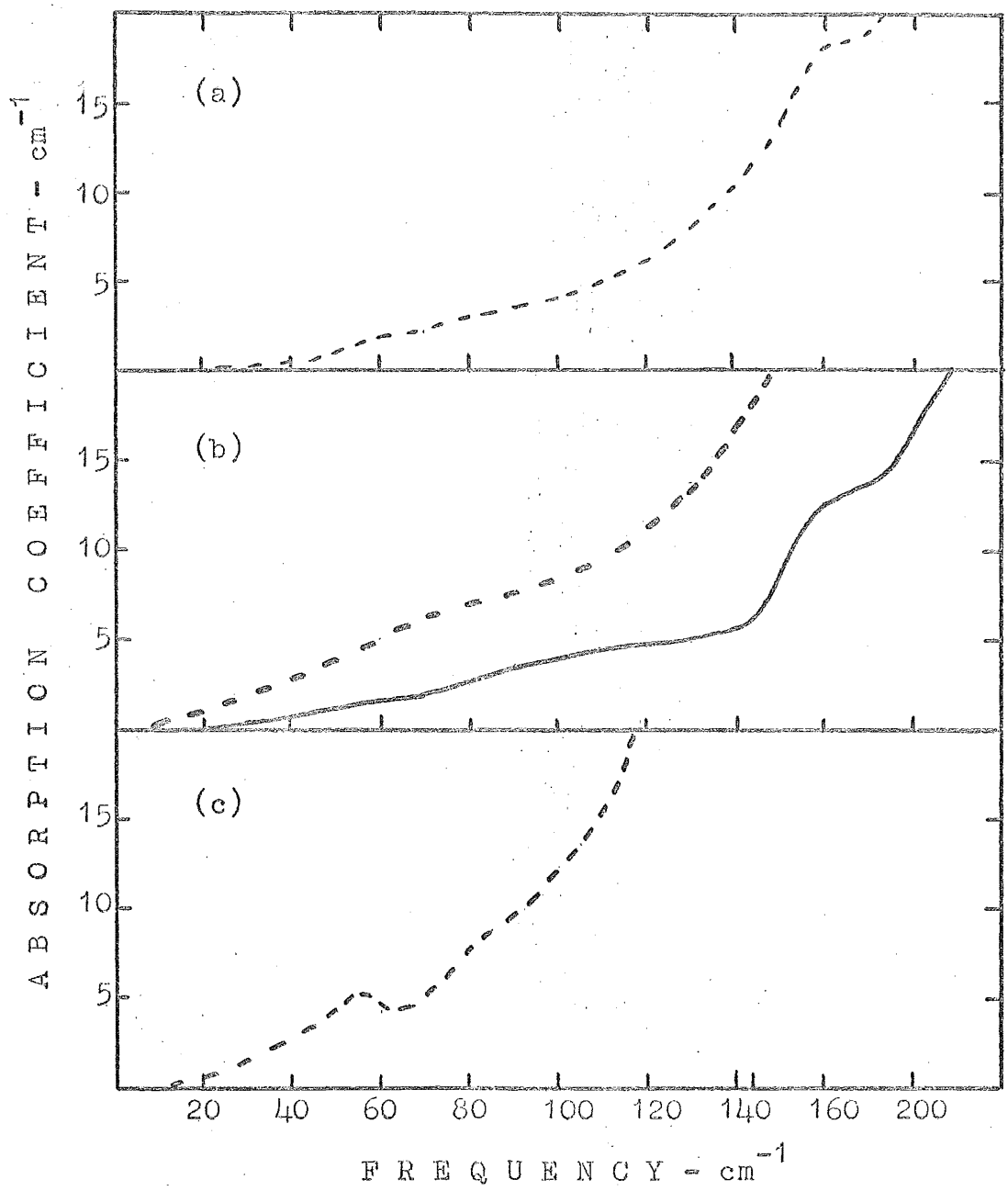

Fig (5.3 a-c) The far infrared absorption spectra of strontium and barium fluorides at 15°K (——) and 85°K (- - - -).
(a) Strontium fluoride (Optovac stock).
(b) Strontium fluoride (regrown Optovac stock).
(c) Barium fluoride (Optovac stock).

5-2 Far Infrared Absorption Spectra of Doped Calcium Fluoride

The far infrared spectra of most of the ions of the lanthanide series in calcium fluoride were obtained. The spectra of calcium fluoride doped with other impurities were also investigated. A complete list of the systems studied together with the sources of the crystals are listed in table 5.2.

All absorption spectra of the lanthanide ions in calcium fluoride were obtained at 15°K (fig. (5.4)) while some were also obtained at 85°K. (All spectra of doped crystals which are presented in this chapter have been ratioed against the spectrum of the pure host crystal so that a measure of the enhancement of absorption arising from the presence of the impurity is obtained.) Certain systems were investigated in some detail using samples from different sources or with varying impurity concentrations. The most thorough study was carried out on CaF_2-Lu and the results will be presented in later sections.

The features which are observed in the spectra, are of two types. The first type, which is characteristic of virtually all the spectra obtained, is the increase in the absorption level. This rises steadily with increasing frequency producing what will be termed a "background" absorption. Three possibilities may produce this effect:

1. A trivalent ion introduces a charge defect into the crystal, possibly giving rise to an absorption spectrum which approximately reflects the density of states.

2. The substitution of a lanthanide ion for a calcium ion introduces strains into the crystal which produce lattice defects (dislocations, vacancies, interstitials) having

TABLE 5.2

IMPURITY	CaF_2	SrF_2	BaF_2
Li^{+}	x C	x C	x C
O^{2-}	x C		
Na^{+}	x C	x C	x C
Cl^{-}	x C	x C	
Ca^{2+}		x C	x C
Sc^{3+}	x I		
Ni^{2+}	x C		
Sr^{2+}	x I		
Y^{3+}	x C	x C	x C
Ba^{2+}	x C		
La^{3+}	x I	x C	x C
Ce^{3+}	X I,C	x C	
Pr^{3+}	x I		
Nd^{3+}	x I	x C	
$Sm^{2+,3+}$	x C	x C	
Gd^{3+}	X J,C	X C	
Tb^{3+}	X I,C	x C	
Dy^{3+}	X I,J	x C	
Er^{3+}	X I,O	X C	x C
Ho^{3+}	x C	x C	
Tm^{3+}	x C	x C	
Yb^{3+}	x J		
Lu^{3+}	X C	x C	x C
$U^{3+,4+}$	x C	x C	x C

x - sample investigated (at 15°K and/or 85°K).

X - investigated in detail (two or more different samples at 15°K and/or 85°K).

Sources: C - grown at University of Canterbury

I - supplied by Hebrew University of Jerusalem

J - supplied by Dr G. D. Jones, University of Canterbury

O - supplied by Optovac Inc.

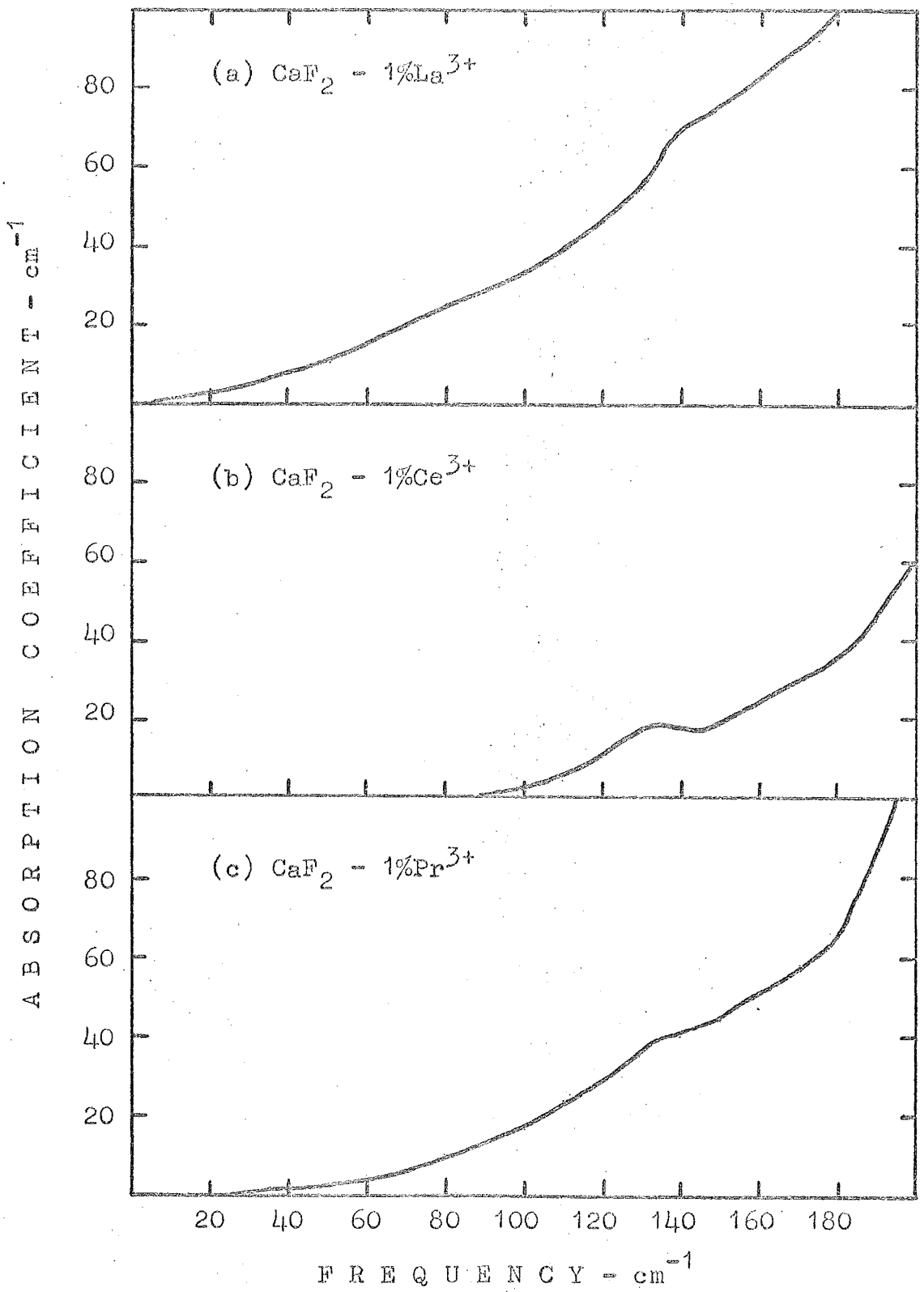

Fig (5.4 a-c). The far infrared absorption spectra of lanthanide ions in calcium fluoride at 15 K.

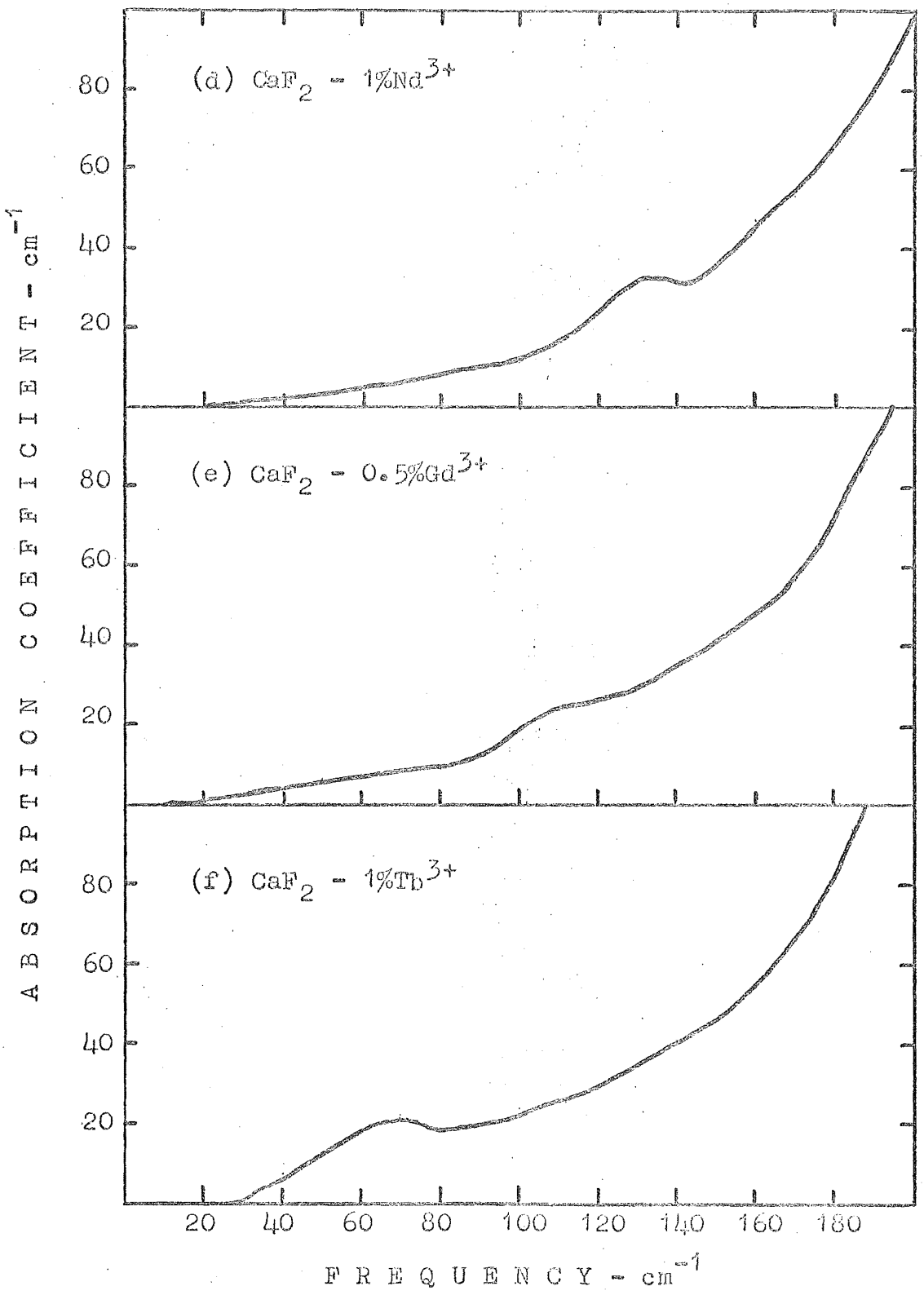

Fig (5.4 d-f). The far infrared absorption spectra of lanthanide ions in calcium fluoride at 15°K.

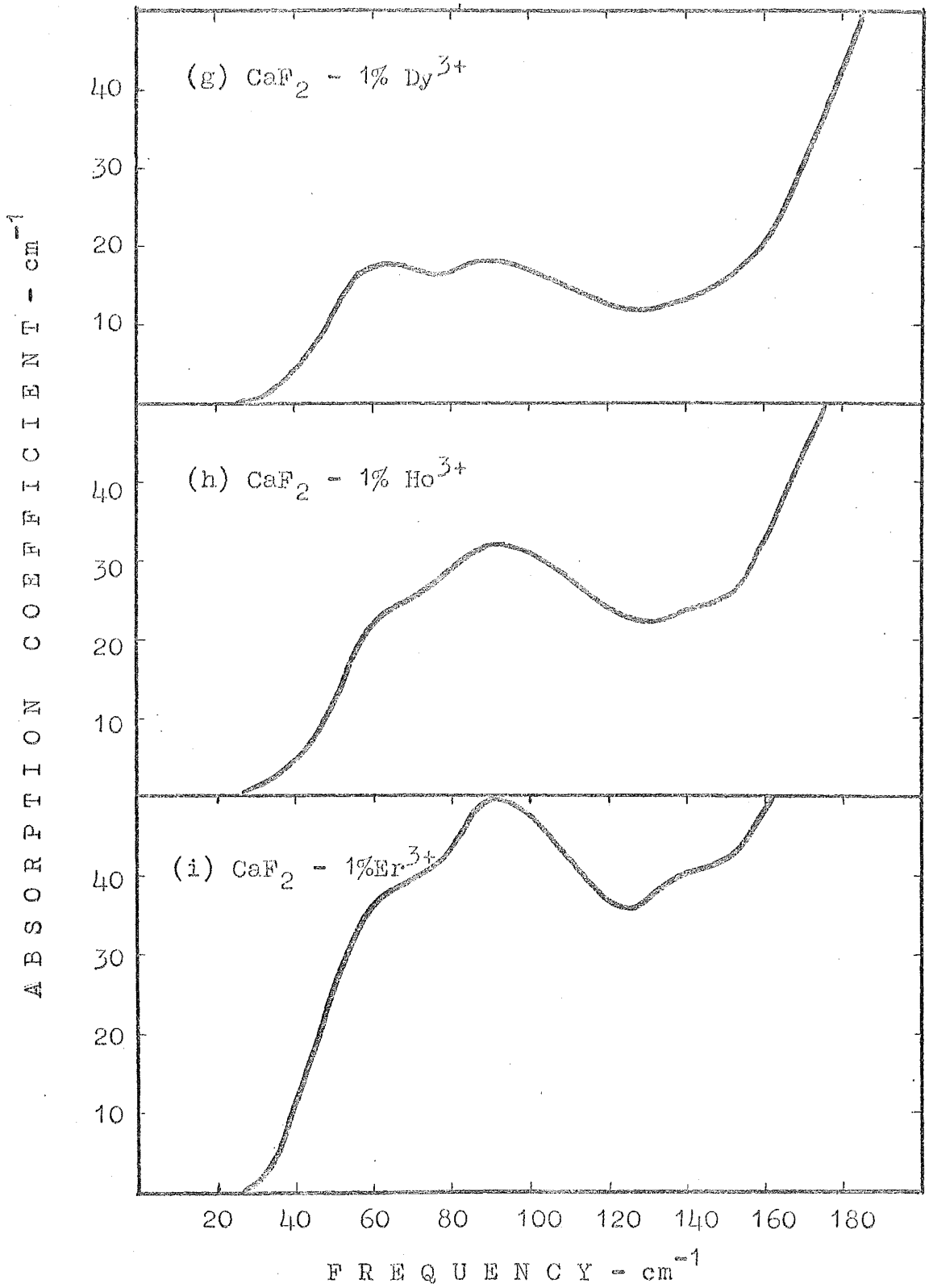

Fig (5.4 g-i). The far infrared absorption spectra of lanthanide ions in calcium fluoride at 15°K.

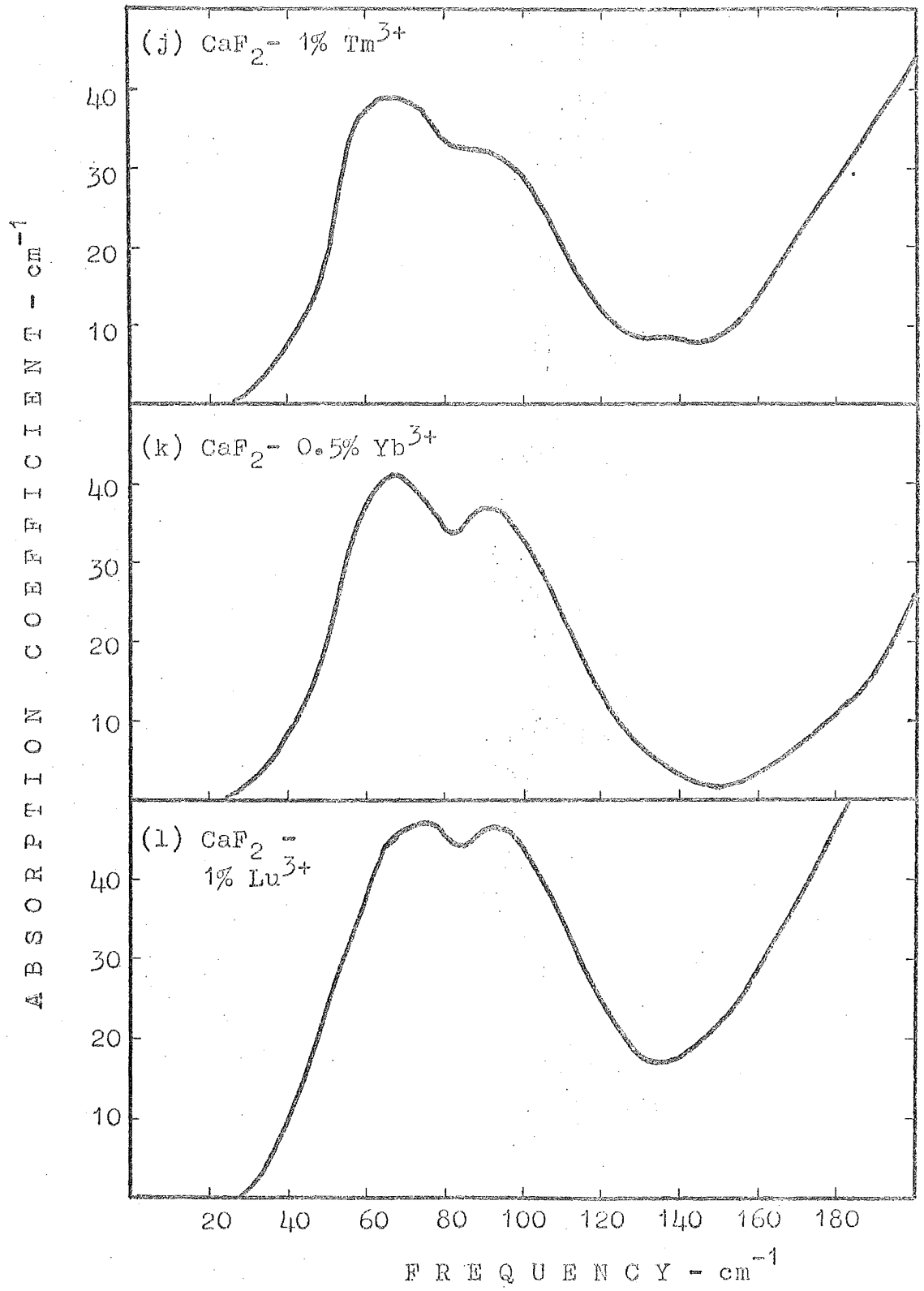

Fig (5.4j-l). The far infrared absorption spectra of lanthanide ions in calcium fluoride at 15°K.

infrared active modes.

3. Strains increase the anharmonicity of the crystal lattice with the result that more extensive multiphonon absorption is possible than for the unperturbed crystal. The background absorption shows little structure corresponding to the peaks in the density of states, increases with increasing temperature and depends to some extent on the origin (growth conditions) of the crystals, so that the third possibility is most likely. Annealing of doped crystals was not able to reduce the background absorption significantly. Some Israeli crystals, for example CaF_2 - 1% Ce and CaF_2 - 1% Nd exhibit weak structure around 135-140 cm^{-1} which means either that certain lanthanide ions enhance the absorption at this frequency or that the absorption which is present even in nominally pure Israeli calcium fluoride is somewhat variable in intensity from crystal to crystal.

The second, more significant feature is the structure in the 40-140 cm^{-1} region which appears with lanthanide ions in the latter half of the series. This structure first appears as a weak absorption band centred at 65 cm^{-1}. On proceeding along the series a second component centred at about 90 cm^{-1} becomes evident, the structure intensifies and becomes resolved into two clearly defined absorption bands. Fig. (5.5) shows the structure separated from the background absorption of the perturbed crystal. (These spectra are uncorrected for probable curvature of the background.) The integrated absorption coefficient S which is represented by the area under the absorption band spectrum is given in table 5.3 (corrected for background curvature) for 1.0% lanthanide ion impurities in calcium fluoride, along with the central

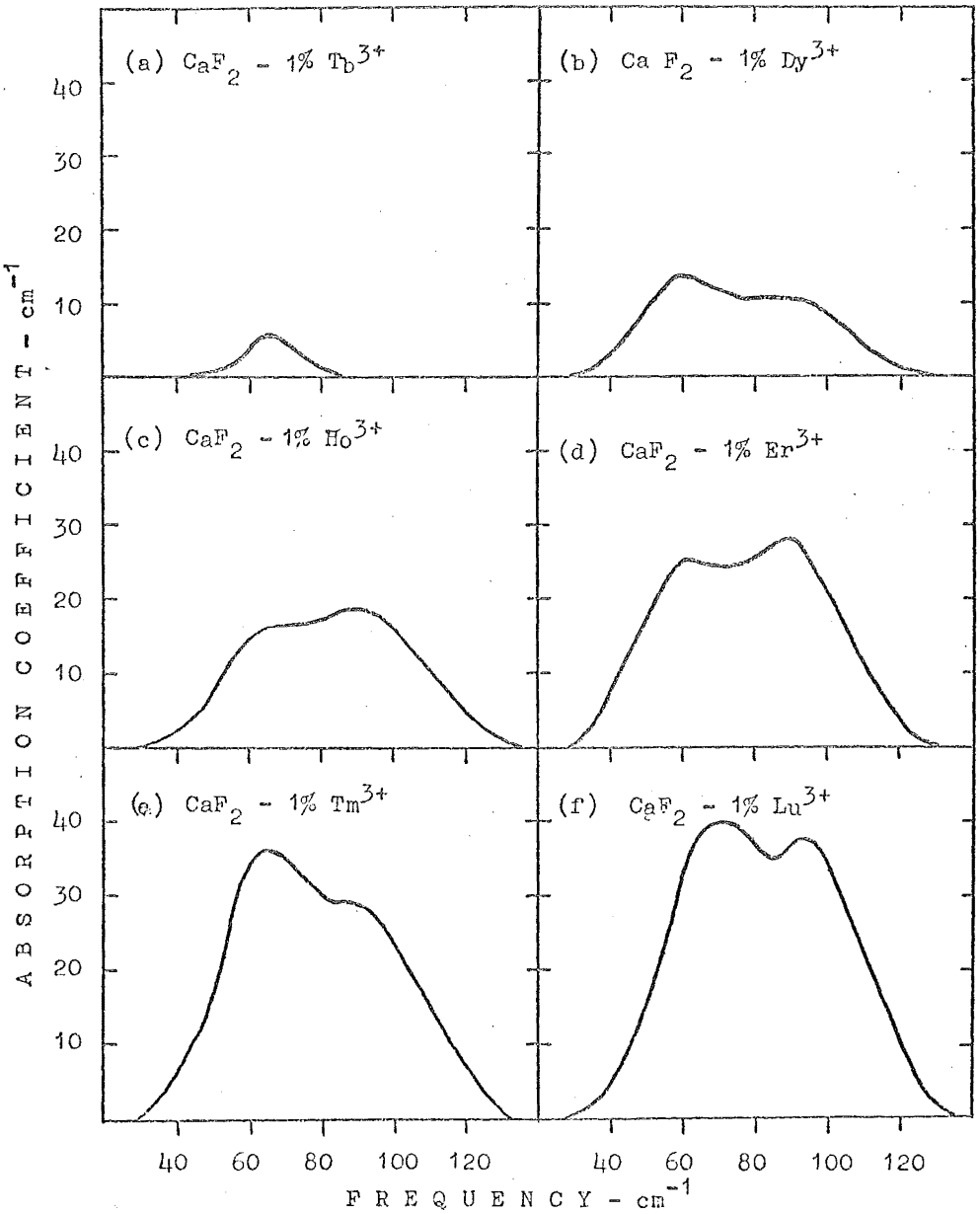

Fig (5.5a-f). The far infrared absorption bands arising from lanthanide ions in calcium fluoride at 15°K.

frequencies ω_1, ω_2 and full widths at half height Γ_1, Γ_2 of the absorption bands. The accurate determination of widths of two bands which are close together requires the fitting of a function using least squares methods. These approximate widths were obtained by inspection of the spectra.

Table 5.3

Absorption bands arising from 1.0 atoms per cent of lanthanide ions in calcium fluoride at 15°K

	Tb	Dy	Ho	Er	Tm	Lu
ω_1 (cm^{-1}) (±2 cm^{-1})	65	62	68	62	67	72
ω_2 (cm^{-1}) (±2 cm^{-1})	-	85	90	89	88	93
$\omega_2 - \omega_1$ (cm^{-1})	-	23	22	27	21	21
Γ_1 (cm^{-1}) (±3 cm^{-1})	19	30	31	32	32	38
Γ_2 (cm^{-1}) (±3 cm^{-1})	-	50	44	38	44	40
$\frac{\omega_1}{\Gamma_1}$ (± 0.3)	3.4	2.07	2.2	1.95	2.1	1.9
$\frac{\omega_2}{\Gamma_2}$ (± 0.3)	-	1.7	2.02	2.34	2.0	2.2
S (cm^{-2})	120±15	880±50	1550±100	1650±100	2350±150	2580±200

No trend is evident in either the central frequencies or the widths of the bands, but the ratios Γ_1/ω_1 and Γ_2/ω_2 are roughly constant when the uncertainties are taken into account. The ratios agree closely with the value of approximately 2 predicted by the Brout-Visscher model of the resonance mode of an isotopic impurity in a monatomic Bravais lattice (section 4-2). Another significant feature is the increase in the integrated absorption coefficient with increasing atomic number, i.e. decreasing ionic radius.

The origin of crystals and thus their growth conditions, have some effect on the shape of the absorption spectrum. Fig. (5.6) shows the spectra of three crystals of different origins to the corresponding crystals (supplied by Hebrew University) whose spectra are shown in Fig. (5.4). All three spectra display marked changes in background absorption level and fig. (5.6c) shows extremely strong bands (S = 1220 cm^{-2}) considering that the concentration of Er^{3+} is 0.5%. It is possible that the latter effect, which is also observed with CaF_2 - 0.5% Yb^{3+} (S = 2600 cm^{-2} at 15°K), may be due to a concentration dependence (see section 5-6). Because under reducing conditions ytterbium enters calcium fluoride with a considerable proportion of ions in the divalent state, no attempt was made to investigate the CaF_2-Yb system further.

In order to elucidate the nature of the far infrared absorption bands in doped calcium fluoride, the range of impurities was extended beyond the lanthanide ions, to include the monovalent ions Li^+ and Na^+. The following impurity concentrations were added to calcium fluoride and the spectra of the doped crystals obtained at either 85°K or 15°K:

0.3% Li^+, 0.3% Na^+, 0.2% Sc^{3+}, 0.3% Y^{3+}, 1.0% U^{3+}.

Without exception, these systems failed to reveal any interesting features in their spectra. The crystals with alkali metal ions as dopants had spectra which were identical with that of the pure host crystal, while the trivalent impurity ions produced spectra which were characterized by enhancement of the background absorption (fig. (5.7a), fig. (5.7b)).

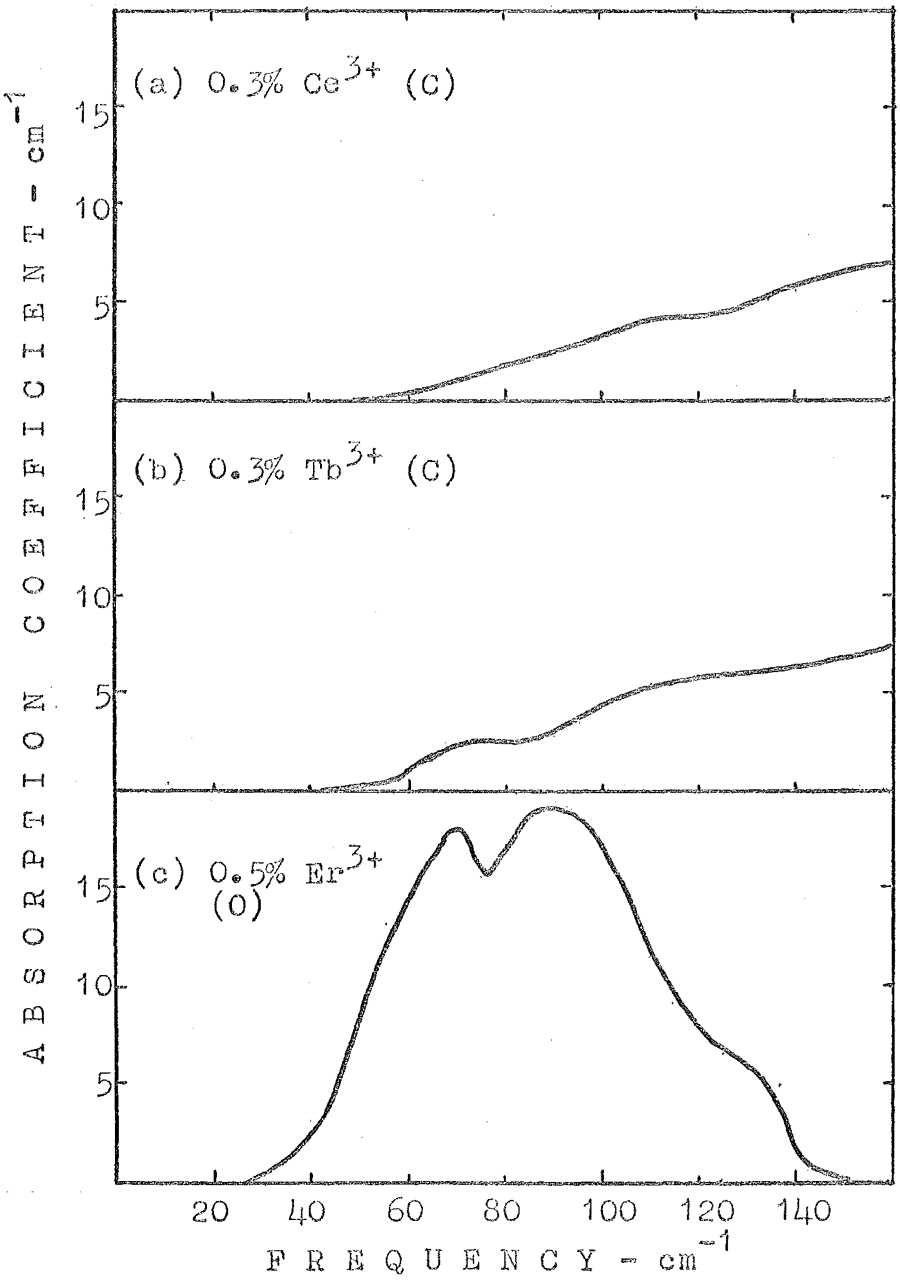

Fig (5.6). The far infrared absorption spectra of lanthanide ions in calcium fluoride: samples obtained from different sources to those shown in fig(5.4). (See table 2.2 for key to abbreviations.)

(Note different vertical scale and concentrations to fig. (5.4).)

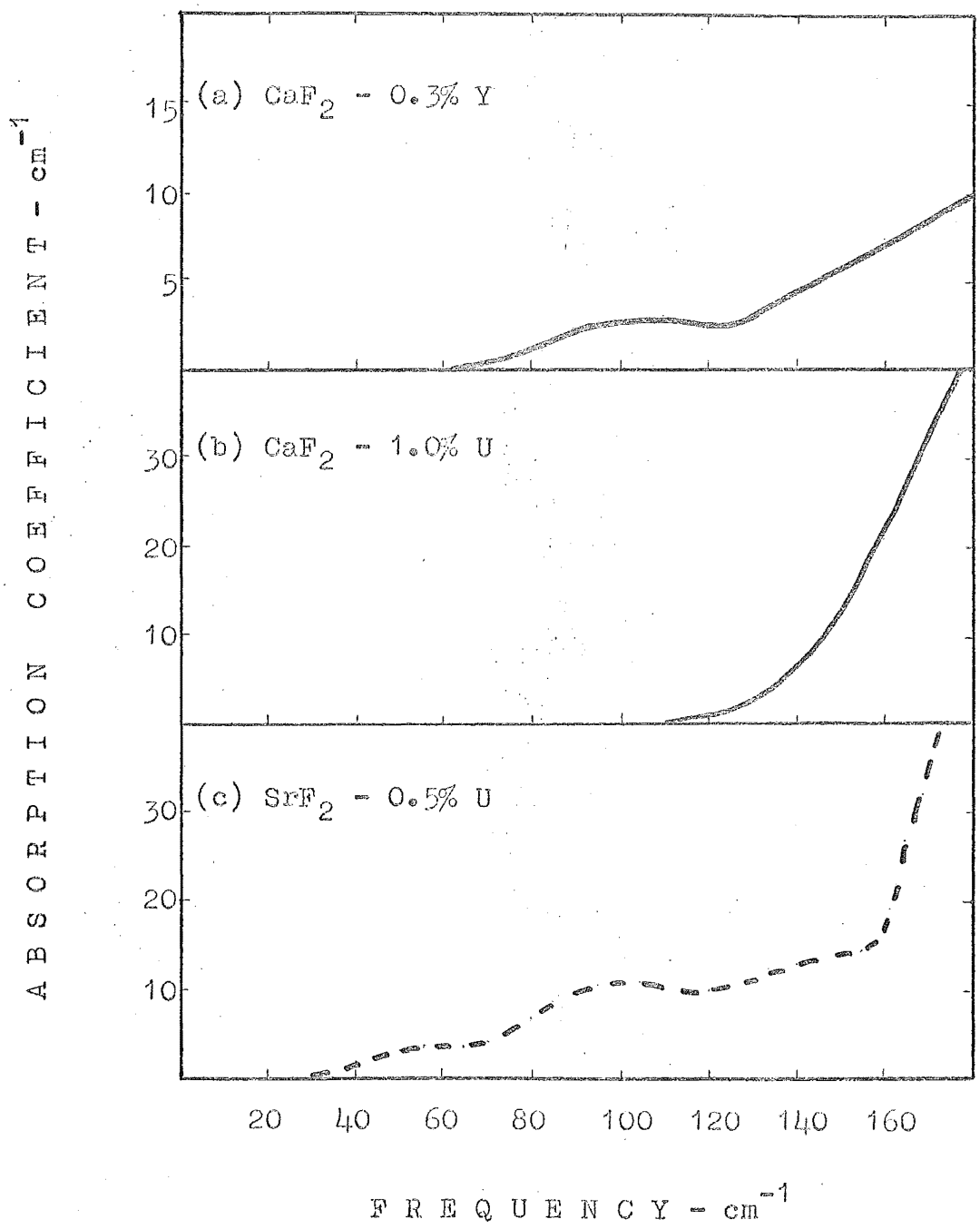

Fig (5.7). ——— 15°K
- - - - - 85°K

5-3 Far Infrared Absorption Spectra of Doped Strontium Fluoride

The far infrared spectra have been obtained for most of the ions of the lanthanide series in the strontium fluoride lattice (Table 5.2) (see fig. (5.8)). All spectra were obtained at 85°K while in certain cases spectra were also obtained at 15°K. Two systems, viz. SrF_2-Er and SrF_2-Gd were investigated in some detail.

As was observed for calcium fluoride, lanthanide ions affect the far infrared spectra of strontium fluoride in two ways. The first is the raising of the absorption level which increases both with frequency and temperature. There is also the occurrence of structure in the 50-130 cm^{-1} region, superimposed on the background absorption level. This structure, which appears as one or more absorption bands, is observed for all lanthanide ions in strontium fluoride but with variations in shape and intensity. Since SrF_2-Gd produces a single strong band around 90 cm^{-1} and electron spin resonance spectra are readily obtained and interpreted, this system received the most thorough study. The results of this study are presented later in this chapter.

Certain other impurities were added to strontium fluoride in the concentrations given below and the spectra of the doped crystals obtained at 85°K:

0.3% Li^+, 1.0% O^{2-}, 0.3% Na^+, 0.25% Ca^{2+}, 0.3% Y^{3+}, 0.5% U^{3+}.

With the exception of yttrium (fig. 5.8a)) and uranium ions (fig. (5.7c)), the doped crystals did not reveal any structure in their spectra. The results for 0.3% lanthanide ions in SrF_2, together with yttrium and uranium are summarized in table (5.4). This table includes the integrated absorption

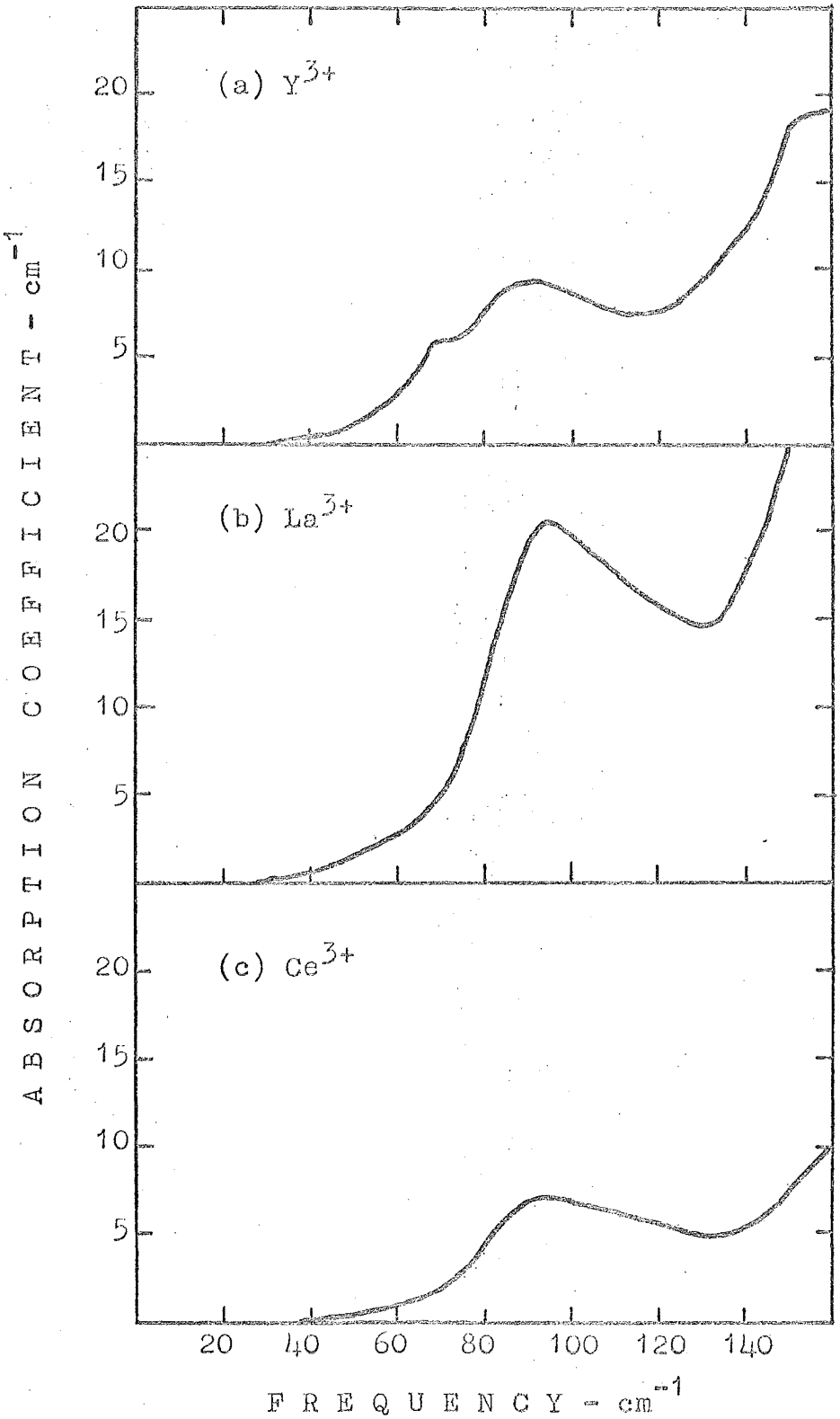

Fig (5.8 a-c). The far infrared absorption spectra of 0.3% lanthanide ions in strontium fluoride at 85°K.

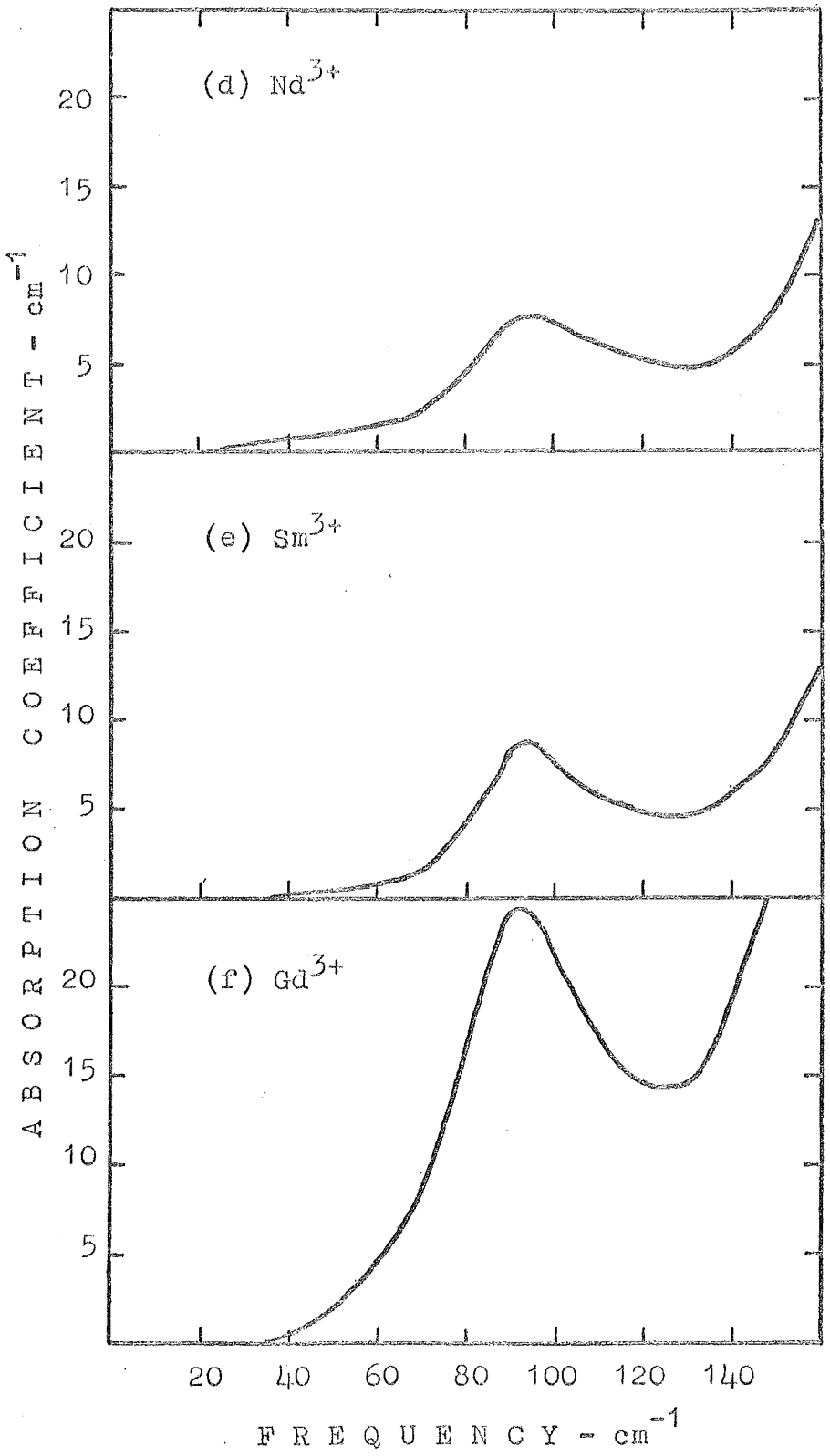

Fig (5.3 d-f). The far infrared absorption spectra of 0.3% lanthanide ions in strontium fluoride at 85°K.

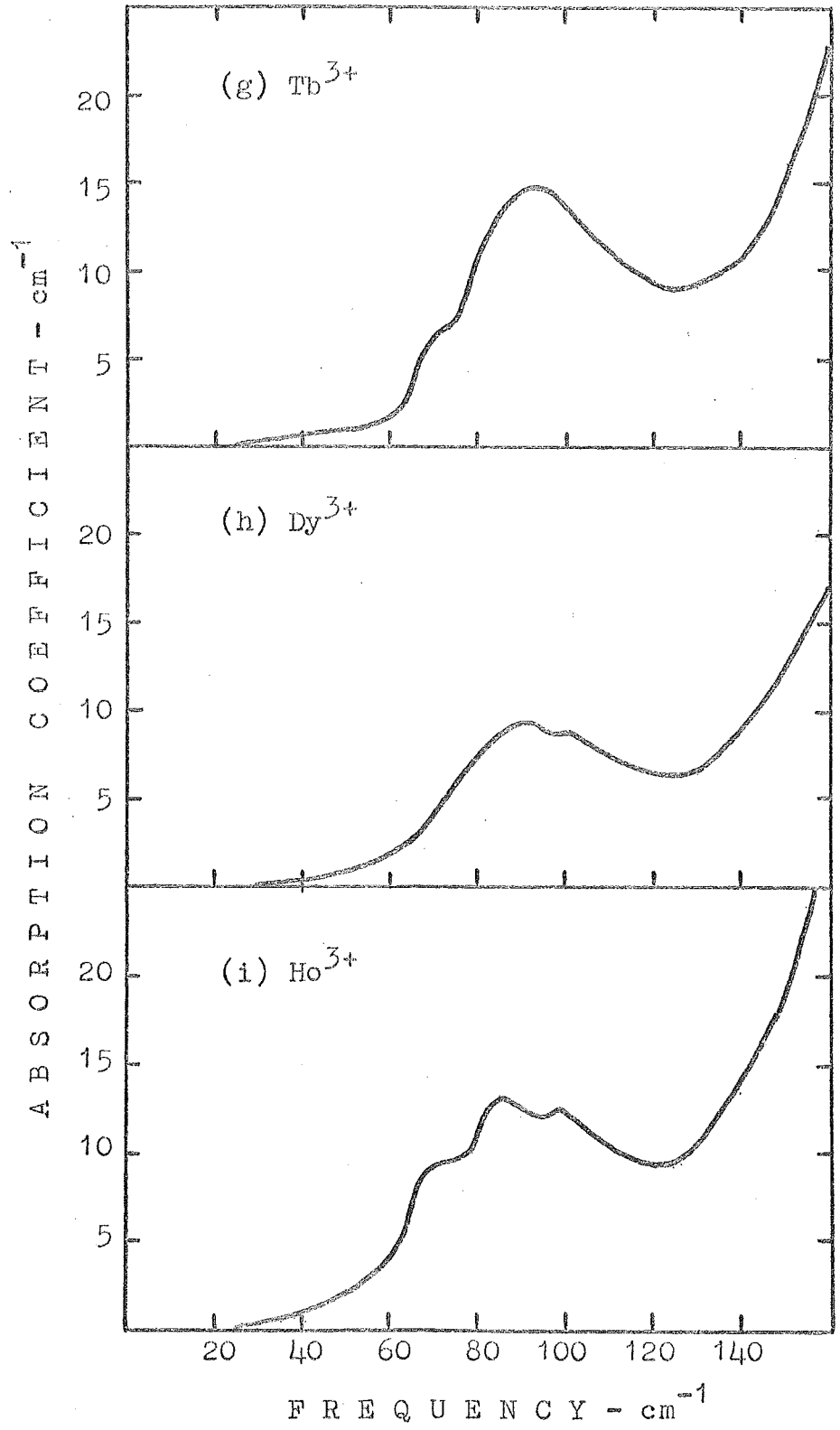

Fig (5.8 g-i). The far infrared absorption spectra of 0.3% lanthanide ions in strontium fluoride at 85°K.

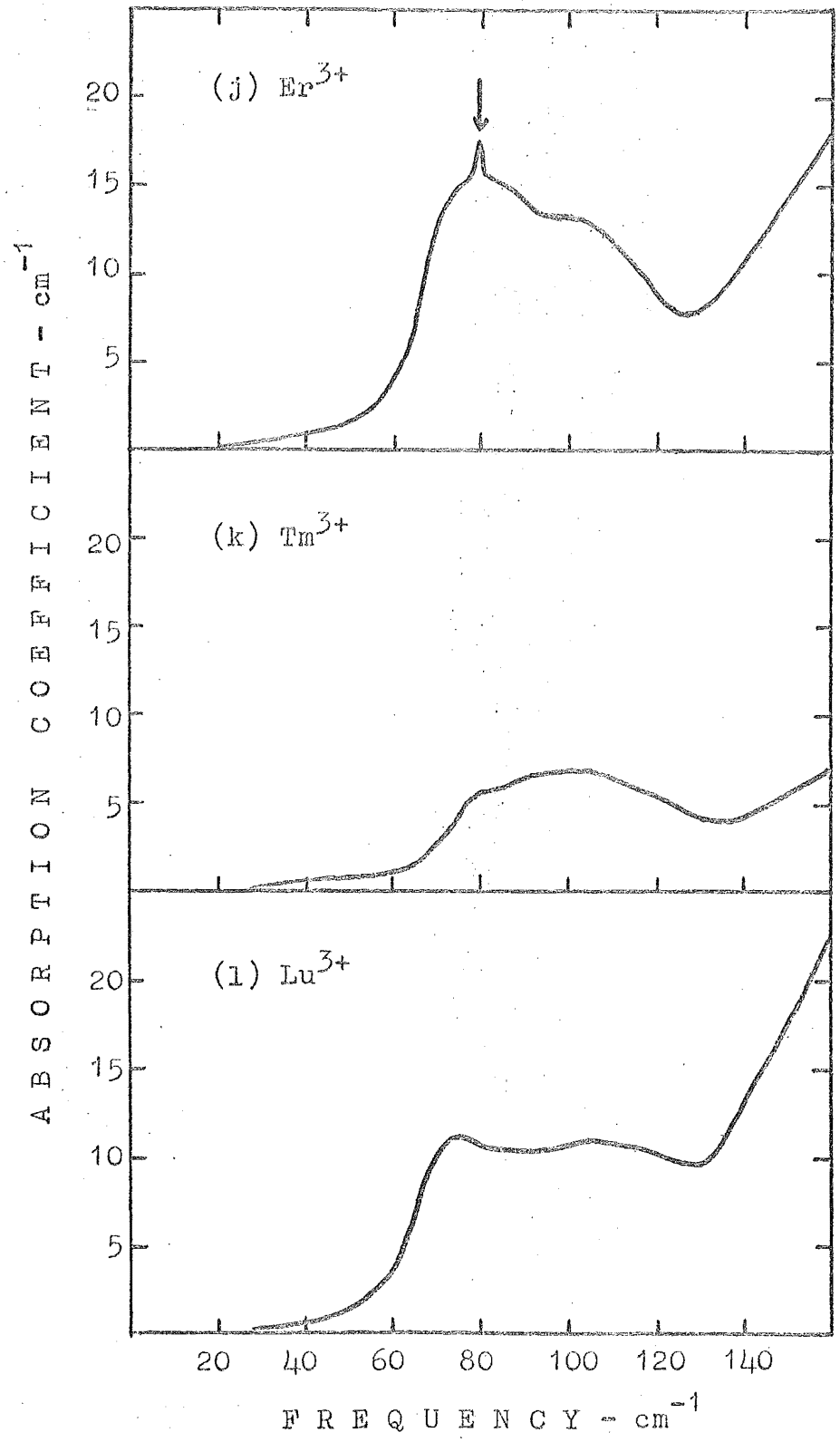

Fig (5.8 j-l). The far infrared absorption spectra of 0.3% lanthanide ions in strontium fluoride at 85°K.

Table 5.4

Absorption bands arising from 0.3 atoms per cent of yttrium, uranium and lanthanide ions in strontium fluoride at 85°K

	Y	La	Ce	Nd	Sm	Gd	Tb	Dy	Ho	Er	Tm	Lu	U[c]
Number of maxima	2	1	1	1	1	1	1	2[a]	3	2[a]	2[a]	3[b]	2[a]
Central frequency of main peak (± 2 cm^{-1}) (cm^{-1})	87	94	93	95	93	91	92	88	85	80	85[a]	75	97
Total width (± 3 cm^{-1}) (cm^{-1})	37	30	31	28	24	28	31	35	39	42	45	46	30
S (cm^{-2})	230±40	450±40	170±15	190±20	180±10	620±60	430±40	240±20	370±40	540±30	260±20	380±40	140±10

(a) tentative

(b) from spectrum at 15°K

(c) 0.5% U

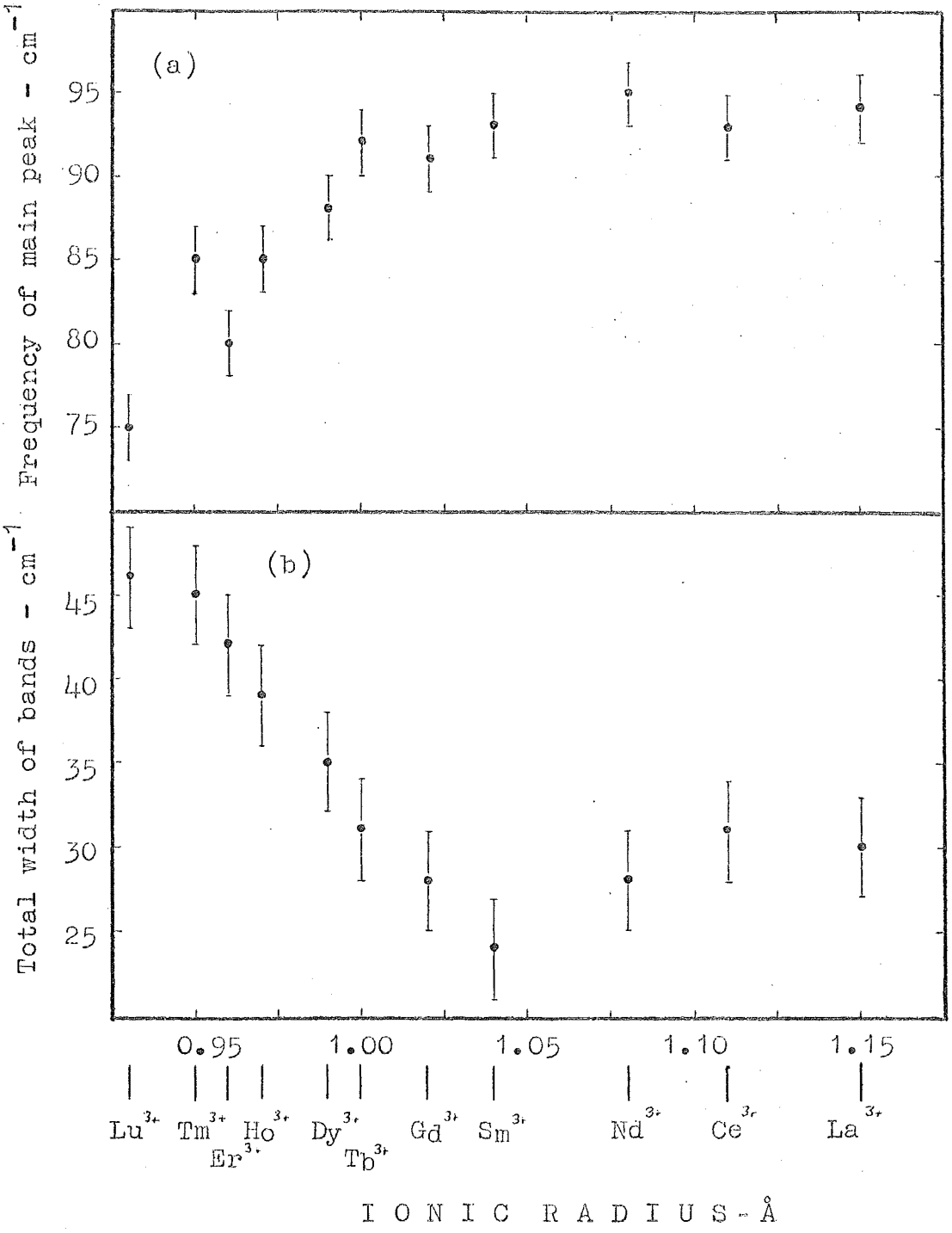

Fig (5.9) Variation in (a) frequency of main peak and (b) total width of the absorption bands in the spectra of strontium fluoride doped with lanthanide ions (85° K).

coefficient S (corrected for curvature of background absorption), the total width of the structure at half the maximum height, the probable number of maxima in the structure and the frequency at which the main peak occurs.

The structure in the spectra of lanthanide ions in the first half of the series consists of a single absorption band centred around 92 cm^{-1}, of varying strength with a maximum for SrF_2-Gd. Beyond SrF_2-Tb the situation becomes increasingly confused as several other peaks appear, with the tendency for the most intense peak to shift to lower frequencies. Another trend is for the total width of the structure to reach a minimum for SrF_2-Sm then increase steadily on proceeding along the series (fig. 5.9).

The arrow in fig. (5.8j) indicates the presence of a particularly sharp absorption line in the spectra of SrF_2-Er. This feature is discussed in section 5-8.

5-4 Far Infrared Absorption Spectra of Doped Barium Fluoride

The far infrared spectra of barium fluoride doped with 0.3% of certain impurities including several lanthanides, have been obtained at 85°K (see table 5.2) (fig. (5.10)). The alkali metal ions produced no change in the spectra of barium fluoride while the trivalent ions Y, Er, Lu and U produced increases in the background absorption upon which are superimposed broad, weak absorption bands in the region of 70 cm^{-1}. The spectrum of BaF_2-Er which was obtained with high resolution at 15°K is discussed in section 5-8.

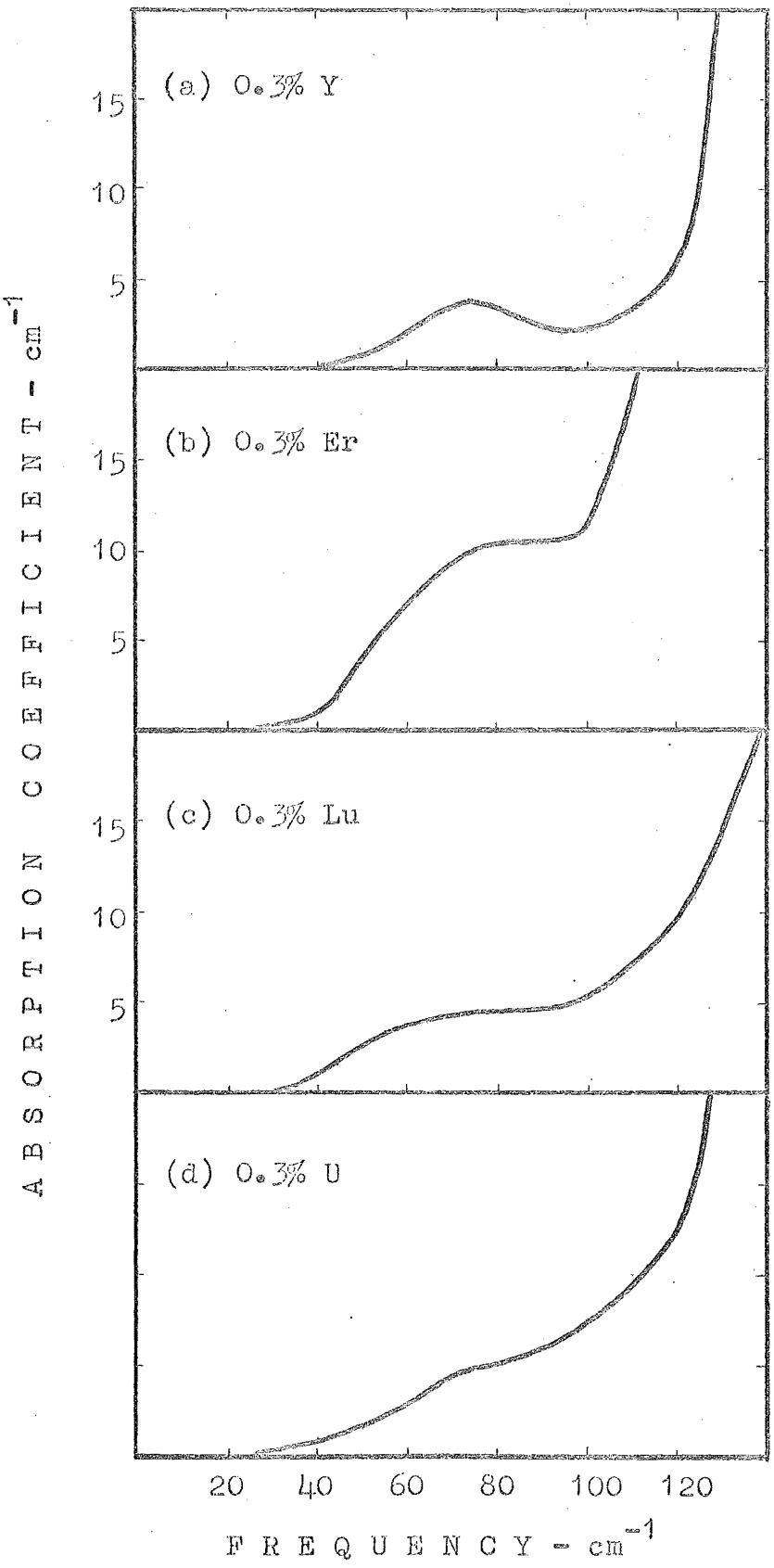

Fig (5.10). The far infrared absorption spectra of doped barium fluoride at 85°K.

5-5 Temperature Dependence of the Absorption Bands in the Spectra of Doped Calcium Fluoride and Strontium Fluoride

For comparison, the spectra of certain crystals have been obtained both at 85°K and 15°K. As typical examples of lanthanide ions in calcium fluoride the spectra of CaF_2 - 0.5% Yb^{3+}, CaF_2 - 1.0% Lu^{3+} and CaF_2 - 0.6% Lu^{3+} are shown in fig. (5.11) (with the structure separated from the background absorption level). Table 5.5 contains the parameters characteristic of the absorption bands at both temperatures.

Table 5.5

Temperature dependence of the absorption bands of lanthanide ions in calcium fluoride

	CaF_2 - 0.5% Yb^{3+}		CaF_2 - 0.6% Lu^{3+}		CaF_2 - 1.0% Lu^{3+}	
	85°K	15°K	85°K	15°K	85°K	15°K
$\omega_1 cm^{-1}$ ($\pm 2\ cm^{-1}$)	72	67	80	74	80	72
$\omega_2 cm^{-1}$ ($\pm 2\ cm^{-1}$)	92	93	93	93	94	93
$\Gamma_1 cm^{-1}$ ($\pm 3\ cm^{-1}$)	34	30	32	24	48	38
$\Gamma_2 cm^{-1}$ ($\pm 3\ cm^{-1}$)	48	42	35	30	42	40
S (cm^{-2})	1880±60	2800±100	960±50	1490±100	1880±60	2580±150

The differences in spectra at the two temperatures can be summarized as follows:

1. In going from 85°K to 15°K the integrated absorption coefficient S increases by approximately 50%.

2. The frequency of the lower band ω_1 is reduced by about 6 cm^{-1} and its width Γ_1 is also reduced.

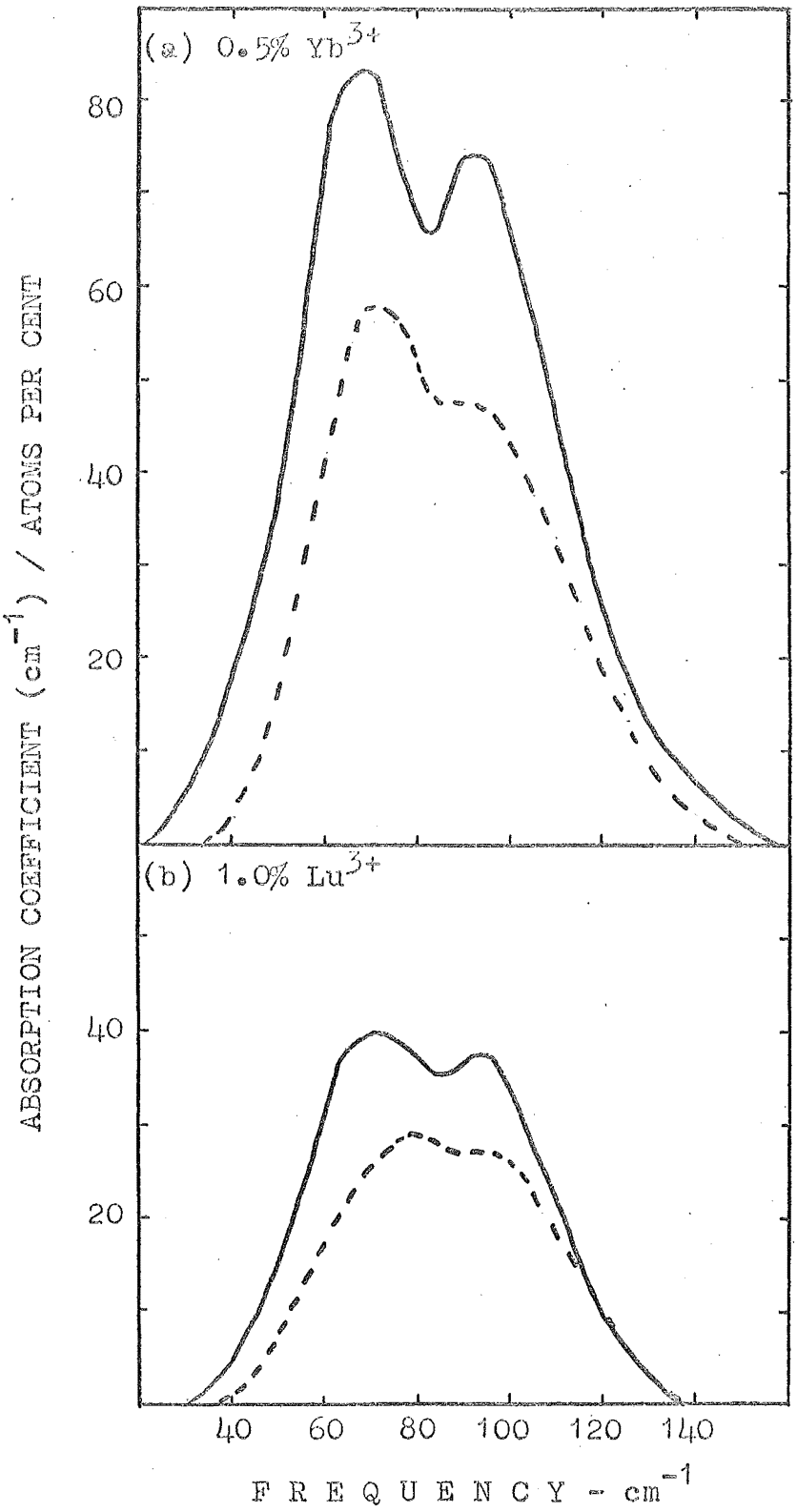

Fig (5.11). The temperature dependence of the absorption bands arising from lanthanide ions in CaF_2.

- - - - - 85° K
——— 15° K

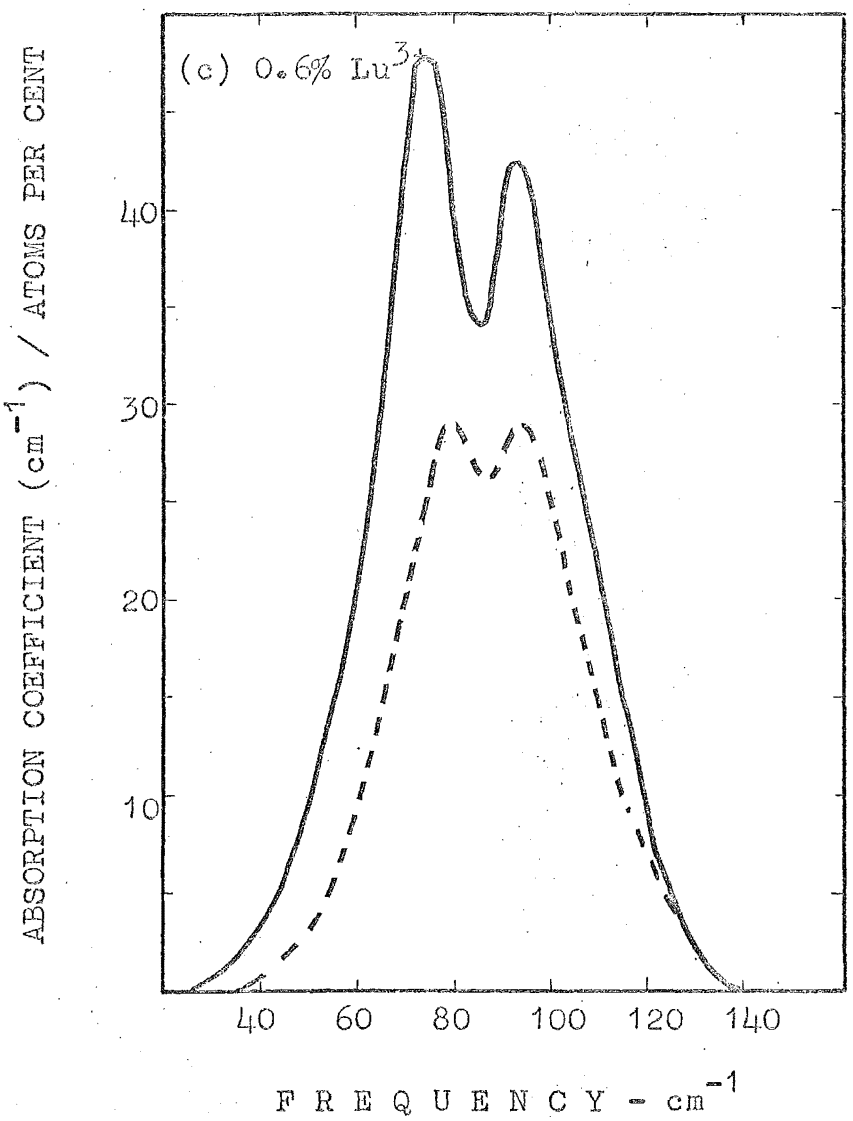

Fig (5.11). The temperature dependence of the absorption bands arising from lanthanide ions in CaF_2.

- - - - 85°K
——— 15°K

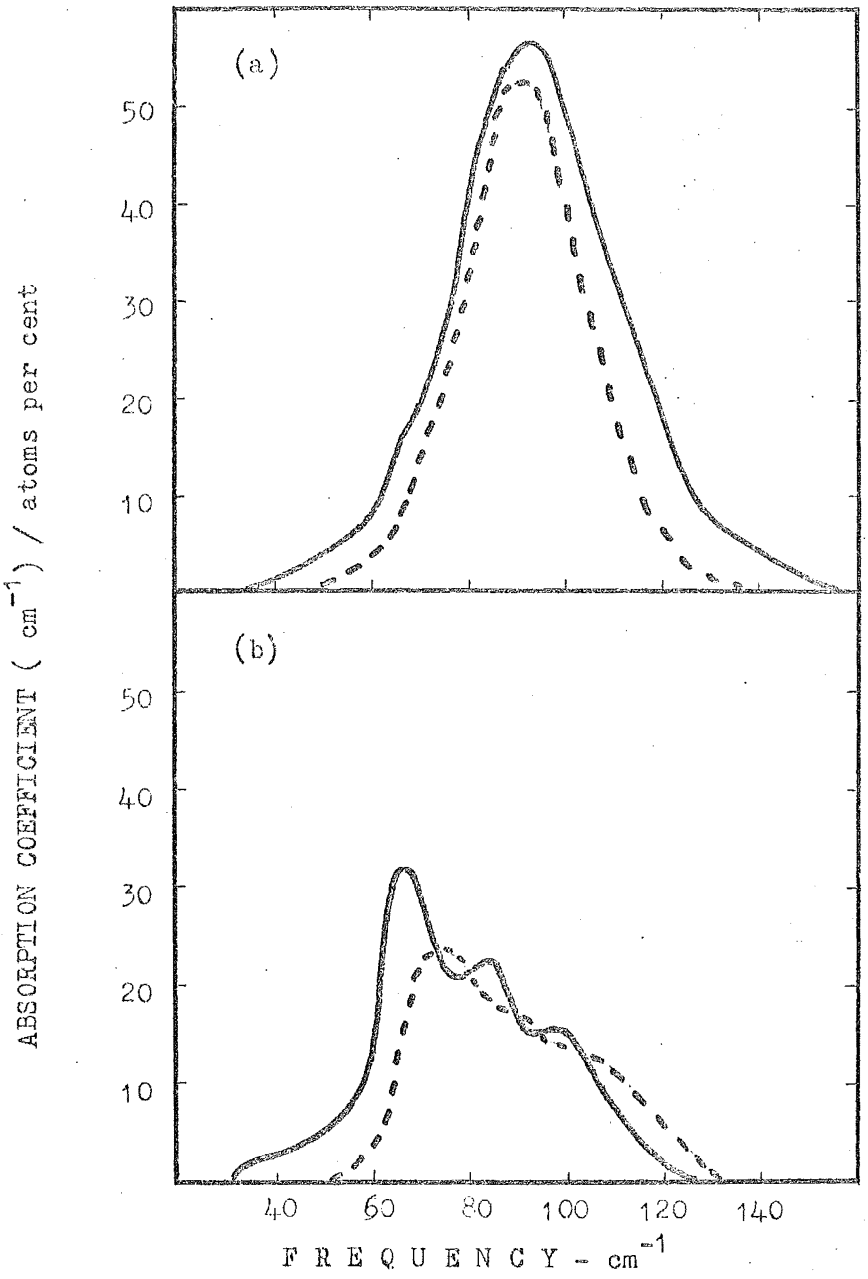

Fig (5.12). The temperature dependence of the absorption bands produced by lanthanide ions in strontium fluoride.

(a) SrF_2 - 0.3% Gd.

(b) SrF_2 - 0.3% Lu.

– – – – 85°K

——— 15°K

3. The frequency of the upper band ω_2 is unchanged while its width Γ_2 is reduced.

While liquid helium temperatures are desirable for the study of this structure, its occurrence is confirmed by spectra obtained at liquid nitrogen temperatures.

For the spectra of lanthanide ions in strontium fluoride, the picture is more confused particularly at 15°K. Fig. (5.12) shows the spectra of SrF_2 - Gd and SrF_2 - Lu. The absorption band in SrF_2 - Gd at 15°K is characterized by a 40% increase in S with a 25% increase in Γ, while the central frequency does not shift significantly. On the other hand for SrF_2 - Lu, the structure appears sharper at 15°K and shifted to lower frequencies.

Table 5.6

Concentration-dependence of the absorption bands in CaF_2 - Lu at 15°K

	2%	1.5%	1.0%	0.6%	0.3%	0.1%	0.05%	0.03%
$\omega_1 cm^{-1} (\pm 2 cm^{-1})$	74	75	72	74	77	78	-	-
$\omega_2 cm^{-1} (\pm 2 cm^{-1})$	94	95	93	93	93	91	91	97
$\Gamma_1 cm^{-1} (\pm 3 cm^{-1})$	32	32	38	24	26	16	-	-
$\Gamma_2 cm^{-1} (\pm 3 cm^{-1})$	42	40	40	30	24	26	-	-
$S(cm^{-2})$	3880±150	3490±100	2580±150	1490±100	790±50	140±15	35±3	13±1.5

5-6 Concentration Dependence of the Absorption Bands in the Spectra of CaF_2 - Lu and SrF_2 - Gd

The absorption spectra of CaF_2 - Lu have been obtained at 15°K for nominal impurity concentrations in the range 2 - 0.03 atoms per cent. The absorption bands occurring in these spectra are shown in fig. (5.13) and the parameters characteristic of the bands are given in table (5.6) for the various concentrations studied.

The results can be summarized as follows:

As the concentration of lutetium ions in calcium fluoride is decreased-

1. The lower band tends to become narrower and shifts to a higher frequency, (fig. 5.14).

2. The upper band tends to become narrower and shift slightly to a lower frequency (fig. 5.14).

3. The strength of the lower band, relative to that of the upper band, decreases.

4. The integrated absorption coefficient S is not a linear function of concentration. (This will be discussed in Chapter 6.)

Table 5.7

Concentration dependence of the absorption band in SrF_2 - Gd at 85°K

	0.6%	0.3%	0.2%	0.1%	0.07%	0.05%
ω (± 2 cm^{-1})	85	91	91	89	92	90
Γ (± 3 cm^{-1})	37	28	26	21	26	22
(cm^{-2})	990±50	490±30	330±20	170±15	60±5	120±10
T	-	0.9	-	2.0	2.2	2.8

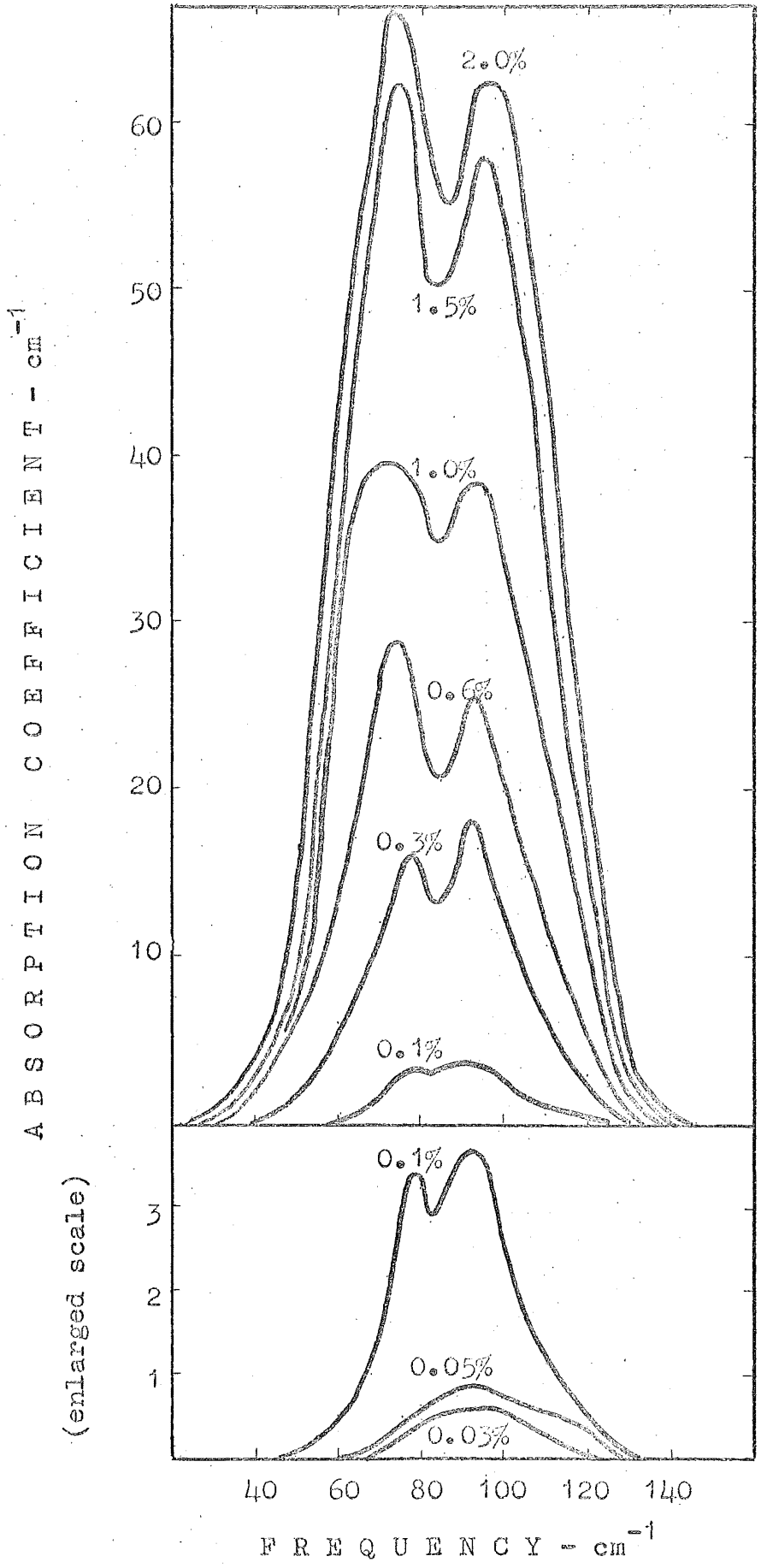

Fig (5.13) The concentration dependence of the absorption bands in CaF_2 - Lu at 15° K.

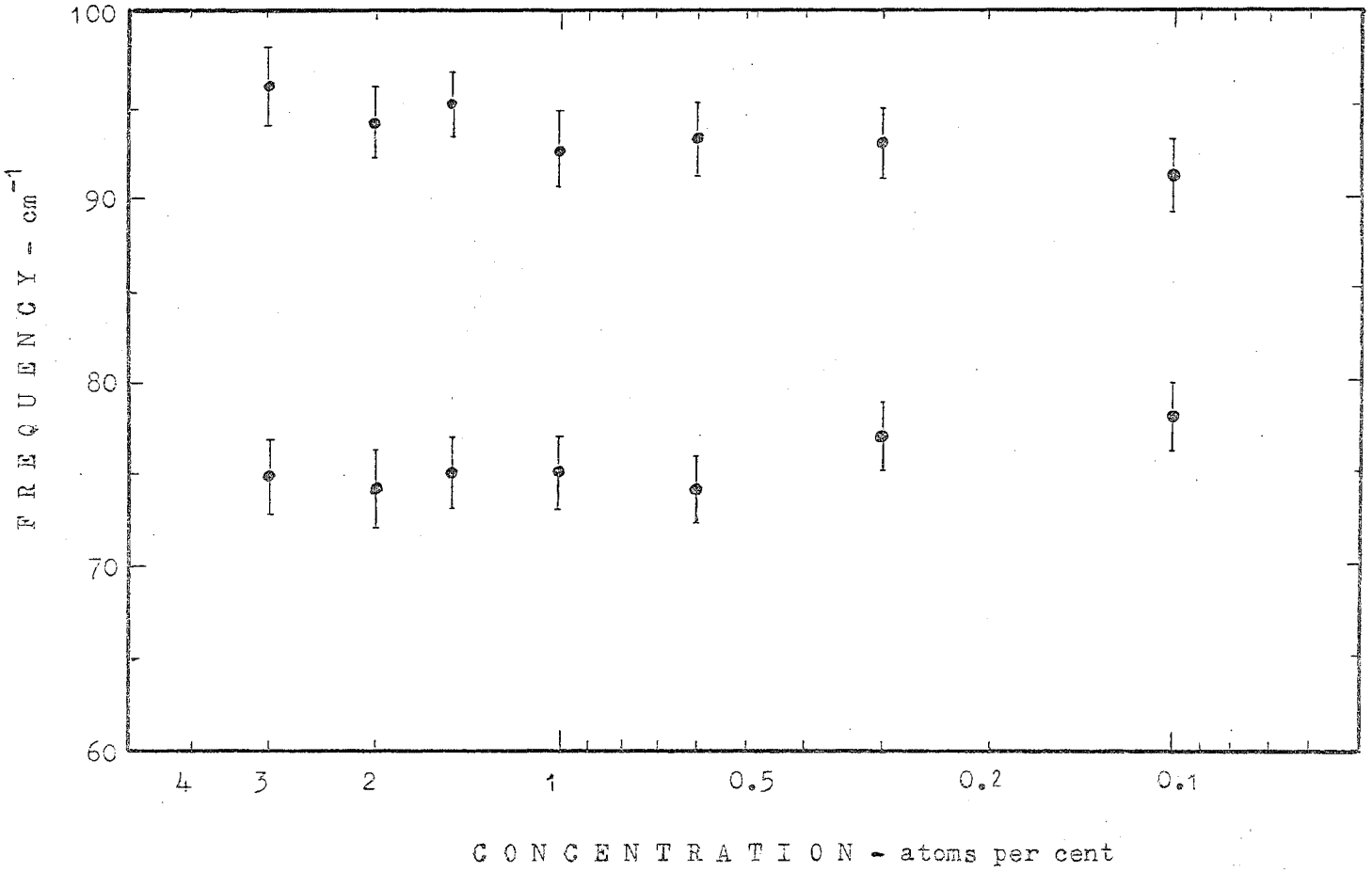

Fig (5.14) Concentration dependence of the central frequencies of the absorption bands in CaF_2-Lu.

The absorption spectra of SrF_2 - Gd were obtained at 85°K for nominal impurity concentrations in the range 0.6 - 0.05 atoms per cent. The absorption bands occurring in these spectra are shown in fig. (5.15). The electron spin resonance spectra of several samples at 300°K were obtained by A. Edgar using the Department's Q-band spectrometer in order to determine what lanthanide ion sites were present and the approximate relative proportion of sites. Predominant sites were found to be tetragonal and trigonal at all concentrations. The ratio of tetragonal sites to trigonal sites T is given in table (5.7) together with the parameters characteristic of the bands for the concentrations studied.

The results can be summarized as follows:

As the concentration of gadolinium ions in strontium fluoride is decreased -

1. The absorption band tends to become narrower but undergoes no significant shift in central frequency.

2. The integrated absorption coefficient S is approximately a linear function of impurity concentration in the range 0.1 - 0.6 atoms percent. (It is not certain to what extent the concentrations 0.07%, 0.05% can be trusted.)

3. The tetragonal site becomes increasingly predominant over the trigonal site.

In the case of SrF_2 - 0.07% Gd, the S value is anomalously low. It is interesting to note that the e.s.r. spectrum of this sample is the only one to show evidence of trigonal O^{2-} compensation.

Since the Lu^{3+} ion has full electronic shells, it has no e.s.r. spectrum so that direct determination of sites present is not possible. However, the e.s.r. spectrum of CaF_2 - 0.3% Gd grown under reducing conditions revealed

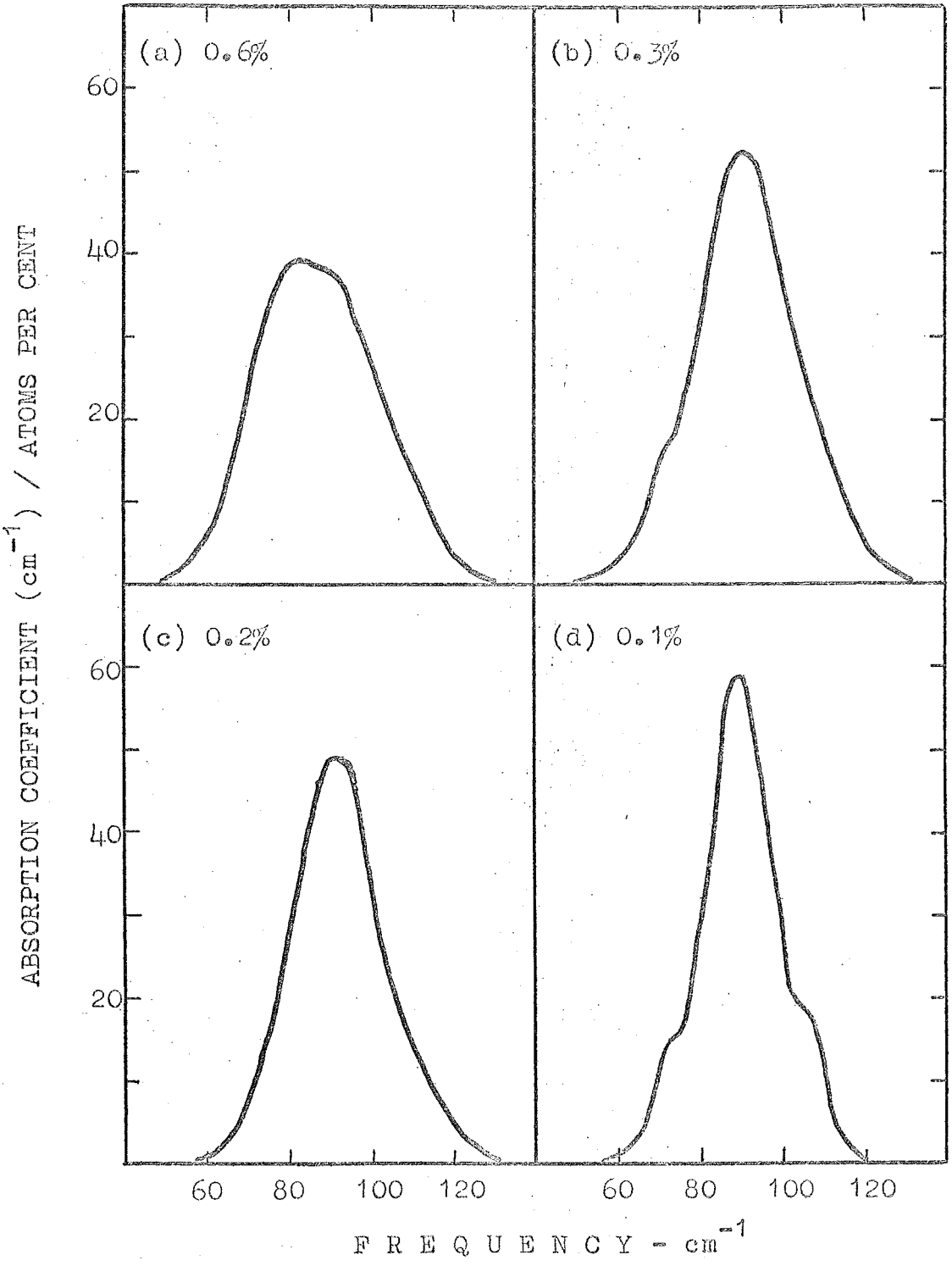

Fig (5.15 a-d) The concentration dependence of the absorption band in SrF_2 - Gd at 85°K.

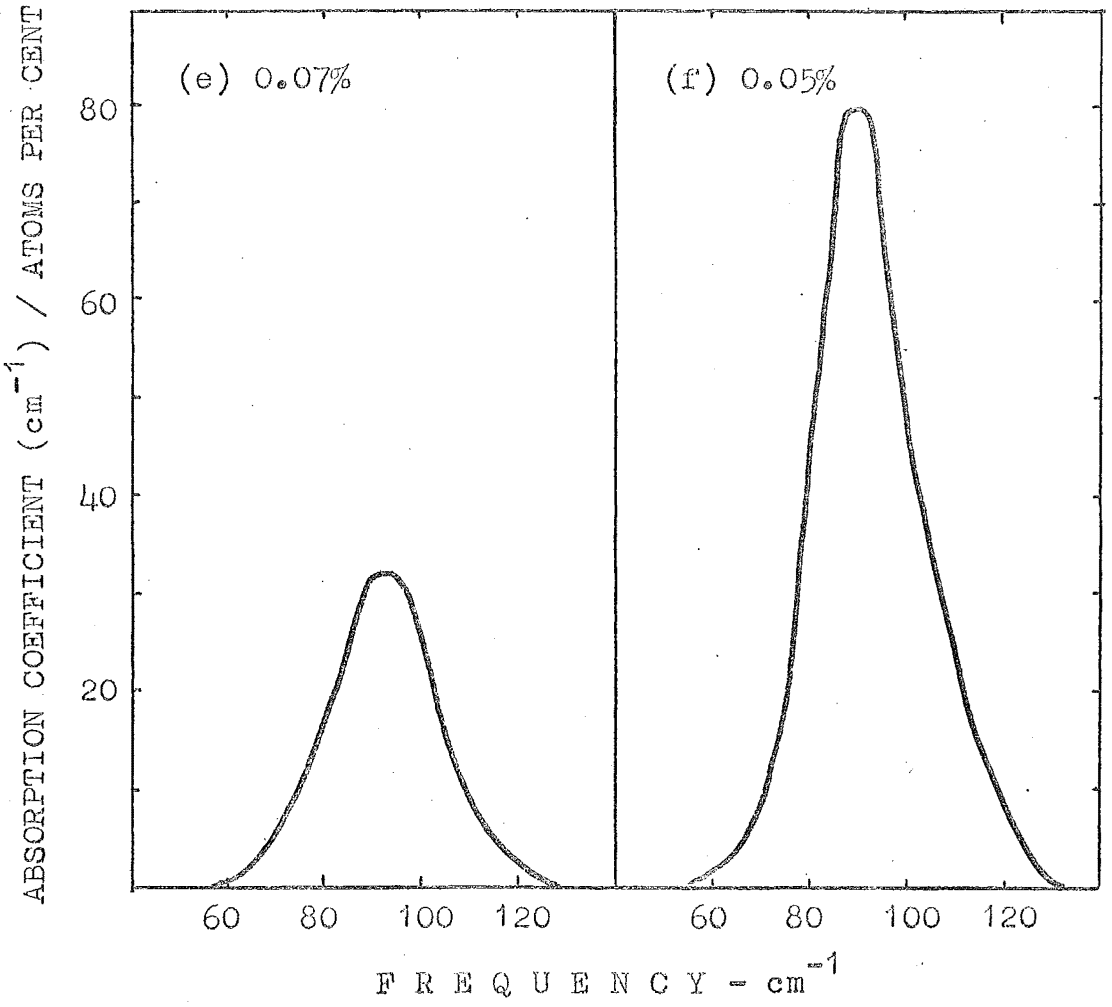

Fig (5.15 e-f). The concentration dependence of the absorption band in SrF_2 - Gd at 85°K.

that tetragonal and cubic sites occur, in the ratio 3 : 2.

5-7 Effects of Growth Conditions on the Far Infrared Spectra of Lanthanide Ions in Calcium and Strontium Fluorides

As discussed in Chapter 3, the occurrence of the various site symmetries of lanthanide ions in alkaline earth fluorides are largely determined by the growth conditions which in turn are affected by the dopants added to the melt prior to growth.

It has been found that the conditions under which a doped calcium fluoride crystal is grown markedly affect the far infrared spectrum, particularly the characteristic absorption bands. The far infrared spectra at 15°K of calcium fluoride doped with the following compounds were obtained:

(a) 0.1% Lu_2O_3 (fig. (5.16))

(b) 0.3% Er_2O_3, 0.1% CaO

(c) 0.3% LuF_3, 1.0% NaF (fig. (5.16))

(d) 0.3% LuF_3, 5.0% NaF

In crystals (a) and (c) the absorption bands appear but significantly diminished in strength when compared with the spectra of crystals having LuF_3 as the sole dopant. For crystals (b) and (d) the bands are completely removed. A reduction in the strength of the bands similar to that obtained for crystals (a) and (c) was produced by heating a CaF_2 - 0.3% LuF_3 crystal at 800°C for four days in a H_2O atmosphere.

It was found that strontium fluoride crystals doped with gadolinium are influenced to a lesser extent by the growth conditions. The far infrared and electron spin resonance spectra of SrF_2 doped with the following compounds were obtained

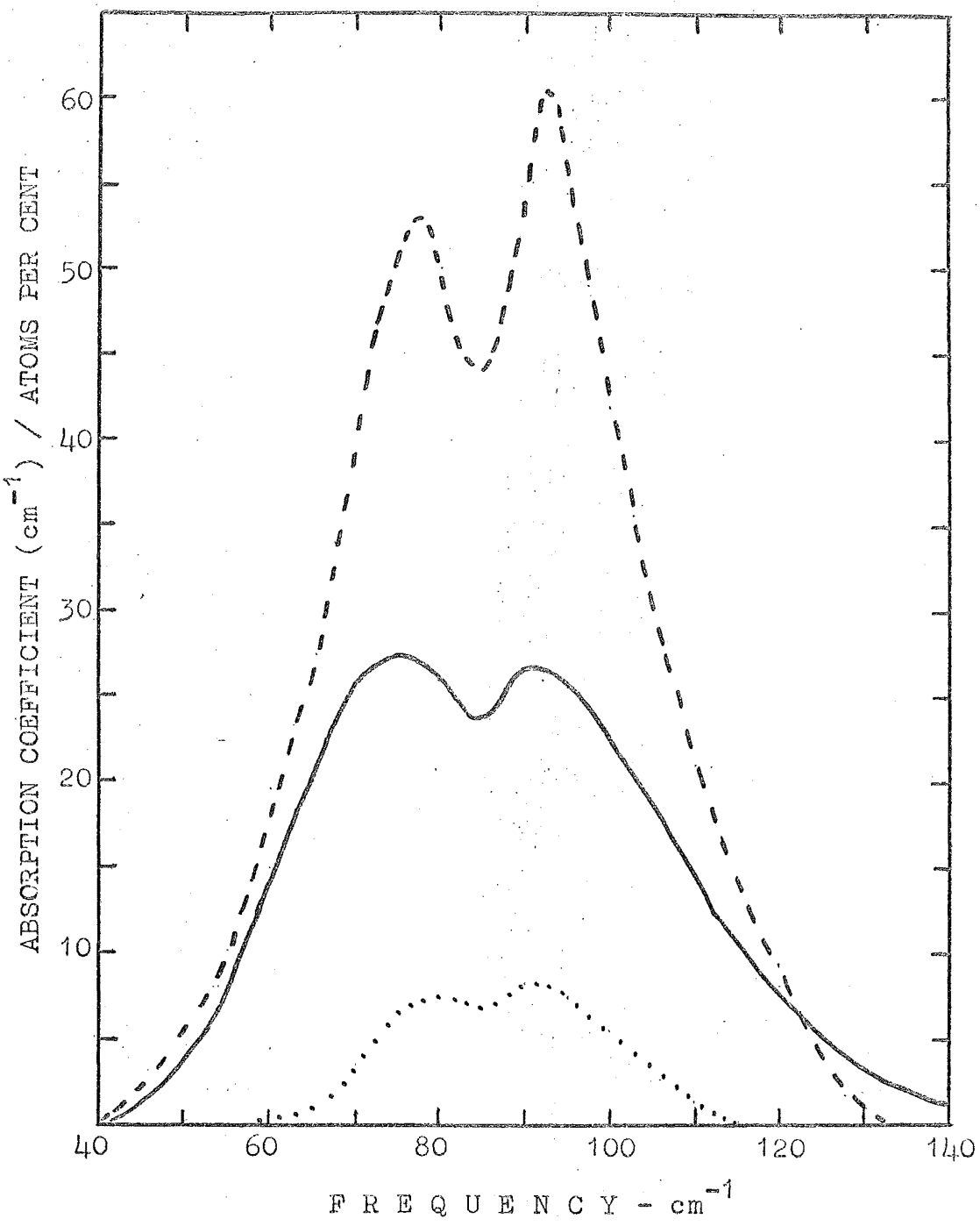

Fig (5.16) Reduction in the intensity of the absorption bands, produced by altering the growth conditions. All spectra are of CaF_2-Lu at 15°K. The starting materials are as follows:

- - - - - 0.3% LuF_3

——— 0.3% LuF_3, 1.0% NaF

..... 0.1% Lu_2O_3

(e) 0.3% Gd_2O_3

(f) 0.3% GdF_3, 5.0% NaF.

Crystal (e) showed evidence of O^{2-} compensation in its e.s.r. spectrum and the far infrared absorption band was reduced in strength by about 50%. The attempt at Na^+ compensation in crystal (f) produced no substantial change in either the far infrared spectrum (possibly a slight enhancement of the absorption band) or the e.s.r. spectrum (predominant sites are tetragonal and trigonal in the approximate ratio of 4 : 1).

5-8 Electronic Lines

It was intended as part of this project, to examine the far infrared spectra of the doped crystals for lines originating from low-lying electronic levels. The spectra of lanthanide ions in calcium fluoride were all obtained with a resolution of 1 cm^{-1} at 15°K. In addition the following systems were examined at higher resolution:

CaF_2 - Ce (0.5 cm^{-1}), CaF_2 - Er (0.5 cm^{-1}),
SrF_2 - Er (0.2 cm^{-1}), BaF_2 - Er (0.2 cm^{-1}),
SrF_2 - Nd (0.2 cm^{-1}).

However, only the system SrF_2 - Er definitely showed a sharp absorption line, although in the noisy spectrum of BaF_2 - Er a weaker line has possibly been seen.

The line in SrF_2 - Er has the following characteristics (fig. 5.17) at 15°K:

(i) The peak frequency is 81.0 cm^{-1}, and with a resolution of 0.2 cm^{-1}, the full width at half height is 1.0 cm^{-1}.

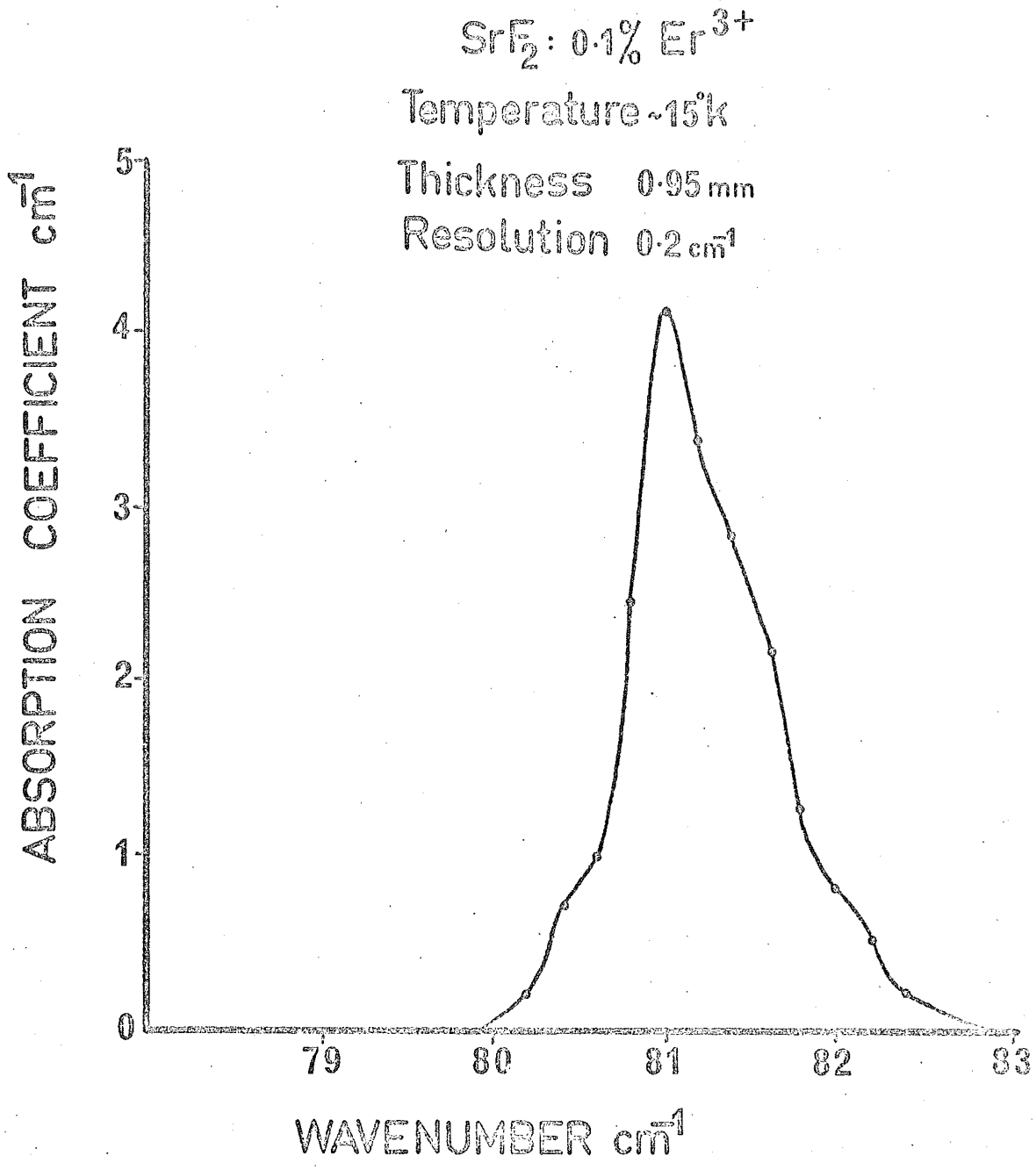

Fig (5.17) The sharp absorption line in the spectrum of SrF_2 - Er at 15°K.

(ii) The lineshape is asymmetric, strongly suggesting the existence of two unresolved lines.

(iii) The line strength varies linearly with erbium concentration, and at 0.1 atoms per cent, the integrated absorption coefficient is 3.9 cm^{-2}.

(iv) The line is still visible at 85°K but has a reduced height and increased width.

(v) Growth conditions do not measurably affect the line.

No fluorescence measurements are available with which to compare our results, but the indications are that this line arises from a low-lying electronic level of Er^{3+} in strontium fluoride. Zeeman studies are necessary to confirm this possibility.

CHAPTER 6

DISCUSSION OF RESULTS

6-1 The Nature of the Absorption Bands in Calcium Fluoride Doped with Lanthanide Ions

Although to date, no results of investigations of the far infrared absorption spectra induced by lanthanide ions in calcium fluoride have been reported, results from other techniques suggest that the strong absorption bands that we have observed arise from vibrational motion of the lanthanide ion impurity and its surroundings in a kind of "resonance" (quasilocalized) mode. Sharp, low frequency resonance modes induced by certain impurities in alkali halide crystals have been extensively studied in the far infrared using direct optical absorption[20,34]. In addition, certain systems display absorption bands in the region of 50 cm^{-1}, which, in spite of their width, are called resonance modes[20,105]. The systems include NaCl : Ag^+ (ω_r = 52.5 cm^{-1}, Γ = 10 cm^{-1}), NaCl : F^- (ω_r = 59 cm^{-1}), NaBr : Ag^+ (ω_r = 48 cm^{-1}). Other authors prefer to call structure which is neither sharp nor at low frequency "band mode" absorption[40].

The optical spectra of lanthanide ions in crystals often display so-called vibronic satellites in addition to lines assigned to pure electronic transitions. These vibronic lines are attributed to a simultaneous electronic excitation of the lanthanide ion and a lattice vibration. A number of workers have assigned peaks in the optical spectra of divalent[43,106] and trivalent[44,107-109] lanthanide ions in calcium fluoride to localized or quasi-localized vibrational modes associated

with the impurity. They hypothesize that since the restrahlen frequency is 270 cm^{-1}, with a mass increase by a factor of 4 on replacing a calcium by a lanthanide ion, the frequency of vibrational modes of the complex formed by the impurity and its nearest neighbours is expected to be about 135 cm^{-1}. The vibronic separation frequencies observed in various systems are somewhat inconsistent and no clear pattern has emerged.

Measurements of spin-lattice relaxation of certain lanthanide ions in calcium fluoride have also revealed evidence of impurity-induced quasilocalized vibrational modes[101]. However, low temperature thermal conductivity measurements on $CaF_2 : Sm^{2+}$ and $CaF_2 : U^{3+}$ by Harrington and Walker[110] showed no evidence of phonon resonances. Our work shows that they made an unfortunate choice of crystals.

Alexander and Sievers[111] have observed low-frequency resonance modes in the far infrared spectra of $MnF_2 : Eu^{2+}$ and $MnF_2 : Tm^{2+}$ but no lines were observed in the following systems: $MnF_2 - Sm^{2+}$, $MnF_2 - Nd^{3+}$, $CaF_2 - Eu^{2+}$, $SrF_2 - Eu^{2+}$.

Since a lanthanide ion is approximately the same size as the calcium ion which it replaces, it is expected that the existence of resonance modes will be determined primarily by the mass difference. However, for a quantitative explanation of the observed features, force constant changes must be taken into account. In the alkali halides it has been found in most cases that substantial weakening of the force constants is necessary to produce resonance modes at low frequency, and the impurity mass plays only a secondary role. Comparison of theory with experiment indicates that a considerable mismatch in ionic radii corresponds to a large change in coupling constant[20,112].

Table 6.1

Ionic Radii (Å)

	Pauling[113]	Shannon & Prewitt[114]	Moeller[115]	Zhdanov[116]
La^{3+}	1.15	1.18	1.061	1.04
Ce^{3+}	1.11	1.14	1.034	1.02
Pr^{3+}	1.09	1.14	1.013	1.00
Nd^{3+}	1.08	1.12	0.995	0.99
Sm^{3+}	1.04	1.09	0.964	0.97
Eu^{3+}	1.03	1.07	0.950	0.97
Gd^{3+}	1.02	1.06	0.938	0.94
Tb^{3+}	1.00	1.04	0.923	0.89
Dy^{3+}	0.99	1.03	0.908	0.88
Ho^{3+}	0.97	1.02	0.894	0.86
Er^{3+}	0.96	1.00	0.881	0.85
Tm^{3+}	0.95	0.99	0.869	0.85
Yb^{3+}	0.94	0.98	0.858	0.81
Lu^{3+}	0.93	0.97	0.848	0.80
Sc^{3+}	-	-	0.68	0.83
Y^{3+}	0.93	1.015	0.88	0.97
U^{3+}	1.111	-	1.03	1.04
Ca^{2+}	0.99	1.12	0.99	1.04
Sr^{2+}	1.13	1.25	1.12	1.20
Ba^{2+}	1.35	1.42	1.34	1.38

The radii of the lanthanide ions and other ions of interest are given in table 6.1. The values which are obtained from several sources show considerable discrepancies arising from differences in definition of effective radius and in differences in methods used for their determination as well as the fact that the effective radius of an ion depends on its environment, in particular the coordination number. Although the lanthanide ionic radii decrease monotonically in going along the series from lanthanum to lutetium, for the different sources the calcium ionic radius does not correspond to the same position in the range of lanthanide radii. While traditionally Pauling's values[113] have been used, where the calcium radius is the same as that for dysprosium, the other sources have the relative size of the calcium ion somewhat larger, corresponding roughly to that of neodymium.

To generalize, it can be said that the first few ions in the lanthanide series, being slightly larger than the calcium ion, will be more strongly coupled to the lattice. Ions occurring towards the end of the series will be less strongly coupled and thus more likely to give rise to resonance modes of vibration. The force constants expected from ionic radii considerations will be altered by (i) the extra change on the trivalent lanthanide ion which will tend to attract the eight surrounding fluorine ions and (ii) the existence of local charge compensation. Both effects will tend to increase the coupling of the lanthanide ion to its surroundings so that it is not surprising that structure in the absorption spectrum, which is attributed to resonance modes, fails to appear until terbium is reached in the series. ENDOR measurements offer the most direct method of obtaining evidence of local

distortion around impurity ions. Analysis of ENDOR spectra of lanthanide ions at cubic sites in calcium fluoride indicate that outward movements occur with larger ions while inward movements occur with smaller ions[117].

In the simplest model of a resonance mode, the Einstein oscillator, the impurity vibrates independent of its surroundings at a frequency ω_r:

$$\omega_r^2 = \frac{\Phi'}{M'}$$

where M' is the impurity mass and Φ' is an effective coupling constant. From dysprosium to lutetium a frequency shift of about 4% is predicted due to the mass increase while a decrease in the force constants would also make a further contribution to the downward shift. The isotope shifts of low frequency resonance modes and local modes are in general well explained by the Einstein oscillator model, because the impurity can be considered to be vibrating in a static potential well. The fact that our results fail to show a consistent mass shift is therefore perhaps an indication of the extended nature of the defect. The frequencies and widths of the observed absorption bands indicate that the impurity cannot be considered to be weakly coupled to the host lattice even though the coupling constants have been somewhat reduced from the values for the calcium ion. Instead of imagining the lanthanide impurity to be vibrating in an optically active mode relatively independent of its surroundings, the motions of the surrounding ions and their contribution to the dipole moment must be included. Any changes in the mass or coupling constants of the impurity would probably have less effect on the frequency of vibration of this "molecule" than it would have on the

vibrational frequency of a lanthanide impurity oscillating in a stationary lattice. The ENDOR results[117] show that for a small lanthanide ion, the surrounding cube of eight fluorine ions relaxes around the impurity. This would have the effect of reducing the lanthanide-fluorine force constant change while decreasing the coupling of these fluorine ions to their other nearest neighbours.

While the resonance mode frequencies differ from one lanthanide ion to another, the results show no obvious relation to the lanthanide ionic radii. Other effects which may produce frequency shifts will be discussed in later sections.

6-2 Concentration Dependence of the Integrated Absorption Coefficient of Resonances Modes in CaF_2 - Lu

The values of the integrated absorption coefficient S from table 5.6 have been ratioed against the nominal lutetium ion concentration. The resulting normalized integrated absorption coefficient S' (cm^{-2}/1 impurity atom per cent) is shown in fig. (6.1a) as a function of concentration. If all impurity ions made an equal contribution to the absorption coefficient, then S' would be constant (provided all the lutetium ions added to the melt enter the crystal by substituting for calcium ions). However our results indicate that this is not the case. Instead S' is a maximum around 0.5 - 1.0 atoms per cent and decreases at low and high concentrations. Since for lanthanide ions in calcium fluoride, centres of different symmetry are known to predominate over different ranges of concentration, the behaviour of S' suggests that resonance modes of vibration are more readily observed by far

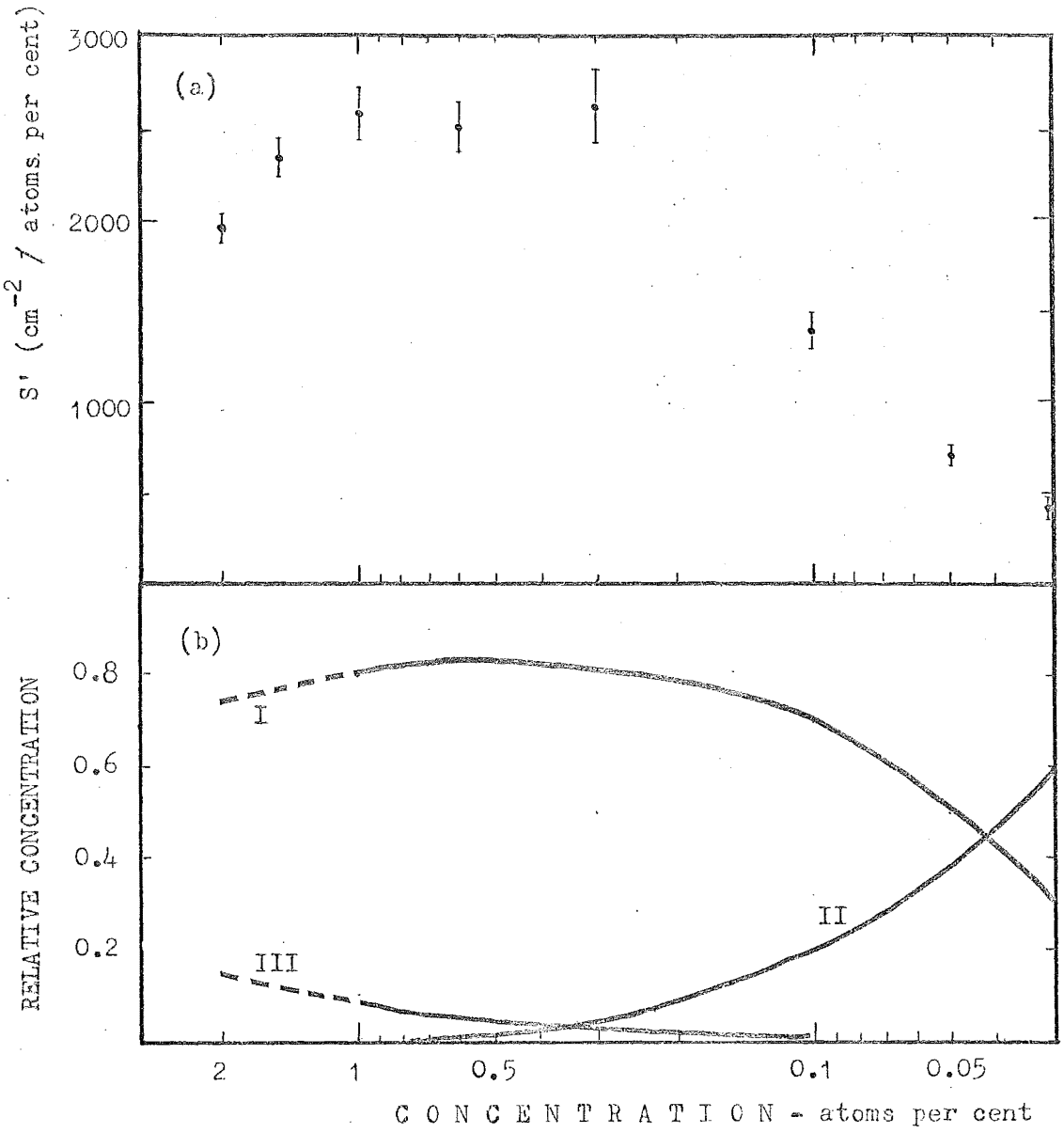

Fig (6./a) The variation in the normalized integrated absorption coefficient S' with concentration for the absorption bands of CaF_2 - Lu.

Fig (6./b) The relative concentration of sites in lanthanide ion-doped calcium fluoride as a function of impurity concentration:

I - tetragonal

II - cubic

III - orthorhombic

(Adapted from Osiko[118])

infrared absorption for some centres than for others.

Osiko[118] has developed a thermodynamic theory for optical centres of lanthanide ions in calcium fluoride. On the basis of the minimum free energy condition, the concentration dependencies of centres of different symmetries were calculated and are shown in fig. (6.1b). It is evident that the concentration curve for centres having tetragonal symmetry shows good agreement with the variation of S' with concentration. Certain absorption lines in the optical spectra of lanthanide ions in calcium fluoride have a similar concentration dependence[119].

Attempts were made to produce sites of different symmetry by growing CaF_2 - Lu crystals in oxidizing conditions, where trigonal O^{2-} sites form at the expense of cubic and tetragonal F^- sites. The absorption spectra of these crystals had the absorption bands greatly reduced in strength as did the spectra of CaF_2 - Lu crystals grown with NaF to produce rhombic Na^+ sites.

Thus it appears that the strong absorption bands, which are observed for certain lanthanide ions in calcium fluoride, are due to resonance modes of the lanthanide ion at a site of tetragonal symmetry and its neighbours.

6-3 The Tetragonal Site

Although in describing the resonance modes produced by lanthanide ions in calcium fluoride, the motion of their neighbours cannot be neglected, by virtue of its mass, coupling constants and central position, the motion of the lanthanide ion is of prime importance in determining the

nature of the vibrations of the "defect molecule".

Because of the equivalence of displacements along the three cartesian axes, an infrared-active resonance mode arising from an impurity occupying a site of cubic symmetry will be triply degenerate. For a lanthanide ion impurity at a calcium site in calcium fluoride, such a mode will transform according to the polar vector irreducible representation T_{1u} of the O_h point group. Resonance modes have been studied mainly with impurities in alkali halides occupying sites of cubic symmetry, and which are observed as single absorption lines in the far infrared[34].

When the impurity site symmetry is lower than cubic, part or all of the degeneracy is removed. If the local point symmetry is tetragonal or trigonal the triply degenerate T_{1u} mode will split into a singly degenerate A_{2u} mode and a doubly degenerate E_u mode. For the tetragonal site in calcium fluoride, the interstitial F^- ion resides in the box next to that of the trivalent lanthanide ion, along the z direction. The coordinates (x,y) form basis functions for two-dimensional irreducible representation (E_u) of the C_{4v} group while z is a basis function for the irreducible representation A_{2u}. Provided the tetragonal perturbation is sufficiently large, these modes will be observed in absorption as two separate lines or bands.

In the limited amount of work which has been carried out on localized and resonance modes arising from impurities at non-cubic sites, the results show the lifting of the three-fold degeneracy[45,55,111,120]. Jones and coworkers[45,55] have examined the spectra of hydrogenated calcium fluoride containing lanthanide ions. The hydride-ion impurity gives

rise to localized modes which are observed by their infrared absorption. The frequencies and number of absorption lines are characteristic of the force constants and of the symmetry of the site. As well as single H^- lines due to the tetrahedral substitutional site and the cubic interstitial site, a pair of lines arising from hydride ions in an interstitial position next to a trivalent lanthanide ion are observed. The frequency separation of these tetragonal-site lines decreases monotonically along the series and can be correlated with the variation of lanthanide ionic radius. In this case the presence of the lanthanide ion produces a substantial tetragonal perturbation.

To decide on the strength of the tetragonal perturbation which the interstitial fluorine ion places on its neighbouring lanthanide ion in calcium fluoride, one must consider the distortion produced by an interstitial F^- ion. In calcium fluoride, the simple cubic lattice of fluorine ions is tight-packed with a large enough space at the centre for a calcium ion. Replacement of a calcium by a lanthanide ion of comparable size produces only limited distortion of the lattice. Because of its large ionic radius (1.36Å) the interstitial fluorine ion is a misfit in its body centre site. The main effect is to push out the eight fluorine ions which surround it. More distant fluorine shells may be similarly displaced, but the magnitude will drop off rapidly with distance. Also the electrostatic attraction of the F^- interstitial for the lanthanide ion may cause the latter to be displaced. The displacement by the interstitial of the four intervening F^- ions may facilitate rather than resist such a movement of the lanthanide ion. From ENDOR experiments on

$CaF_2 - Yb^{3+}$ and $CaF_2 - Ce^{3+}$, Baker et al.[121] found that around cubic sites, the second shell neighbours are moved by only 0.7% from their positions in the undistorted lattice. The incorporation of the interstitial F^- ion in the lattice causes the following distortions[121]: (i) the eight F^- ions are pushed radially outward mainly because of the large interstitial ion, (ii) the lanthanide ion is moved towards the interstitial by 6%, keeping approximately the same distance between its nucleus and the four intervening F^- ions.

A further indication of the distortion produced by interstitial F^- ions in calcium fluorine comes from measurements of the volume changes produced by tetragonal centres[122]. The fractional change in volume as a function of lanthanide concentration shows a similar dependence to our results for S' but $\frac{\Delta V}{V}$ is a maximum at about 0.2% for $CaF_2 - Dy$.

In view of the large lattice distortion produced by the interstitial fluorine ion it therefore seems likely that the force constant matrix will lose its cubic symmetry sufficiently for two discrete modes of vibration to appear.

An impurity which is vibrating in a static harmonic potential of tetragonal symmetry will give rise to two infrared absorption lines. One line corresponds to the singly-degenerate z vibration while the other which corresponds to the doubly-degenerate x-y vibration should be twice as strong. Although this 2 : 1 intensity ratio is expected for local modes or low-frequency resonance modes of impurities at sites of tetragonal symmetry, it is seldom obtained. This means that assignment of vibration type to absorption lines on the basis of relative intensities could be in error.

While no quantitative estimate of the relative strengths of the two absorption bands in $CaF_2 - Lu$ has been carried out,

inspection of their widths and heights shows that in most cases the high frequency band is stronger, but not necessarily twice as strong. Tentative assignment of vibration type to these bands is delayed until section 6-4.

An ambiguity in line assignment from relative intensities may arise from the possibility that two modes of vibration of the same defect molecule have different effective charges. The role of effective (or apparent) charges in impurity-induced infrared absorption by covalent crystals has been studied theoretically by Leigh and Szigeti[123,124]. A charged impurity atom in a covalent crystal polarizes the surrounding electrons, but since the equilibrium configuration is symmetrical, the net dipole moment is zero. It is possible for a lattice displacement to change the electronic polarizability so that an unsymmetrical polarization is obtained, giving rise to a net electronic dipole moment. Vibrational modes having this property are optically active even if they involve no motion of the impurity. Leigh and Szigeti attribute "effective charges" to the impurity and surrounding atoms and show that absorption by neighbours is similar in magnitude to (or larger than) the absorption by the impurity vibration. They considered impurities at sites of cubic symmetry and expressed the integrated absorption coefficient for a perturbed crystal in terms of elements of an effective charge tensor.

For impurity complexes, the effective charge tensor will have a correspondingly lower symmetry. The result is that the absorption strengths of the two vibrational modes of an impurity which is paired with another may be very different from that expected from the residual degeneracy. This could

be true in ionic as well as covalent crystals[125]. These effects are likely to be most significant when the second impurity is radically different from the host ion which it replaces.

As previously discussed, the local change in the force constants when an impurity is introduced into an ionic crystal causes a shift of the surrounding ions from regular lattice points to new equilibrium positions. The shift of these ions is accompanied by distortion of their electron clouds so that they have induced electric dipole moments. In addition to distortion of the lattice, trivalent lanthanide ions at cubic sites in calcium fluoride have been shown to give rise to considerable polarization of the surrounding ions[126]. In view of the lattice distortion which it produces, the interstitial fluorine ion in calcium fluoride is expected to also produce large polarization. These considerations lead to two conclusions:

(1) The effective charge tensor for the tetragonal centre in calcium fluoride will have tetragonal rather than cubic symmetry. The relative absorption strengths of the two vibrational modes associated with this centre will thus differ from that expected from the degeneracies, and assignment of vibration type on the basis of line strength is likely to be unreliable.

(2) Strong polarization of the surrounding host lattice ions by a lanthanide ion and a substitutional fluorine ion means that the effective charges associated with vibrational modes of the tetragonal centre are likely to be considerably greater in magnitude than the effective charges associated with vibrational modes of other types of centres.

Consequently, modes of vibration associated with lanthanide ions at tetragonal sites in calcium fluoride will be more strongly absorbing than modes associated with other centres which have smaller effective charges.

The second conclusion is substantiated by our observations in two ways:

(i) The absorption bands, which we attribute to resonance modes of vibration of certain lanthanide ions at tetragonal sites in calcium fluoride, have an extremely large integrated absorption coefficient compared to values obtained for resonance modes in other systems.

(ii) In CaF_2 - Lu, at lanthanide concentrations where the proportion of tetragonal centres is low, no absorption bands appear at other frequencies which can be positively identified with centres of different symmetry.

However, it is observed that on decreasing the concentration of lutetium ions in calcium fluoride, the strength of the high frequency band relative to that of the low frequency band increases (Fig. 5.13). This effect could be due to either a vibrational mode of a lutetium ion at a site of cubic symmetry occurring at a frequency around 95 cm^{-1}, or a slight change in the effective charges associated with the two modes of the tetragonal centre. If the former is the case then it is most likely that the high frequency band arises from the xy vibration rather than the z vibration.

Another concentration effect which remains to be discussed is the shift in the central frequencies of the absorption bands (Fig. 5.14). Clayman and coworkers[127,128] have investigated the concentration dependence of resonance modes arising from certain impurities in alkali halide

crystals. The upward frequency shifts which occur for increasing impurity concentrations are correlated with reductions in the average lattice spacing. It is not understood why changing the concentration of lutetium ions in calcium fluoride should produce an upward frequency shift of one band and a downward shift of the other. However, the volume changes which have been observed for calcium fluoride containing lanthanide ions at tetragonal sites, appear to affect one mode as a lattice dilation and the other as a lattice contraction. The similarity between fig. (5.14) and the variation in the local mode frequencies of hydride ions at tetragonal sites in calcium fluoride with lanthanide ionic radius is noted here[55].

6-4 Temperature Dependence of Resonance Modes

The temperature dependence of impurity-induced resonance modes in crystals has been extensively studied for a variety of systems. Some resonance mode systems are relatively temperature independent; for example, the broad resonance in $NaCl - Ag^{+}$ at 52 cm^{-1} [105]. Others show marked changes in central frequency, width and absorption strength with changing temperature[129,130]. These are the low frequency resonance modes, which have greatly weakened harmonic force constants so that anharmonic coupling begins to be important. Generally, the anharmonicity of atomic vibrations depends on their degree of excursion, i.e. the extent which they are displaced from their equilibrium positions.

For a harmonic oscillator, the absorption strength is temperature independent. Low frequency resonance modes must be represented by an anharmonic oscillator which has an

absorption strength dependent upon

(i) population changes

(ii) dynamic effects.

In the latter effect, anharmonic coupling causes the impurity vibration to be affected by the positions of neighbouring ions and their relative displacements. The resulting coupling of the resonance mode to the lattice vibrations gives its absorption strength a temperature dependence.

Anharmonic coupling will also produce a temperature shift in the central frequency. While thermal expansion of the lattice, through linear coupling between resonance mode and the lattice, always lowers the frequency, higher order anharmonic coupling may shift the resonance to a higher frequency.

The absorption bands that we observe for lanthanide ions in calcium fluoride do not alter markedly with temperature, agreeing with the observation of Weber and Nette[130] that broad resonance mode absorption lines show only a weak temperature dependence (Fig. 5.11). Apart from a 30% reduction in the total integrated absorption coefficient and a slight increase in the widths in going from $15^{o}K$ to $85^{o}K$, the only interesting feature is the upward shift of the low frequency band while the high frequency band remains fixed. This indicates that the vibrational mode having the lower frequency is more anharmonic in nature. It is reasonable to expect this because weaker harmonic coupling constants are required for the lanthanide ion to vibrate in this mode, giving slightly greater importance to the anharmonic coupling constants.

The lanthanide - F^- interstitial coulomb attraction displaces the lanthanide ion from its normal position at the centre of the cube of eight fluorine ions, in the z direction. As a consequence, the z vibration is expected to show the larger degree of anharmonicity, as well as a large shift in frequency from that expected for a lanthanide ion at a cubic site in calcium fluoride. The temperature dependencies of the two absorption bands, and their relative strengths at low impurity concentrations (section 6-3) lead us to tentatively assign the low frequency band to the z vibration, and the high frequency to the xy vibration. These assignments could be confirmed or disproved by uniaxial stress measurements, which enable the residual degeneracy to be lifted.

6-5 Activation of Perfect Crystal Phonons by Impurities

The absorption spectra of lanthanide ions in strontium fluoride do not present such a regular pattern as they do in calcium fluoride. For this reason, most of the discussion will be directed at the spectrum of gadolinium ions in strontium fluoride, which shows a single strong band at about 90 cm^{-1} (section 5.3). Because a maximum in the phonon density of states of strontium fluoride occurs in this region (fig. 1.5), this structure cannot be attributed to impurity-induced resonance modes. Instead we must consider the enhancement of infrared absorption produced by the breakdown of translational symmetry and the $k = 0$ selection rule when an impurity is introduced into a perfect crystal lattice (section 1-4).

The presence of the impurity reduces the symmetry group of the system from the crystal space group to the point group of the impurity site. The corresponding reduction of the space group irreducible representations enables selection rules for impurity-activated absorption to be determined from the requirement that the space group reduction of a phonon must contain the vector representation of the point group.

The two lowest frequency phonon branches at the symmetry points X and L in the Brillouin zone contribute to the first maximum in the density of states of strontium fluoride (fig. 1.5). Using the reduction tables of Lowdon[25] selection rules have been determined which include these phonons in those which can contribute to impurity-activated single-phonon absorption. However, it is not clear why only the phonon at L appears to be activated for SrF_2 - Gd. Lanthanide ions at sites having lower symmetry than cubic will produce further relaxation of the selection rules, but since these phonons are already infrared active, the site symmetry is expected to have little influence on the absorption spectrum.

In barium fluoride, the lowest frequency branches at the points X and L, contribute to a maximum in the density of states at about 80 cm^{-1} (fig. 1.6). The weak structure in the absorption spectra of lanthanide ions in barium fluoride appears to result from the activation of the phonon at L.

Some impurities in calcium fluoride give rise to structure in the absorption spectra in the region of 130-160 cm^{-1}, which is in the vicinity of a maximum in the density of states (fig. (1.4)). While "pure" Israeli calcium fluoride and calcium fluoride containing certain lanthanide ions display structure at about 140 cm^{-1}, calcium fluoride doped

with CaO and $CaCl_2$ (fig. (5.2)) has absorption lines closer to 160 cm^{-1}. It appears that once again, the phonons at X and L are responsible. Although both phonons can be impurity-activated, the absorption spectrum depends on the type of impurity.

Lanthanide ions in strontium fluoride do not have a sufficiently large mass or force constant difference to produce resonance modes. Instead the lanthanide ion activates a phonon at a symmetry point in the Brillouin zone, giving rise to an absorption spectrum that bears some resemblance to the phonon density of states of strontium fluoride. The closeness of this resemblance depends to some extent on the nature of the impurity. While a lanthanide ion of large radius may fit easily into the lattice and show some similarity to the strontium ion (apart from its extra charge), a smaller lanthanide ion at the end of the series will have reduced coupling constants. For this reason it is not surprising that the structure in the absorption spectrum becomes increasingly complex for lanthanide ions in the latter half of the series, and reflects less and less the density of states of the host crystal. The major features in the structure shift to lower frequencies, suggesting that a sufficiently large reduction in the coupling constants will produce a resonance mode at low frequencies.

The reduction in harmonic coupling constants in SrF_2 - Lu shows as an anharmonic temperature shift of the major peak in the structure (fig. 5.12b). On the other hand, the system SrF_2 - Gd, where harmonic coupling constants predominate, shows no temperature shift (fig. 5.12a).

CHAPTER 7

CONCLUSION

This thesis contains the results of far infrared investigations on calcium, strontium and barium fluorides containing lanthanide ions as impurities. The strong pair of absorption bands which are observed in calcium fluoride for lanthanide ions in the latter half of the series, are shown by the concentration dependence of the integrated absorption coefficient to be due to resonance modes arising from lanthanide ions at tetragonal sites. While the existence of such resonance modes is predicted by an isotopic impurity model, for a quantitative explanation of the observed features force constant reductions must be invoked. For a resonance to occur at about 90 cm^{-1}, the force constants must be reduced by approximately 20%, while a reduction of 50% is necessary to produce a resonance at 60 cm^{-1}. The weak temperature dependence of the absorption bands reflects the predominantly harmonic nature of these modes. On the basis of our results, the band at higher frequency is tentatively assigned to an xy mode of vibration, while the lower frequency band is assigned to a z vibration of the lanthanide ion. Conclusive evidence would be furnished by uniaxial stress experiments.

Our results indicate that Harrington and Walker[110] made an unfortunate choice of impurities when they investigated the thermal conductivity of doped calcium fluoride. Thermal conductivity measurements on calcium fluoride doped with lanthanide ions in the latter half of the series are expected to show dips at temperatures corresponding to the resonance

mode frequencies. It is hoped to carry out measurements soon on CaF_2 - Lu.

Lanthanide ions in strontium and barium fluorides are not heavy enough to produce a mass resonance. Instead, structure appears in the absorption spectra of these systems, which is related to maxima in the density of states of the host crystals. The lanthanide ion impurities cause phonons at high-symmetry points in the Brillouin zone to become infrared-active. For strontium fluoride, on proceeding down the lanthanide series, the structure becomes rather more complex and tends to shift to lower frequencies. As the lanthanide ionic radii decrease, the coupling constants will be reduced, the absorption spectra will become increasingly divorced from the density of states of pure strontium fluoride, and begin to resemble resonance mode absorption.

The far infrared spectra of a number of systems were examined with a resolution of 0.5 cm^{-1} or higher, but only in the case of SrF_2 - Er was there observed a sharp absorption line, which could originate from a low-lying electronic level of the erbium ion.

REFERENCES

1. A.E. Hughes, Contemp. Phys. 12, 275 (1971).
2. "Spectroscopic Techniques", ed. D.H. Martin, (North Holland, 1967).
3. M.F. Kimmitt, "Far Infrared Techniques", (Pion Press, 1970).
4. H. Rubens and O.V. Baeyer, Phil. Mag. 21, 689 (1911).
5. H.A. Gebbie, N.W.B. Stone and F.D. Findlay, Nature 202, 685 (1964).
6. H. Steffen, P. Steffen, J.F. Moser and F.K. Kneubühl, Phys. Letters 23, 313 (1966).
7. J.M. Besson, Appl. Phys. Letters 7, 706 (1965).
8. D.W. Faries, K.A. Gehring, P.L. Richards and Y.R. Shen, Phys. Rev. 180, 363 (1969).
9. B.C. Johnson, H.E. Puthoff, J. Soo Hoo and S.S. Sussman, Appl. Phys. Letters 18, 181 (1971).
10. E.H. Putley and D.H. Martin in "Spectroscopic Techniques" (ibid.).
11. P.L. Richards in "Far Infrared Properties of Solids", ed. S. Nudelman and S.S. Mitra (Plenum Press, 1970).
12. M.J.E. Golay, Rev. Sci. Instr. 16, 347 (1947).
13. P.L. Richards and M. Tinkham, Phys. Rev. 119, 575 (1960).
14. F.J. Low, J. Opt. Soc. Am. 51, 1300 (1961).
    S. Zwerdling, R.A. Smith and J.P. Theriault, Infrared Physics 8, 271 (1968).
    H.D. Drew and A.J. Sievers, Phys. Rev. Letters 19, 697 (1967).
15. W.J. Moore and H. Shenker, Infrared Physics 5, 99 (1965).

16. M.A. Kinch and B.V. Rollin, Brit. J. Appl. Phys. 14, 672 (1963).

17. M.A.C.S. Brown and M.F. Kimmitt, Infrared Physics 5, 93 (1965).

18. K.D. Moller and W.G. Rothschild, "Far Infrared Spectroscopy" (Wiley, 1971).

19. "Far Infrared Properties of Solids", ed. S. Nudelman and S.S. Mitra (Plenum Press, 1970).

20. A.J. Sievers in "Elementary Excitations in Solids", ed. M. Balkanski, (Plenum Press, 1969).

21. D. Bloor, Infrared Physics 10, 1 (1970).

22. D.H. Martin, Advances in Physics 14, 39 (1965).

23. C. Kittel, "Introduction to Solid State Physics", (Wiley 1966).

24. A.A. Maradudin, E.W. Montroll and G.H. Weiss, "Theory of Lattice Dynamics in the Harmonic Approximation" - Solid State Physics Supplement 3 (Academic Press, 1963).

25. R. Lowdon, Proc. Phys. Soc. (London) 84, 379 (1964).

26. P.G. Dawber and R.J. Elliott, Proc. Phys. Soc. (London), 81, 453 (1963).

27. K.F. Renk, Z. Physik 201, 445 (1967).

28. R. Weber, Ph.D. dissertation, Phys. Inst. Univ. Freiburg i. Br. (1967).

29. Lord Rayleigh, "Theory of Sound", vol. I (Dover 1945).

30. I.M. Lifshitz, Nuovo Cimento 3 suppl., 716 (1956).

31. G. Schaefer, J. Phys. Chem. Solids 12, 233 (1960).

32. C.T. Walker and R.O. Pohl, Phys. Rev. 131, 1433 (1963).

33. A.J. Sievers, Phys. Rev. Letters 13, 320 (1964).

34. M.V. Klein in "Physics of Colour Centres", ed. W.B. Fowler, (Academic Press, 1968).

35. A.A. Maradudin, Solid State Physics 18, 274 (Academic Press, 1966).

36. ibid, Solid State Physics 19, 1 (Academic Press, 1966).

37. A.A. Maradudin in "Elementary Excitations in Solids", ibid.

38. A.A. Maradudin, Rep. Prog. Phys. 28, 331 (1965).

39. Proceedings of the International Conference on Localized Excitations in Solids, ed. R.F. Wallis (Plenum Press, 1968).

40. L. Genzel in "Optical Properties of Solids", ed. S. Nudelman and S.S. Mitra, (Plenum Press, 1969).

41. R. Kaiser and W. Möller, Phys. Letters 28A, 619 (1969).

42. A. Kiel and J. Scott, Phys. Rev. B3, 2033 (1970).

43. B.Z. Malkin, Soviet Physics JETP 21, 1101 (1965).

44. E. Loh, Phys. Rev. 154, 270 (1967).

45. I.T. Jacobs, G.D. Jones, K. Zdansky and R.A. Satten, Phys. Rev. B3, 2033 (1970).

46. R.W.G. Wyckoff, "Crystal Structures", vol. I, 2nd ed., (Wiley, 1965).

47. "Handbook of Chemistry of Physics", 51st edition (Chemical Rubber Company, 1971).

48. D.R. Bosomworth, Phys. Rev. 157, 709 (1967).

49. W.B. Lacina and P.S. Pershan, Phys. Rev. B1, 1775 (1970).

50. M.M. Elcombe, J. Phys. C. 5, 2702 (1972).

51. J.P. Hurrell and V.J. Minkiewicz, Solid State Commun. 8, 463 (1970).

52. G.A. Slack, Phys. Rev. 122, 1451 (1961).

53. M.M. Elcombe and A.W. Pryor, J. Phys. C 3, 492 (1970).

54. A.D.B. Woods, W. Cochran and B.N. Brockhouse, Phys. Rev. 119, 980 (1960).

55. G.D. Jones, S. Peled, S. Rosenwaks and S. Yatsiv, Phys. Rev. 183, 353 (1969), and references herein.

56. M.J. Weber and R.W. Bierig, Phys. Rev. 134, A1492 (1964) and references herein.

57. C.W. Rector, B.C. Pandey and H.W. Moos, J. Chem. Phys. 45, 171 (1966).

58. U. Ranon and A. Yariv, Phys. Letters 9, 17 (1964).

59. B. Bleaney, P.M. Llewellyn and D.A. Jones, Proc. Phys. Soc. (London), B69, 858 (1956).

60. J.M. Baker, W. Hayes and M.C.M. O'Brien, Proc. Roy. Soc. (London), A254, 273 (1960).

61. N. Rabbiner, Phys. Rev. 130, 502 (1963).

62. R.W. Ure, J. Chem. Phys. 26, 1363 (1957).

63. E. Friedman and W. Low, J. Chem. Phys. 33, 1275 (1960).

64. M.R. Brown, K.G. Roots, J.M. Williams, W.A. Shand, C. Groter and H.F. Kay, J. Chem. Phys. 50, 891 (1969).

65. R.H. Heist and F.K. Fong, Phys. Rev. B1, 2970 (1970).

66. I.V. Stepanov and P.O. Feofilov, Soviet Physics Doklady 1, 350 (1967).

67. J. Sierro, J. Chem. Phys. 34, 2183 (1961).

68. W. Low and U. Ranon in "Paramagnetic Resonance", ed. W. Low, (Academic Press, 1963).

69. T.Rs. Reddy, E.R. Davies, J.M. Baker, D.N. Chambers, R.C. Newman and B. Özbay, Phys. Letters 36A, 231 (1971).

70. J. Sierro, Phys. Letters 4, 178 (1963).

71. J. Kirton and S.D. McLaughlan, Phys. Rev. 155, 279 (1967).

72. S.D. McLaughlan, Phys. Rev. 160, 287 (1967).

73. E.V. Lowenstein, Applied Optics 5, 845 (1968).

74. L. Mertz, "Transformations in Optics", (Wiley, 1965).

75. G.R. Wilkinson and D.H. Martin in "Spectroscopic Techniques" (ibid.)
P. Jacquinot, "Applied Optics 8, 479 (1969).
H.A. Gebbie, Applied Optics 8, 501 (1969).

76. P. Jacquinot, Repts Prog. Phys. 23, 267 (1960).

77. P.B. Fellgett, Thesis, University of Cambridge (1951).

78. J. Connes, Rev. d'Optique 40, 45, 116, 171, 231 (1961). An English translation is available as a report (NAV-WEPS Rept No. 8099 NOTS TP3157), published by U.S. Naval Ordinance Test Station, China Lake, California.

79. J. Strong and G.A. Vanasse, J. Opt. Soc. Am. 49, 844 (1959).

80. H.A. Gebbie, G.A. Vanasse and J. Strong, J. Opt. Soc. Am. 46, 377 (1956).

81. P.O. Richards in "Spectroscopic Techniques" (ibid).

82. G.A. Vanasse and H. Sakai in "Progress in Optics" VI, ed. E. Wolf, (North Holland, 1967).

83. J. Strong and G.A. Vanasse, J. Phys. Radium 19, 192 (1958).

84. H.A. Gebbie, N.P.L. Symposium on Interferometry (H.M. Stationary Office, London, 1960).

85. L. Genzel, J. Mol. Spectroscopy 4, 241 (1960).

86. A.S. Filler, J. Opt. Soc. Am. 54, 762 (1964).

87. S. Goldman, "Information Theory", p.73 (Prentice-Hall, 1955).

88. M.L. Forman, W.H. Steele and G.A. Vanasse, J. Opt. Soc. Am. 56, 59 (1966).

89. J.M. Watt, Computer Journal 1, 162 (1959).

90. G. Goertzel, American Maths Monthly, 65, 34 (1958).

91. M.L. Forman, J. Opt. Soc. Am. 56, 978 (1966).

92. J.W. Cooley and J.W. Tukey, Mathematics of Computation 19, 296 (1965).

93. R.H. Pennington, "Introductory Computer Methods and Numerical Analysis", 2nd edition (Collier-MacMillan, 1970).

94. L.V. Berman and A.G. Zhukov, Opt. Spectry 19, 433 (1965).

95. Department of Physics, The Hebrew University of Jerusalem,

96. Optovac Inc., North Brookfield, Massachusetts, U.S.A.

97. A.A. Maradudin in "Astrophysics and the Many-Body Problem", (Benjamin, 1963).

98. I.M. Lifshitz and A.M. Kosevich, Rep. Prog. Phys. 29, 217 (1966).

99. R. Brout and W.M. Visscher, Phys. Rev. Letters 9, 54 (1962).

100. S. Ganesan and R. Srinivasan, Canad. J. Phys. 40, 74 (1962).

101. K.K. Pukhov and V.P. Sakun, Soviet Physics - Solid State, 10, 1148 (1968).

102. J.R. O'Connor and J.H. Chen, Phys. Rev. 130, 1790 (1963).

103. W. Hayes, H.F. McDonald, G.D. Jones, C.T. Sennett and R.J. Elliott, Proc. Roy. Soc. 289, 1 (1965).

104. M. Foguel, Department of Physics, Hebrew University of Jerusalem, (pers. comm.).

105. R. Weber and F. Siebert, Z. Physik 213, 273 (1968).

106. Z.J. Kiss, Phys. Rev. 127, 718 (1962).

107. H. Nara and M. Schlesinger, Solid State Comm. 9, 1247 (1971).

108. S.A. Pollack, J. Chem. Phys. 40, 2751 (1964).

109. J.L. Merz and P.S. Pershan, Phys. Rev. 162, 235 (1967).

110. J.A. Harrington and C.T. Walker, Phys. Rev. B1, 882 (1970).

111. R.W. Alexander and A.J. Sievers in "Optical Properties of Ions in Solids", ed. H.M. Crosswhite and H.W. Moos (Wiley Interscience, 1967).

112. S. Takeno, Prog. Theoret. Phys. 38, 995 (1967).

113. L. Pauling, "The Nature of the Chemical Bond", (Cornell University Press, 1960).

114. R.D. Shannon and C.T. Prewitt, Acta Cryst. B25, 935 (1969).

115. T. Moeller, "The Chemistry of the Lanthanides", (Reinhold, 1963).

116. G.S. Zhdanov, "Crystal Physics (Oliver and Boyd, 1965).

117. J.M. Baker, J. Phys. C 1, 1670 (1968).

118. V.V. Osiko, Soviet Physics - Solid State 7, 1047 (1965).

119. Yu.K. Voronko, A.A. Kaminskii and V.V. Osiko, Soviet Physics JETP 22, 501 (1966).

120. M.A. Nusimovici, M. Balkanski and J.L. Birman, preprint, Laboratoire des Physique des Solides de la Faculté des Sciences de Paris, France.

121. J.M. Baker, E.R. Davies and J.P. Hurrell, Proc. Roy. Soc. A. 308, 403 (1968).

122. M.S. Tyutin and B.I. Maksakov, Soviet Physics - Solid State 11, 168 (1969).

123. R.S. Leigh and B. Szigeti, Proc. Roy. Soc. A 301, 211 (1967).

124. B. Szigeti, J. Phys. Chem. Solids 24, 225 (1963).

125. R.C. Newman, Advances in Physics 18, 545 (1969).

126. Z.I. Ivanenko and B.Z. Malkin, Soviet Physics - Solid State, 11, 1498 (1970).

127. B.P. Clayman, Ph.D. Thesis, Cornell University, New York, (1969).

128. B.P. Clayman, I.G. Nolt and A.J. Sievers, Solid State Comm. 7, 7 (1969).

129. R.W. Alexander, A.E. Hughes and A.J. Sievers, Phys. Rev. B1, 1563 (1970).

130. R. Weber and P. Nette, Physics Letters 20, 493 (1966).

A P P E N D I X

COMPUTER PROGRAMS

```
C          MAIN FOURIER TRANSFORM PROGRAM
C
C
C          A NUMERICAL FOURIER TRANSFORM PROGRAM FOR EITHER SINGLE OR
C          DOUBLE SIDED INTERFEROGRAMS. IT HAS A CHOICE OF 3 APODIZATION
C          FUNCTIONS AND A SUBROUTINE FOR CORRECTING THE ERROR IN THE
C          CENTRAL MAXIMUM POSITION. THE FOURIER COEFFICIENTS ARE
C          OBTAINED BY WATT'S METHOD (SEE MERTZ - TRANSFORMATIONS IN
C          OPTICS).
C
C     PARAMETERS
C        1)APOD IS SET TO 0,1,2,3, DEPENDING ON THE APODIZATION FUNCTION
C          REQUIRED. (NONE, LINEAR, QUADRATIC, OR COSINE)
C        2)IPU,IPC ARE SET TO 0 WHEN PRINT-OUTS OF THE UNCORRECTED OR
C          CORRECTED INTERFEROGRAM ARE NOT REQUIRED.
C        3)SIDE IS 0,1,2 FOR SINGLE-SIDED LEFT HAND, SINGLE-SIDED RIGHT
C          HAND, DOUBLE-SIDED INTERFEROGRAMS RESPECTIVELY.
C        4)CARD IS SET TO 1 IF PUNCHED CARD OUTPUT OF THE SPECTRUM IS
C          DESIRED. THE FIRST CARD SPECIFIES THE RESOLUTION, THE
C          FREQUENCY RANGE AND THE NUMBER OF SPECTRAL POINTS PER
C          RESOLUTION ELEMENT. THE REMAINING CARDS CONTAIN THE SPECTRUM
C          WITH 10 POINTS PER CARD.
C        5)KP IS THE NUMBER OF SPECTRAL POINTS PER RESOLUTION ELEMENT
C          TO BE PLOTTED.
C        6)NE IS THE EXPERIMENT NO.
C        7)SP DESCRIBES THE SAMPLE. IT IS AN ALPHAMERIC STRING WHICH
C          OCCUPIES 24 COLUMNS.
C
C          ARRAY DIMENSIONS ARE SET BY THE COMMON STATEMENT IN THE
C          MAIN PROGRAM.
C
C                    NOTE  & = +
C
      EXTERNAL GRUBB
      COMMON /ALPHA/A(10000)/BETA/SPEC(2000)/GAMMA/B(4200)
      DIMENSION SP(6)
      INTEGER SIDE, APOD,CARD
      REAL K1,K2
      K=20
      IZERO=0
      PRINT 98
   98 FORMAT('1'40X'**********FOURIER TRANSFORM SPECTROSCOPY**********')
C
C       READ DATA CARD
C
      READ 1,SIDE,APOD,IPU,IPC,CARD,K1,K2,N,DELTAX,KP,NE,SP
    1 FORMAT(5I5,2F5.0,I5,F5.0,2I5,6A4)
      PRINT 103,NE
  103 FORMAT('1'8X'EXPERIMENT NO. 'I3)
      PRINT 203,SP
  203 FORMAT('0'8X'SAMPLE - '6A4)
      PRINT 2,N
    2 FORMAT('0NO. OF INPUT POINTS(N) TO BE USED='I5)
      PRINT 3,DELTAX
    3 FORMAT('0SAMPLING INTERVAL = 'F4.1' MICRONS')
      PRINT 4,K1,K2
    4 FORMAT('0LIMIT FREQUENCIES ='F5.0' - 'F5.0' WAVE NUMBERS')
      PRINT 6,KP
    6 FORMAT('0NO.OF OUTPUT POINTS PER RESOLUTION ELEMENT = 'I1)
      NS=0
  100 ITOT=KLOCK(X5)
      ITAPE=KLOCK(X1)
C
C       CALL THE PAPER TAPE SUBROUTINE
C
      CALL PTAPE(A,56000,IX,GRUBB)
      ITAPE=KLOCK(X1)-ITAPE
      NS=NS+1
      IF(IX.LE.-1) STOP
      NO=(56000-IX)/5
      PRINT 102
  102 FORMAT('1'60X'************')
      PRINT 103,NE
      PRINT 101,NS
  101 FORMAT('0'10X' RUN NO.'I2)
      PRINT 5,NO
    5 FORMAT('0NO. OF INPUT POINTS READ ='I5)
      CALL PREP(SIDE,M,IPU,NO)
   10 IF(SIDE.EQ.2) GO TO 20
C
C       CHECK FOR UNDERSIZE INTERFEROGRAM
C
      IF(M.LE.(K+30)) GO TO 30
      IF((N*K-1).GT.(NO-M)) GO TO 40
      IZERO=KLOCK(X3)
C
      CALL ERROR(DELTAX,N,M,K,IPC)
      IZERO=KLOCK(X3)-IZERO
      DELTAK=10000./(FLOAT(N-1)*DELTAX)
      PRINT 11,DELTAK
   11 FORMAT(//'0RESOLUTION = 'F5.2' WAVE NUMBER')
      X=1.0/FLOAT(N-1)
      IAPOD=KLOCK(X2)
C
      CALL APODS(N,APOD,M,X)
      IAPOD=KLOCK(X2)-IAPOD
      IFT=KLOCK(X4)
C
```

```
      CALL COSINE(DELTAX,DELTAK,K1,K2,M,N,KP)
      IFT=KLOCK(X4)-IFT
      GO TO 25
C
C      CHECK FOR UNDERSIZE INTERFEROGRAM
C
   20 IF(M.LT.(N+1)/2) GO TO 30
      IF((N-1)/2.GT.(NO-M)) GO TO 40
      DELTAK=1.0000./(FLOAT((N-1)/2)*DELTAX)
      PRINT 21,DELTAK
   21 FORMAT(//'ORESOLUTION = 'F5.2' WAVE NUMBER')
      X=1.0/FLOAT((N-1)/2)
      IAPOD=KLOCK(X2)
C
      CALL APODD(N,APOD,M,X)
      IAPOD=KLOCK(X2)-IAPOD
      IFT=KLOCK(X4)
C
      CALL COMP(DELTAX,DELTAK,K1,K2,M,N,KP)
      IFT=KLOCK(X4)-IFT
   25 PRINT 26,NS
   26 FORMAT('1'10X'SPECTRUM NO.'I2)
      PRINT 203,SP
      NK=KP*(K2-K1)/DELTAK+1.1
      PRINT 27,NK
   27 FORMAT(//'ONO. OF OUTPUT POINTS TO BE PLOTTED='I4)
      IPLOT=KLOCK(X5)
C
      CALL PLOT(NK,K1,DELTAK,KP)
      IPLOT=KLOCK(X5)-IPLOT
      IF(CARD.NE.1) GO TO 99
      WRITE(7,28)DELTAK,K1,K2,KP,NE,NS
   28 FORMAT(5X,3F10.2,I10,10X,2I10)
      WRITE(7,29)(SPEC(I),I=1,NK)
   29 FORMAT(10F8.0)
   99 ITOT=KLOCK(X6)-ITOT
      PRINT 300
  300 FORMAT('1'10X'OPERATION  - READ TAPE  APODIZATION  ZERO ERROR  FOU
     5RIER TRANSFORM  PLOT      TOTAL')
      PRINT 301,ITAPE,IAPOD,IZERO,IFT,IPLOT,ITOT
  301 FORMAT('0'10X'TIME(SECS) -'4X,I3,9X,I3,9X,I3,12X,I3,11X,I3,5X,I3)
      GO TO 100
   30 PRINT 31
   31 FORMAT(//'0****TOO FEW POINTS AT START OF THIS INPUT****'/)
      IF(NO.LT.95) NS=NS-1
      GO TO 100
   40 PRINT 41
   41 FORMAT(//'0****TOO FEW POINTS AT END OF THIS INPUT****'/)
      IF(NO.LT.95) NS=NS-1
      GO TO 100
      END



      SUBROUTINE APODD(N,APOD,M,X)
C
C        THE BASE-LINE IS CORRECTED AND THE DOUBLE-SIDED
C        INTERFEROGRAM IS APODIZED.
      COMMON /ALPHA/A(1)/BETA/SPEC(1)/GAMMA/B(1)
      INTEGER APOD
      PI=3.14159265358990
      BASE=0.0
      N1=(N-1)/2+1
      M1=M+1
      M2=M+(N-1)/2
      DO 10 I=1,10
      BASE=BASE+A(M-N1+I)+A(M+N1-I)
   10 BASE=0.05*BASE
      IF(APOD.NE.0) GO TO 13
      DO 11 I=1,N
      J=M-N1+I
   11 A(J)=A(J)-BASE
      PRINT 12
   12 FORMAT(//'ONO APODIZATION'/)
      RETURN
   13 IF(APOD.EQ.1) GO TO 20
      IF(APOD.EQ.2) GO TO 30
      IF(APOD.EQ.3) GO TO 40
   20 PRINT 21
   21 FORMAT(//'OLINEAR APODIZATION'/)
      DO 22 I=1,M
   22 A(I)=(A(I)-BASE)*(1.0-(M-I)*X)
      DO 23 I=M1,M2
   23 A(I)=(A(I)-BASE)*(1.0-(I-M)*X)
      RETURN
   30 PRINT 31
   31 FORMAT(//'OQUADRATIC APODIZATION'/)
      DO 32 I=1,M
   32 A(I)=(A(I)-BASE)*(1.0-((M-I)**2)*X**2)**2
      DO 33 I=M1,M2
   33 A(I)=(A(I)-BASE)*(1.0-((M-I)**2)*X**2)
      RETURN
   40 PRINT 41
   41 FORMAT(//'OCOSINE APODIZATION'/)
      DO 42 I=1,M
   42 A(I)=(A(I)-BASE)*0.5*(1.0+COS(PI*(M-I)*X))
      DO 43 I=M1,M2
   43 A(I)=(A(I)-BASE)*0.5*(1.0+COS(PI*(I-M)*X))
      RETURN
      END



      SUBROUTINE PREP(SIDE,M,IPU,NO)
C
      COMMON /ALPHA/A(1)/BETA/SPEC(1)/GAMMA/B(1)
      INTEGER SIDE
      IF(SIDE.NE.0) GO TO 10
C
C       A LEFT-HANDED INTERFEROGRAM IS INVERTED.
      DO 2 I=1,NO
      J=NO+1-I
    2 A(I)=B(J)
   10 IF(SIDE.EQ.0) SIDE=1
C
C     FIND CENTRE (MAXIMUM) POINT OF INTERFEROGRAM.
      AMAX=0.
      DO 6 I=1,NO
      IF(A(I).LE.AMAX) GO TO 6
      AMAX=A(I)
      M=I
    6 CONTINUE
      PRINT 7,M
    7 FORMAT('0CENTRAL POINT IS NO.'I5//)
      IF(IPU.EQ.0) GO TO 11
      PRINT 8
    8 FORMAT(//'0INTERFEROGRAM'/)
      WRITE (6,9)(A(I),I=1,NO)
    9 FORMAT(' '20F6.0)
   11 RETURN
      END
```

```
      SUBROUTINE ERROR(DELTAX,N,M,K,IPC)
C
CCC     THE ZERO ERROR CORRECTION IS DETERMINED AND
CCC     THE INTERFEROGRAM IS ADJUSTED ACCORDINGLY
C       USING THE METHOD OF FORMAN ET AL (JOSA 56,59)
      COMMON /ALPHA/A(1)/BETA/SPEC(1)/GAMMA/B(1)
      DIMENSION SINC(41),HOLD(40)
      ICN=1
      DO 13 I=1,40
   13 HOLD(I)=0.0
  100 D=A(M+1)-A(M-1)
      D2=A(M+1)-2*A(M)+A(M-1)
      D3=A(M+2)-2*D-A(M-2)
      D4=A(M+2)-4*A(M+1)+6*A(M)-4*A(M-1)+A(M-2)
      D5=A(M+3)-4*A(M+2)+5*D+4*A(M-2)-A(M-3)
      D6=A(M+3)-6*A(M+2)+15*A(M+1)-20*A(M)+15*A(M-1)-6*A(M-2)+A(M-3)
      I=0
      P=-0.5*D/D2
      S=0.
    1 I=I+1
      S=P
      S3=(3.0*P*P-1.0)/12.0
      S4=P*(2.0*P*P-1.0)/12.0
      S5=((5.0*P*P)*(P*P-3.0)+4.0)/240.0
      S6=((20.0*P**3)*(3.0*P*P-10.0)+8.0*P)/720.0
      P=-(0.5*D+S3*D3+S4*D4+S5*D5+S6*D6)/D2
      IF(ABS(P-S).GT.1.0E-4.AND.I.LE.10) GO TO 1
      ZERROR=P*DELTAX
      IF(ABS(ZERROR).LT.0.1.AND.ICN.EQ.1) GO TO 8
      IF(ABS(ZERROR).LT.0.4) GO TO 101
      PRINT 2,ICN,ZERROR
    2 FORMAT('0ZERO ERROR PRIOR TO CORRECTION NO.'I2' = 'F6.3' MICRONS')
      KI=2*K+1
      DO 3 I=1,KI
      R=3.141592653590*((I-K-1)-ZERROR/DELTAX)
      IF(R.EQ.0) SINC(I)=1.0
    3 IF(R.NE.0) SINC(I)=SIN(R)/R
      M1=M+N-1
      ML=M-10
      DO 5 I=ML,M1
      A(I-40)=HOLD(1)
      L1=I-K
      L2=I+K
      D=0.0
      DO 4 L=L1,L2
    4 D=D+A(L)*SINC(L-L1+1)
      DO 12 JOE=1,39
   12 HOLD(JOE)=HOLD(JOE+1)
      HOLD(40)=0
    5 CONTINUE
      DO 14 JOE=1,40
   14 A(M1-40+JOE)=HOLD(JOE)
      ICN=ICN+1
      IF(ICN.GT.20) RETURN
      GO TO 100
  101 IF(IPC.EQ.0) GO TO 11
      PRINT 6
    6 FORMAT(//'0CORRECTED INTERFEROGRAM'/)
      WRITE(6,7) (A(I),I=ML,M1)
    7 FORMAT(' '20F6.0)
    9 RETURN
    8 PRINT 10
   10 FORMAT(//'0***ZERO ERROR IS NEGLIBLE***')
   11 RETURN
      END


      SUBROUTINE COMP(DELTAX,DELTAK,K1,K2,M,N,KP)
C
CCC     A COMPLEX(AMPLITUDE) FOURIER TRANSFORMATION IS PERFORMED ON
C       A DOUBLE-SIDED INTERFEROGRAM.
      COMMON /ALPHA/A(1)/BETA/SPEC(1)/GAMMA/B(1)
      REAL KV,K1,K2
      TKP=1.0/FLOAT(KP)
      PRINT 1
    1 FORMAT(//'0COMPLEX (AMPLITUDE) TRANSFORM OF THE DOUBLE-SIDED
     3 INTERFEROGRAM'/)
      PI=3.141592653590*2.0*DELTAX/10000.
      N1=(N-1)/2
      DO 2 L=1,N1
      B(L)=A(M+L)-A(M-L)
    2 A(M+L)=A(M+L)+A(M-L)
      JMAX=IFIX(KP*(K2-K1)/DELTAK+1.1)
      DO 4 J=1,JMAX
      KV=K1+(J-1)*DELTAK*TKP
      SUMC=A(M)
      SUMS=0.0
      X=COS(PI*KV)
      Y=SIN(PI*KV)
      C=1.0
      S=0.0
      DO 3 I=1,N1
      C1=C
      C=X*C-Y*S
      S=Y*C1+X*S
      SUMC=SUMC+A(M+I)*C
    3 SUMS=SUMS+B(I)*S
      SUMC=SQRT(SUMC*SUMC+SUMS*SUMS)
    4 SPEC(J)=DELTAX*SUMC
      RETURN
      END


      SUBROUTINE COSINE(DELTAX,DELTAK,K1,K2,M,N,KP)
C
CCC     A COSINE FOURIER TRANSFORMATION IS PERFORMED ON A
C       SINGLE-SIDED INTERFEROGRAM.
      COMMON /ALPHA/A(1)/BETA/SPEC(1)/GAMMA/B(1)
      REAL KV,K1,K2,PI
      TKP=1.0/FLOAT(KP)
      N1=N-1
      PRINT 1
    1 FORMAT(//'0COSINE TRANSFORM OF THE SINGLE-SIDED INTERFEROGRAM'/)
      PI=3.141592653590*2.0*DELTAX/10000.
      JMAX=IFIX(KP*(K2-K1)/DELTAK+1.1)
      DO 3 J=1,JMAX
      KV=K1+(J-1)*DELTAK *TKP
      C=COS(PI*KV)
      C1=1.0
      A1=C+C
      SUMC=A(M+1)*C
      DO 2 I=2,N1
      C2=C
      C=A1*C-C1
      C1=C2
    2 SUMC=SUMC+A(M+I)*C
      SUMC=SUMC+SUMC+A(M)
    3 SPEC(J)=DELTAX*SUMC
      RETURN
      END
```

```
      SUBROUTINE PLOT(N,K1,DELTAK,KP)
C
      COMMON /ALPHA/A(1)/BETA/SPEC(1)/GAMMA/B(1)
      EQUIVALENCE (SPEC(1),X(1))
      DIMENSION X(780)
      REAL  PL/' '/,ST/'*'/,XI/'I'/,OUT(111),K,K1
      TKP=1.0/FLOAT(KP)
      K=K1
      XMA=-1.0E40
      DO 11 I=1,N
   11 XMA=AMAX1(XMA,X(I))
      SC=XMA/1000
      PRINT 30,SC
   30 FORMAT('0SCALING FACTOR = 'F9.0)
      PRINT 1
    1 FORMAT(///'0WAVE NO.  TRANSMITTANCE----------PLOTTED'/)
      DO 20 I=1,N
      DO 10 IKE=1,111
   10 OUT(IKE)=BL
      OUT(11)=XI
      OUT(111)=XI
      IR=X(I)*100./XMA+11.0
      X(I)=(X(I)*1000.)/XMA
      IF(IR.GE.1) OUT(IR)=ST
      WRITE(6,12)K,X(I),OUT
   12 FORMAT(' 'F6.2,3X,F6.0,3X,111A1)
      K=K+DELTAK*TKP
   20 CONTINUE
      RETURN
      END


      SUBROUTINE APODS(N,APOD,M,X)
C
CCC     THE BASE-LINE IS CORRECTED AND THE SINGLE-SIDED
        INTERFEROGRAM IS APODIZED.
      COMMON /ALPHA/A(1)/BETA/SPEC(1)/GAMMA/B(1)
      INTEGER APOD
      PI=3.14159265358 9
      BASE=0.0
      DO 10 I=1,10
      J=M+N-I
   10 BASE=BASE+A(J)
      BASE=0.1*BASE
      M1=M+N-1
      IF(APOD.NE.0) GO TO 13
      DO 11 I=M,M1
   11 A(I)=A(I)-BASE
      PRINT 12
   12 FORMAT(//'0NO APODIZATION'/)
      RETURN
   13 IF(APOD.EQ.1) GO TO 20
      IF(APOD.EQ.2) GO TO 30
      IF(APOD.EQ.3) GO TO 40
   20 PRINT 21
   21 FORMAT(//'0LINEAR APODIZATION'/)
      DO 22 I=M,M1
   22 A(I)=(A(I)-BASE)*(1.0-(I-M+1)*X)
      RETURN
   30 PRINT 31
   31 FORMAT(//'0QUADRATIC APODIZATION'/)
      DO 32 I=M,M1
   32 A(I)=(A(I)-BASE)*(1.0-((I-M+1)**2)*X**2)**2
      RETURN
   40 PRINT 41
   41 FORMAT(//'0COSINE APODIZATION'/)
      DO 42 I=M,M1
   42 A(I)=(A(I)-BASE)*0.5*(1.0+COS(PI*(I-M)*X))
      RETURN
      END
```

```
C            RUT  PROGRAM
C
CCC     THIS PROGRAM USES THE CARD OUTPUT FROM THE FOURIER TRANSFORM
CCC    PROGRAM. IN EACH OF NE EXPERIMENTS IT AVERAGES NB BACKGROUND RUNS
CCC    AND NS SPECTRUM RUNS , WHERE NB,NS ARE LESS THAN 6, AND RATIOS
CCC    THE RESULTS. THE RATIOED TRANSMITTANCE IS THEN CONVERTED INTO THE
CCC    FREQUENCY-DEPENDENT ABSORPTION COEFFICIENT. IT IS POSSIBLE TO
CCC    INSERT NINT POINTS BETWEEN EACH OF THE SPECTRAL POINTS USING AN
CCC    INTERPOLATION SUBROUTINE. NBEG AND NEND POINTS ARE DISCARDED AT
CCC    BEGINNING AND END OF THE SPECTRUM.
CCC    CARD IS SET TO 0 IF PUNCHED CARD OUTPUT IS NOT REQUIRED.
C
      DIMENSION SAM(6),TEMP(4),ALFA(1000)
      COMMON S1(2000),S2(2000),S3(2000),S4(2000),S5(2000),S6(2000)
      REAL K1,K2
      INTEGER CARD,HOST
      PRINT 8
    8 FORMAT('1'40X'**********FOURIER TRANSFORM SPECTROSCOPY**********')
      NCOUNT=0
   50 NCOUNT=NCOUNT+1
      PRINT 51,NCOUNT
   51 FORMAT('1'15X'SPECTRUM NO. 'I2)
      READ 1,NE,NB,NS,NINT,KP,NBEG,NEND,DELTAK,K1,K2,EXPO,BACKO,SAM,TEMP
    1 FORMAT(4I1,3I2,F5.1,2F5.0,2I5,6A4,4A4)
      PRINT 52,SAM,TEMP
   52 FORMAT('0'15X'SAMPLE - '6A4,10X'TEMPERATURE - '4A4//)
      READ 200,HOST,THICK,CONC
  200 FORMAT(I5,2F5.3)
      PRINT 100
  100 FORMAT(' ')
      IF(NB.NE.0) PRINT 53,NB,BACKO
   53 FORMAT('0 AVERAGE OF 'I1' BACKGROUND RUNS FROM EXPERIMENT NO.'I4)
      PRINT 54,NS,EXPO
   54 FORMAT('0 AVERAGE OF 'I1' RUNS FROM EXPERIMENT NO.'I4)
      DK=DELTAK/FLOAT(KP)
      N=(K2-K1)/DK+1.1
      PRINT 55,DELTAK
   55 FORMAT('0 RESOLUTION = 'F5.1' WAVE NUMBER')
      PRINT 56,N,DK,K1,K2
   56 FORMAT('0 THE INPUT SPECTRA HAVE 'I4' POINTS AT INTERVALS OF 'F5.1
     1' WAVE NO. BETWEEN 'F4.0' - 'F5.0' WAVE NOS.')
      PRINT 100
      NO=0
      IF(NB.EQ.0) NO=1
    3 CALL WAVE(NB,NS,NO,N)
    4 IF(NO.EQ.0) PRINT 53,NB,BACKO
      IF(NO.EQ.1) PRINT 54,NS,EXPO
      IF(NO.EQ.2) PRINT 52,SAM,TEMP
      CALL GRAPH(NO,N,K1,DK,NINT,NBEG,NEND)
```

```
      PRINT 100
      NO=NO+1
      IF(NO.EQ.1) GO TO 3
      IF(NR.EQ.0.AND.NCOUNT.EQ.NE) STOP
      IF(NR.EQ.0) GO TO 50
      IF(NO.EQ.2) GO TO 70
      PRINT 101
  101 FORMAT('1'55X'**********')
      TH=THICK
      CALL ALPHA(N,TH,ALFA,K1,DELTAK,HOST)
      WRITE(7,29)K1,K2,DELTAK,DK,EXPO,BACKO,SAM,TEMP
   29 FORMAT(2F5.0,2F5.1,2I5,6A4,4A4)
      WRITE(7,200)HOST,THICK,CONC
      WRITE(7,30)(ALFA(I),I=1,N)
   30 FORMAT(10F8.3)
   60 IF(NCOUNT.EQ.NE) STOP 1
      GO TO 50
   70 DO 5 I=1,N
    5 S5(I)=S5(I)/S6(I)
      GO TO 4
      END



      SUBROUTINE ALPHA(N,TH,ALFA,K1,DELTAK,HOST)
C
      COMMON S1(2000),S2(2000),S3(2000),S4(2000),S5(2000),S6(2000)
      DIMENSION D(2000),ALFA(1000)
      EQUIVALENCE (S1(1),D(1))
      REAL NR,KR,NW,K1,BL/' '/,ST/'*'/,XI/'I'/,OUT(111),K
      INTEGER HOST
      PI=3.141592653
      IF(CONC.GT.0.) GO TO 80
      IF(HOST.NE.1) GO TO 1
      NR=2.6
      EO=6.38
      WTO=267.
      EINF=2.047
      GO TO 10
    1 IF(HOST.NE.2) GO TO 2
      NR=2.55
      EO=6.04
      WTO=225.
      EINF=2.07
      GO TO 10
    2 NR=2.65
      EO=6.56
      WTO=189.
      EINF=2.157
   10 DMAX=-1.0E40
      REF=(NR-1.)**2/(NR+1.)**2
      SC=((1.-REF)**2)/(1.-(REF**2))
      DO 11 I=1,N
   11 DMAX=AMAX1(DMAX,D(I))
      DO 12 I=1,N
   12 D(I)=D(I)*SC/DMAX
      I=1
   13 IF(D(I).LE.0.0) GO TO 100
      DI=D(I)
      A=DI*(REF**2)
      B=(1.-REF)**2
      C=-DI
      DISC=B**2-4.*A*C
      FAC=SQRT(DISC)
      SUM=-B+FAC
      DEN=2.*A
      X=SUM/DEN
      IF(X.GT.0.)  CLOG=ALOG(X)
      IF(X.LE.0.) CLOG=0.
      ALF=-CLOG/TH
      K=K1+(I-1)*DELTAK
      KR=ALF/(4.*PI*K)
      REF=((NR-1.)**2+KR**2)/((NR+1.)**2+KR**2)
      A=DI*(REF**2)
      B=(1.-REF)**2
      C=-DI
      X=(-B+SQRT(B**2-4.*A*C))/(2.*A)
      IF(X.GT.0.) ALF=-ALOG(X)/TH
      IF(X.LE.0.) ALF=0.
      NW=SQRT((EO*WTO**2-EINF*K**2)/(WTO**2-K**2))
      REF=((NW-1.)**2+KR**2)/((NW+1.)**2+KR**2)
      A=DI*(REF**2)
      B=(1.-REF)**2
      C=-DI
      X=(-B+SQRT(B**2-4.*A*C))/(2.*A)
      IF(X.GT.0.) ALF=-ALOG(X)/TH
      IF(X.LE.0.) ALF=0.
      ALFA(I)=ALF
      I=I+1
      IF(I.LE.N) GO TO 13
      GO TO 20
  100 ALFA(I)=0.
      I=I+1
      IF(I.LE.N) GO TO 13
      GO TO 20
   80 DMAX=-1.0E40
      DO 81 I=1,N
   81 DMAX=AMAX1(DMAX,D(I))
      DO 82 I=1,N
   82 D(I)=D(I)/DMAX
      I=1
   83 IF(D(I).LE.0.) GO TO 90
      DI=D(I)
      IF(DI.GT.0.) DLOG=ALOG(DI)
      IF(DI.LE.0.) DLOG=0.
      ALF=-DLOG/TH
      ALFA(I)=ALF
      I=I+1
      IF(I.LE.N) GO TO 83
      GO TO 20
   90 ALFA(I)=0.
      I=I+1
      IF(I.LE.N) GO TO 83
   20 PRINT 25
   25 FORMAT(//'0 WAVE NO.'5X'ABSORPTION COEFFICIENT--------PLOTTED'/)
      K=K1
      ALFMA=-1.0E40
      DO 30 I=1,N
   30 ALFMA=AMAX1(ALFMA,ALFA(I))
      DO 50 I=1,N
      DO 35 IKE=1,111
   35 OUT(IKE)=BL
      OUT(1)=XI
      OUT(111)=XI
      IR=ALFA(I)*100./ALFMA+11.
      IF(IR.GE.1) OUT(IR)=ST
      WRITE(6,40)K,ALFA(I),OUT
   40 FORMAT(' 'F6.2,3X,F6.2,3X,111A1)
      K=K+DELTAK
   50 CONTINUE
      RETURN
      END
```

```
      SUBROUTINE GRAPH(NO,N,K1,DK,NINT,NBEG,NEND)
C
      COMMON S1(2000),S2(2000),S3(2000),S4(2000),S5(2000),S6(2000)
      DIMENSION X(2000)
      EQUIVALENCE(S1(1),X(1))
      REAL BL/' '/,ST/'*'/,XI/'I'/,OUT(111),K,K1
      M=4
      IF(NO.NE.0) GO TO 10
      DO 2 I=1,N
    2 X(I)=S6(I)
      GO TO 90
   10 IF(NO.NE.1) GO TO 21
      DO 3 I=1,N
    3 X(I)=S5(I)
      GO TO 90
   21 DELTAK=DK
      DK=DK/FLOAT(NINT+1)
      NP=N
      N=(NINT+1)*(N-1)+1
      IF(NINT.GE.1) PRINT 50,N,DK
   50 FORMAT(//'0 BECAUSE OF INTERPOLATION, 'I4' SPECTRAL POINTS ARE NOW
     1 PLOTTED AT INTERVALS OF 'F4.1' WAVE NUMBERS')
      I=1
   51 K=K1+(I-1)*DK
      J=FLOAT(I-1)/FLOAT(NINT+1)+1
      DD=K-K1
      IF(AMOD(DD,DELTAK).NE.0.) GO TO 80
      X(I)=S5(J)
      IF(I.EQ.N) GO TO 90
      I=I+1
      GO TO 51
C
C      CHECK THAT MTH DIFFERENCES EXIST FOR S5(I).
   80 IF((J-M-NBEG).GT.0) GO TO 81
98    X(I)=0.0
      IF(I.EQ.N) GO TO 90
      I=I+1
      GO TO 51
   81 IF((NP-M-NEND-J).GT.0) GO TO 82
      X(I)=0.0
      IF(I.EQ.N) GO TO 90
      I=I+1
      GO TO 51
   82 CALL TWERP(DELTAK,K1,K,S,M)
      X(I)=S
      IF(I.EQ.N) GO TO 90
      I=I+1
      GO TO 51
   90 K=K1
      IF(NO.NE.2) GO TO 84
      IF(NBEG.EQ.0) GO TO 86
      MBEG=(NINT+1)*NBEG
      DO 76 I=1,MBEG
   76 X(I)=0.0
   86 IF(NEND.EQ.0) GO TO 84
      MEND=(NINT+1)*NEND
      DO 77 I=1,MEND
   77 X(N+1-I)=0.0
   84 CONTINUE
      XMA=-1.0E40
      DO 11 I=1,N
   11 XMA=AMAX1(XMA,X(I))
      PRINT 1
    1 FORMAT(///'0WAVE NO.  TRANSMITTANCE--------------------PLOTTED'/)
      DO 20 I=1,N
      DO 22 IK=1,111
   22 OUT(IK)=BL
      OUT(1)=XI
      OUT(111)=XI
      IF(X(I).LT.0.) X(I)=0.0
      IR=X(I)*100./XMA+1.5
      X(I)=(X(I)*1000.)/XMA
      IF(IR.GE.1) OUT(IR)=ST
      WRITE(6,12)K,X(I),OUT
   12 FORMAT(' 'F6.2,3X,F6.0,3X,111A1)
      K=K+DK
   20 CONTINUE
      RETURN
      END
```

```
      SUBROUTINE TWERP(DELTAK,K1,K,S,M)
C
      COMMON S1(2000),S2(2000),S3(2000),S4(2000),S5(2000),S6(2000)
      DIMENSION D(2000)
      EQUIVALENCE (D(1),S2(1))
      REAL K,K1,KS
      MS=(K-K1+DELTAK)/DELTAK
      RMS=MS-1
      KS=K1+RMS*DELTAK
      U=(K-KS)/DELTAK
      A=U
      S=S5(MS)
      DO 42 IT=1,M
      JT=MS+IT-1
   42 D(IT)=S5(JT+1)-S5(JT)
      IF(M.EQ.1) GO TO 40
      DO 49 KT=2,M
      DO 49 NT=KT,M
      L=M+KT-NT
   49 D(L)=D(L)-D(L-1)
   40 DO 44 KO=1,M
      S=S+A*D(KO)
      FK=KO
   44 A=A*(U-FK+1.)/FK
      RETURN
      END
```

```
      SUBROUTINE RAVE(NB,NS,NO,N)
C
      COMMON S1(2000),S2(2000),S3(2000),S4(2000),S5(2000),S6(2000)
      IF(NO.EQ.1) NB=NS
      READ(5,1) (S1(I),I=1,N)
    1 FORMAT((10F8.0))
      IF(NB.EQ.1) GO TO 10
      READ(5,1)(S2(I),I=1,N)
      IF(NB.EQ.2) GO TO 10
      READ(5,1)(S3(I),I=1,N)
      IF(NB.EQ.3) GO TO 10
      READ(5,1)(S4(I),I=1,N)
      IF(NB.EQ.4) GO TO 10
      READ(5,1)(S5(I),I=1,N)
   10 T2=1.0
      T3=1.0
      T4=1.0
      T5=1.0
      IF(NB.LE.1) T2=0.0
      IF(NB.LE.2) T3=0.0
      IF(NB.LE.3) T4=0.0
      IF(NB.LE.4) T5=0.0
      DO 11 I=1,N
      S=(S1(I)+T2*S2(I)+T3*S3(I)+T4*S4(I)+T5*S5(I))/NB
      IF(NO.EQ.0) S6(I)=S
   11 IF(NO.EQ.1) S5(I)=S
      RETURN
      END
```

```
C               FUN  PROGRAM
C
      DIMENSION X(2000),SAM(6),TEMP(4)
      INTEGER EXPO,BACKO,HOST
      REAL  BL/' '/,ST/'*'/,XI/'I'/,OUT(111),K,K1,K2,KS,KF
      NCOUNT=1
      READ 1,NE
    1 FORMAT(I2)
      PRINT 40
   40 FORMAT('1'/45X'******FOURIER TRANSFORM SPECTROSCOPY******')
      PRINT 21
   21 FORMAT(/'0'35X'FAR INFRARED SPECTRA OF LUTECIUM IONS IN CALCIUM
     2FLUORIDE-TYPE LATTICES')
    2 READ(5,3) K1,K2,DELTAK,DK,EXPO,BACKO,SAM,TEMP
    3 FORMAT(2F5.0,2F5.1,2I5,6A4,4A4)
      PRINT 50
   50 FORMAT('1')
      PRINT 15,NCOUNT
   15 FORMAT(//'0'58X'SPECTRUM NO. 'I2//)
      READ 70,HOST,THICK,CONC,KS,KF
   70 FORMAT(I5,2F5.3,2F5.1)
      N=(K2-K1)/DK+1.1
      PRINT 5,EXPO,SAM,TEMP
    5 FORMAT(///'0'10X'EXPERIMENT NO. 'I3' - '6A4,5X'TEMPERATURE - '4A4/
     1/)
      PRINT 71,CONC
   71 FORMAT('0'10X'IMPURITY CONCENTRATION = 'F5.2' ATOMS PER CENT'//)
      IF(HOST.EQ.1) PRINT 72
   72 FORMAT('0'10X'HOST CRYSTAL IS CALCIUM FLUORIDE'//)
      IF(HOST.EQ.2) PRINT 73
   73 FORMAT('0'10X'HOST CRYSTAL IS STRONTIUM FLUORIDE'//)
      IF(HOST.EQ.3) PRINT 74
   74 FORMAT('0'10X'HOST CRYSTAL IS BARIUM FLUORIDE'//)
      PRINT 75,THICK
   75 FORMAT('0'10X'CRYSTAL THICKNESS = 'F5.3' CENTIMETERS'//)
      PRINT 6,BACKO
    6 FORMAT('0'10X'EXPERIMENT NO. 'I3' - BACKGROUND'//)
      PRINT 7,DELTAK
    7 FORMAT(///'0'10X'RESOLUTION = 'F5.1' WAVE NUMBER'//)
      READ(5,4)(X(I),I=1,N)
    4 FORMAT(10F8.3)
      PRINT 8
    8 FORMAT(///'0 WAVE NO.  ABSORPTION COEFFICIENT----------PLOTTED'//)
      K=K1
      XMA=-1.0E40
      DO 11 I=1,N
   11 XMA=AMAX1(XMA,X(I))
      DO 20 I=1,N
      DO 10 IKE=1,111
   10 OUT(IKE)=BL
      OUT(11)=XI
      OUT(111)=XI
      IF(X(I).LT.0.0)X(I)=0.0
      IR=X(I)*2.+11.
      IF(IR.GE.1.AND.IR.LE.111) OUT(IR)=ST
      WRITE(6,12)K,X(I),OUT
   12 FORMAT(' 'F6.2,3X,F7.3,2X,111A1)
      IF(DK.EQ.5.0) PRINT 37,XI,XI
   37 FORMAT(' '28X,A1,99X,A1)
      K=K+DK
   20 CONTINUE
      IF(KS.GT.10.) CALL BASE(X,DK,K1,KS,KF,CONC)
      NCOUNT=NCOUNT+1
      IF(NCOUNT.GT.NE) STOP
      GO TO 2
      END
```

```
      SUBROUTINE BASE(X,DELTAK,K1,KS,KF,CONC)
C
      DIMENSION X(1000),Y(1000)
      REAL K1,KS,KF,BL/' '/,ST/'*'/,XI/'I'/,OUT(111),K
      IS=(KS-K1)/DELTAK+1.1
      NO=(KF-KS)/DELTAK+1.1
      DO 1 I=1,NO
    1 Y(I)=X(I+IS-1)
      YS=X(IS)
      YF=X(NO+IS-1)
      DIFF=(YF-YS)/(NO-1.)
      DO 2 I=1,NO
    2 Y(I)=Y(I)-(I-1)*DIFF-YS
      PRINT 3
    3 FORMAT(///'0WAVE NO.    NORMALIZED ABSORPTION COEFFICIENT----------
     1--------------------PLOTTED'///)
      K=KS
      YMA=-1.0E40
      DO 4 I=1,NO
    4 YMA=AMAX1(YMA,Y(I))
      SC=2.
      IF(YMA.LE.10.) SC=10.
      IF(YMA.GT.50.) SC=1.
      DO 50 I=1,NO
      DO 35 IKE=1,111
   35 OUT(IKE)=BL
      OUT(1)=XI
      OUT(111)=XI
      IF(DELTAK.GE.5.) PRINT 45,OUT
   45 FORMAT(' '18X,111A1)
      IR=Y(I)*SC+1.1
      IF(IR.GE.1.AND.IR.LE.111) OUT(IR)=ST
      WRITE(6,40) K,Y(I),OUT
   40 FORMAT(' 'F6.2,3X,F6.2,3X,111A1)
      K=K+DELTAK
   50 CONTINUE
      SUM=0.
      DO 10 I=1,NO
   10 SUM=SUM+Y(I)
      ALFINT=DELTAK*SUM
      PRINT 11,ALFINT
   11 FORMAT(///'0'10X'INTEGRATED ABSORPTION COEFFICIENT OF FAR INFRARED
     2 ABSORPTION BAND = 'F7.2' (CM**-2)'//)
      IF(CONC.EQ.0.) GO TO 100
      PRINT 60,CONC
   60 FORMAT(///'0'10X'IMPURITY CONCENTRATION (NOMINAL) = 'F4.2' ATOMS P
     3ER CENT'//)
      DO 61 I=1,NO
   61 Y(I)=Y(I)/CONC
      PRINT 63
   63 FORMAT(///'0WAVE NO.    ABSORPTION COEFFICIENT/ATOMS PER CENT-------
     4--------------------PLOTTED'///)
      K=KS
      YMA=-1.0E40
      DO 74 I=1,NO
   74 YMA=AMAX1(YMA,Y(I))
      SC=1.
      DO 80 I=1,NO
      DO 85 IKE=1,111
   85 OUT(IKE)=BL
      OUT(1)=XI
      OUT(111)=XI
      IF(DELTAK.GE.5.) PRINT 45,OUT
      IR=Y(I)*SC+1.1
      IF(IR.GE.1.AND.IR.LE.111) OUT(IR)=ST
      WRITE(6,40) K,Y(I),OUT
      K=K+DELTAK
   80 CONTINUE
      SUM=0.
      DO 90 I=1,NO
   90 SUM=SUM+Y(I)
      ALFIE=DELTAK*SUM
      PRINT 91,ALFIE
   91 FORMAT(///'0'10X'INTEGRATED ABSORPTION / ATOMS PER CENT = 'F7.2' (
     5CM**-2)'//)
  100 CONTINUE
      RETURN
      END
```